Conceptual Modelling of
Climate-Biosphere Interactions
over Geological Time

Master's thesis by

Peter Nørtoft Nielsen

Centre for Ice and Climate
The Niels Bohr Institute
University of Copenhagen
Juliane Maries Vej 30
2100 Copenhagen Ø

January 2008

Supervisor: Peter D. Ditlevsen

Abstract

Observations indicate that Earth during most of the time since its formation $\sim 4.6 \cdot 10^9$ years ago has had surface temperatures similar to, or perhaps even higher than now, in spite of a considerably less luminous young Sun. Only few geologically brief extreme glacations seem to have occured in Earth's history. These phenomena can be explained by changes in Earth's greenhouse effect over time. Such variations could be tigthly coupled to the biosphere since biology heavily influences the atmospheric content of greenhouse gases. Daisyworld is a simple climate-biosphere model that strongly advocates for a long-term stabilizing effect on climate due to biology, thus pointing towards a biospheric explanation of Earth's relatively constant surface temperature back in time. This stabilizing mechanism is, however, related to a more speculative biological influence on the planetary albedo. In this thesis we review the hypothesized biological stabilization of climate in the Daisyworld model, and we show that the model actually exhibits climatic bistability due to the presence of biology. An introduction to the art of conceptual climate modelling is given, and based on this we present an alternative conceptual climate-biosphere model with focus on the biological influence on the greenhouse effect through atmospheric carbon dioxide. As the primary results, this model does *not* support a biological stabilization of climate. Instead, it points toward a biospheric explanation of one of Earth's extreme glaciations.

Contents

List of Figures

List of Tables

Preface

The following pages present my master's thesis work, the final part of my graduate education in geophysics at the Niels Bohr Institute at the University of Copenhagen. This has been carried out under the supervision of associate professor Peter D. Ditlevsen.

My thesis work unites the study of climate with the art of doing simple modelling, both fields that have my great interest and passion.

In the field of conceptual modelling, many details are crudely simplified. Being a generalist in a world of specialists can be rather challenging. I like to think that specialists produce all the little pieces of a jigzaw puzzle, and my job has been to put some of these together to draw a sketch of the full picture of the puzzle.

Through the work I have come across several, to me as a geophysicist, new fields of science, primarily in evolutionary biology, population ecology, geology and (bio-geo-) chemistry. Trying to grasp these new subjects has been highly interesting, but also challenging. I kindly ask any expert in these fields to bare over with me if they, when reading my thesis, feel their domain improperly treated or over-simplified.

My thesis work has, by my own choice, been an open process, in the sense that no clear track was lain from the start. My supervisor and I had a vague idea of the direction to follow, but the target of the search has been defined along the way. Much of the work has been lain in putting simple things together for the first time, as opposed to improving or adjusting a more complex entity. As often happens, many dead ends are explored before the simple shortcut was found.

During my thesis work, I have been given the opportunity to participate in an informal workshop on climate-biosphere interactions in Paris in fall 2006, and to present a poster of my work at EGU general assembly in Vienna

in spring 2007. These were both very fruitful and entertaining experiences.

This thesis is, naturally, like a child to me, put in this world from the big question of whether life and climate could be working together to shape Earth's history. Raising this child of mine has been a great experience—but not without complications, I should say; birth was painful, and the child grew up to become somewhat different from what I expected. Still, it *is* a love child.

I would like to thank my supervisor, Peter D. Ditlevsen, for suggesting this study, for helpful supervision, and for good ideas and comments along the way. Furthermore I thank Mads Dam Ellehøj and Thomas Bjerring Kristensen for comments on the manuscript and upgrading its readability, Peter L. Langen for good comments and suggestions, all my friends at NBI for both helpful discussions and for being talented opponents at the fuss-ball table during breaks, and my family for their unconditional support and love. Last but not least, I thank my girlfriend, Pia, for being there for me, for your amazing patience with me, your love, and your fantastic cooking. Without you, this thesis had never been finished.

Peter Nørtoft Nielsen
Copenhagen, January 30, 2008

1 Introduction

Palaeoclimatology, the study of Earth's climate over the entire history of the planet, is subjected to two fundamental puzzles. The first is related to the observation that Earth during most of the time since its formation $\sim 4.6 \cdot 10^9$ years ago has had surface temperatures similar to, or perhaps even higher than now, in spite of a considerably less luminous young Sun. This is the socalled *Faint Young Sun paradox* [*Kasting and Catling*, 2003; *Kasting and Ono*, 2006]. Thus, surface temperatures appear to have been within habitable limits for most of Earth's history. The second is related to the evidence of geologically brief extreme glacations in Earth's history $\sim 2.4 \cdot 10^9$ and $\sim 0.7 \cdot 10^9$ years ago, perhaps of global extent—the socalled *Snowball* or *Slushball Earth* events [*Kopp et al.*, 2005; *Hoffman et al.*, 1998].

A likely path to follow in order to understand these somewhat contrasting phenomena is through the greenhouse effect. The Faint Young Sun paradox can be resolved by an intensified greenhouse atmosphere on early Earth due to enhanced concentrations of CO_2 and/or CH_4, whereas the extreme glaciations can be explained as temporary collapses of this greenhouse atmosphere [*Kasting and Catling*, 2003]. Many aspects of this explanation of Earth's climatic evolution being shaped by variations in the greenhouse effect can be related to biology, due to the biospheric influence on the atmospheric content of greenhouse gases. Methanogenic bacteria could have served to fill early Earth's atmosphere with CH_4 before $\sim 2.4 \cdot 10^9$ years ago, and thus keept early Earth warm [*Kasting and Siefert*, 2002]. On the other hand, photosynthetic biology could have served to draw down atmospheric contents of CO_2 $\sim 0.7 \cdot 10^9$ years ago, and thus initiating the extreme glaciation event at that time [*Heckman et al.*, 2001]. The focus of the model presented in this thesis will relate to the latter of these possible effects.

The notion of a co-evolution of Earth's climate and biosphere is at the

very heart of the socalled *Gaia* theory [*Lenton*, 1998]. Daisyworld, an imaginary planet inhabited by only black and white dasies, is a simple theoretical foundation of Gaia theory [*Watson and Lovelock*, 1983]. In Daisyworld, focus is on the planetary albedo as the important biosphere-climate mediator. The model investigates the response of climate to a less luminous Sun back in time, as dictated by the Faint Young Sun paradox; it strongly advocates for a stabilizing, homeostatic effect of the biosphere on climate over long timescales.

The current study is motivated from the two sides outlined above: A qualitiative *observational*, as dictated by the Faint Young Sun paradox, the extreme glaciations, and the potential importance of biology, and a more quantitative *modelling* part, as dictated by the Daisyworld.

1.1 Purpose

In this thesis we thus take up the idea of conceptually modelling the interactions between climate and biosphere over geological timescales. This involves two steps. As a first step, we wish firstly to investigate the hypothesized biotic stabilization of climate in the Gaian Daisyworld, and its tentative biological explanation of the Faint Young Sun paradox. As the second and primary step, we wish to set up an alternative simple biosphere-climate model with focus on the atmospheric content of carbon dioxide CO_2, as oppossed to the Gaian effects from the planetary albedo in Daisyworld. With this model we shall examine the biological effects on climate. Hereby we wish, firstly, to shed new light over the concept of biological homeostasis, and secondly, to investigate possible biological explanations of the Snowball Earth events.

1.2 Outline

The aim of the structure of the thesis is to introduce the reader to the work in a coherent and intuitively clear way. First, in chapter 2, an introduction to palaeoclimatology is given as motivation of the study. Then we will review Daisyworld as a conceptual climate-biosphere model and comment on the concept of biotic homeostasis in Daisyworld in chapter 3. After this, in chapter 4, we introduce the basics of climate theory and motivate the approach of conceptual modelling of the climate system, biosphere and CO_2. Then, in chapter 5, a conceptual climate-biosphere model with focus on CO_2 is set up. This is followed by a presentation of the results of the model in chapter 6 that also contains the perspectives of these results within the context of biological climate stabilization and palaeclimatology. The validity of the model results and the assumptions of the model are then

discussed in chapter 7, and finally, in chapter 8, the conclusions of the thesis are summarized.

2 Background

In this chapter a short introduction to Earth's climatic history on a geological timescale is presented. This is followed by a few comments on biological evolution. It should be stressed that these introductions are only inteded as crude, qualitative sketches and are in no way exhaustive of the subjects. The issues presented here will serve as the qualitiative, observational motivation of the study, whereas the Daisyworld model presented in the next chapter will serve as a more quantitative, modelling motivation.

2.1 Palaeoclimatology

Palaeoclimatology is the study of Earth's climate on long timescales. The focus of this thesis is the longest possible timescale for Earth: the *geological timescale*, spanning from the time of Earth's formation some $4.5 \cdot 10^9$ years ago and up to present day. The geological timescale is characterized by a wealth of names of the different parts of the time line of Earth. All these names can certainly be rather challenging, see figure 2.1 on page 7 for a helping hand. On the broadest line, *eons* separate Earth's history into four: The Hadean ($\sim$4.5–3.8 Ga), the Archaean ($\sim$3.8–2.5 Ga), the Proterozoic ($\sim$2.5–0.55 Ga), and the Phanerozoic eon (from $\sim$0.55 Ga an onwards). Here, and in the following, 1 Ga = 1 giga-anni = 1 billion years, and likewise 1 Ma = 1 mega-anni = 1 million years. Please also refer to appendix A.1 for some explanations of terminology. The Precambrian *super-eon* covers the Hadean, the Archaean, and the Proterozoic eons. Eons are subdivided into eras, eras into periods, and periods into epochs. Often used prefixes are *Palaeo*, meaning early or old, *Meso*, meaning mid or middle, and *Neo*, meaning late or new. The classification, i.e. the definition of super-eons, eons, eras, periods and epochs, and the exact timing and duration of these

are naturally subjected to debate. The focus of this thesis is primarely within this Precambrian super-eon.

A formal definition of climate and the climate system is given later in chapter 4; for now, let us just say that climate is the state of Earth's atmosphere, ocean, ice-caps and lithosphere. *Kasting and Catling* [2003] presents a nice review of the evolution of our planet, see also e.g. *Kasting and Ono* [2006].

Planet Earth was formed $\sim$4.55 Ga ago during the planetary accretion that formed the Solar System. The first $\sim$700 Ma of our planet were characterized by frequent impacts, one of these was the Moon-forming impact known as the 'Big Splat'. This period is referred to as the heavy-bombardment epoch. At some point during or after this violent heavy-bombardment epoch, a solid surface on Earth would have appeared. When and how the atmosphere and oceans were formed is subjected to debate. This question is also relevant for biology, since water is highly important for the habitability of the planet. In one view, the delivery of volatiles, such as H_2O, CO_2, and N_2, to Earth happened during accretion, meaning that both the atmosphere and ocean should have started to form as Earth formed, although the energy associated with these impacts should have worked against this. However, other theories suggest that water on Earth has been delivered to Earth with comets over a somewhat later and longer period in Earth's history. All in all, it is fair to believe that a *climate system* was established at a relatively early time in Earth's history not too long after the end of the heavy-bomardement epoch, although the state of the climate was probably very different from the present.

An interesting question in the history of Earth's climate is how surface temperatures has evolved. No clear measure exists that allow us to construct a curve of Earth's global mean surface temperature as function of time before present. However, some proxy indicators are available. Here, the results of two are briefly described: The first is related to the fractionation of isotopes of, e.g., oxygen extracted from old rocks. The other is related to the finding of glacial deposits that can shown to have formed near equator. In general, the farther back in time we go, the less certain is the evidence (older rocks are hard to find and date).

The oxygen isotope method is based on isotopic fractionation between the two oxygen isotopes ^{18}O and ^{16}O in old sedimentary rocks. This fractionation is measured by $\delta^{18}O$ which is the relative deviation of the ratio of these isotopes compared to some standard. $\delta^{18}O$ in the sedimentary rock reflects the isotopic composition of the seawater in which it was formed. The difference between $\delta^{18}O$ of the seawater and $\delta^{18}O$ of the rock is a result of an isotopic fractionation during formation, and it depends on the seawater temperature. By estimating the value for $\delta^{18}O$ of seawater, the temperature can then be estimated from the measured $\delta^{18}O$ of the rock. The age of the rock can be estimated by radiometric dating. *Robert and Chaussidon*

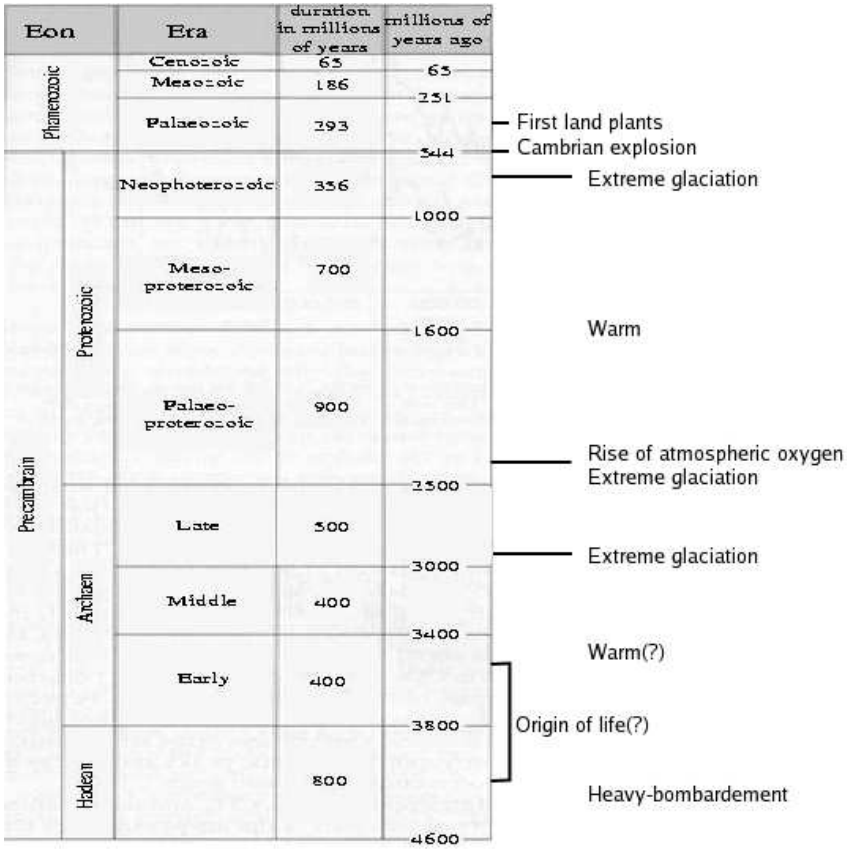

Figure 2.1: A schematic illustration of the geological timescale showing some important climatic and biological happenings. Redrafted from [*Kasting and Ono*, 2006].

[2006] present some recent measurements. Here, the δ^{18}O measurements are further supported by measurements on silicon Si. From this, tentative ocean temperatures are computed back to ∼3.5 Ga, showing a change in seawater temperatures from ∼70°C at 3.5 Ga to ∼20°C at 0.8 Ga. It should be stressed that such high temperatures are not supported by the entire scientific community. Instead, more temperate climates are suggested, cf. [*Kasting and Ono*, 2006]

The other line of evidence comes from geological findings of what is interpreted as evidence of glaciations at low latitudes from different times in Earth's history. This method can be used as more crude proxy of surface temperatures. Diamictites are clusters of rock fragments that are bound in a matrix. This is a glacial deposited rock type. The latitude at which the glacial deposit was formed can be inferred from the magnetic orientation within the rock, compared to the plumbline if this can be determined some

how. Evidence of glacial deposits at low latitudes, i.e. towards equatorial regions, at a given time in history is strongly indicative of low mean surface temperatures at this time. This line of evidence adds to the story of Earth's climate back in time. It appears that during 2–3 distinct periods in Earth's history, the planet has been subjected to extreme glaciations, where ice and snow covered equatorial regions. Each of these periods, it seems, could actually contain several distinct episodes of glaciations, but they are in general relatively brief episodes with typical durations on the order of ∼10Ma [*Hoffman et al.*, 1998]. These extreme glaciations are described further below in section 2.1.2).

Figure 2.1 shows the qualitative, very crude sketch of the history of Earth's climate, as indicated by the above proxiee. Also a few biological happenings have been pointed out—these are commented below in section 2.2. Concerning the climatic issues, we will focus on two main points that are highlighted by the figure: Firstly, the general view is that temperatures through *most* of Earth's history since ∼3.8 Ga have been similar to, or perhaps even higher than now, although scientists disagree on how high the temperatures actually were. As we shall see below, this poses a paradox due to the evolution of the Sun. Secondly, the idea of a constantly, warm Earth is not completely true; rather, the relatively warm Earth has been dramatically disturbed by some briefer, extremely cold climatic episodes, where ice and snow have covered most of Earth's surface, and the global mean temperature was well below freezing. These two points are discussed below.

2.1.1 The Faint Young Sun Paradox

In order to understand why the long periods in Earth's early history with relatively high surface temperatures are actually a paradox, we need to take a brief detour into the evolution of the Sun. The Sun as a *main sequence star* is fueled by nuclear fusion of hydrogen into helium, which takes place in the stellar interiors. With time, this process tends to densify the solar core, which in turn increases the flux of radiant energy that is being emmited from the Sun. Going *back* in time, the solar constant S was therefore *less* than its present value $S_0 \approx 1370\mathrm{Wm}^{-2}$ (thus making the use of the word *constant* somewhat unfortunate). The solar constant S is the flux of radiant energy at one astronomical unit AU away from the Sun, the average Sun–Earth distance. A convenient relation of the evolution of the solar constant S with time is, cf. [*Kasting*, 2005]:

$$\frac{S(t)}{S_0} = \frac{1}{1 + \frac{2}{5}\frac{t}{t_0}}, \tag{2.1}$$

where t is time *before present*, and $t_0 = 4.6\,\mathrm{Ga}$. At $t \approx 3.8\,\mathrm{Ga}$ we have $S/S_0 \approx 0.75$ and the solar constant was thus ∼25% less than today. In

figure 2.2, this relation is illustrated with the solid black line, showing the slow increase in S/S_0 with time. Now, coming back to Earth, this stellar

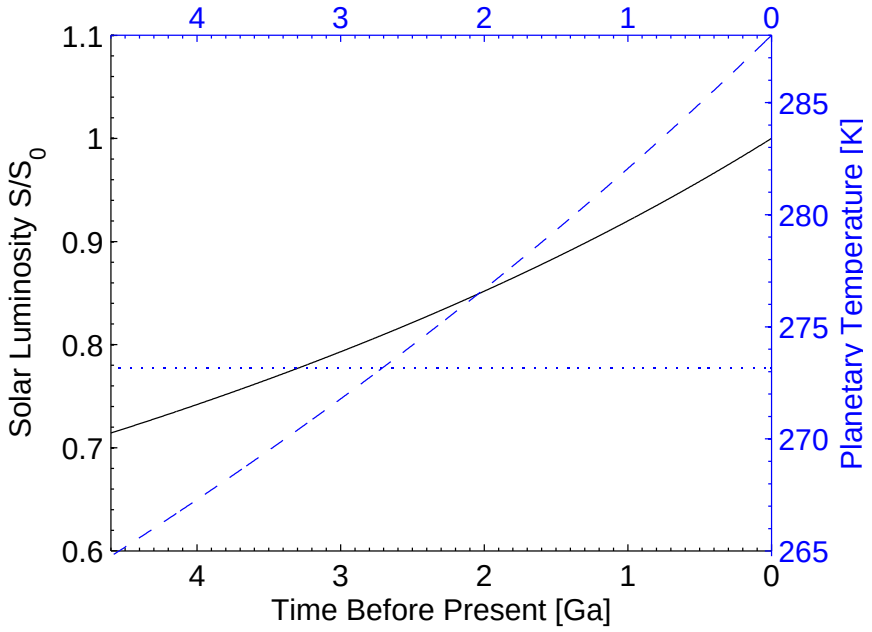

Figure 2.2: Illustration of the Faint Young Sun paradox. The black line shows the evolution of the solar constant (the left axis), while the blue line shows the planetary temperature (the right axis) computed from the simple energy balance of the planet (2.2). The dotted blue line indicates the freezing point of water.

evolution should, all other things being equal, influence the conditions on Earth considerably, since the Sun acts as energy source to climate. Let us consider a simple zero-dimensional energy balance for our planet. Here, the (effective) temperature T of the planet is determined by balancing the incoming shortwave radiation R_{in} and the outgoing longwave radiation R_{out}:

$$\overbrace{\frac{S}{4}\left(1-\alpha_p\right)}^{R_{\text{in}}} = \overbrace{g\sigma T^4}^{R_{\text{out}}}, \tag{2.2}$$

where α_p is the planetary albedo, measuring how much of the incoming radiant energy that is reflected back to space, g the planetary emmisivity, measuring the deviation of the planet from a perfect blackbody, and σ the Stefan-Boltzmann constant. This equation is explained in greater detail in chapter 4. For now, we will just use it to compute an estimate of the planetary temperature in face of the increasing solar constant over time. This is illustrated by the blue line in figure 2.2, showing the planetary temperature as function of time, as computed from the energy balance (2.2). Here, we

have assumed a temperature of 15°C for present day $t = 0$. The relation (2.2) indicates that, everything else being equal, a 25% reduction in S, as is found at $t = 3.8\,\text{Ga}$, should be accompanied by a $1 - \sqrt[4]{1 - 0.25} \approx 7\%$ reduction in T in order to maintain the radiative balance of the planet. With present day surface temperature of 15°C this corresponds to an early surface temperature of some −5°C at $t = 3.8\,\text{Ga}$. These simple calculations assumes that the albedo α_p and the emmisivity g have not changed with time. This, of course, is highly unrealistic, and we should thus not give the exact values of the calculations *too* much weight. Nevertheless, from these simple considerations, we would expect early Earth to have been a chilly globe partially covered in ice. As discussed above, however, geological evidence suggests otherwise. This apparant inconsistency between the expected cold conditions from simple theoretical considerations, and the actually observed warm conditions with only few, shorter extreme glaciations, as inferred from geological findings, has been dupped the *Faint Yong Sun paradox*, or simply the FYS paradox. So, how is this enigma solved? Let us assume that the geological observations are indeed true. Then the FYS paradox must be resolved by rejecting some of the assumptions made in the simple theoretical considerations. The energy balance demonstrates where to look for potential solutions of the FYS paradox, see also [*Shaviv*, 2003].

The first option is that the solar constant S on early Earth was actually *not* less than today. This could be accomplished if the mass of the Sun was higher by ∼10%, which would have made the young Sun at least as luminous as today. Increased mass ejection, i.e. stronger solar winds, should then have caused the Sun to loose its additional mass over time. This explanation contradicts with standard models of stellar evolution, making the hypothesis less tenable.

A somewhat more appealing possibility is that a lower planetary albedo on early Earth counteracted the dimmer Sun. Such changes in planetary albedo could be due to changes in cloud-cover. This mechanism could be linked to stronger solar winds of the young Sun which would have blocked more cosmic rays from hitting the Earth. With less cosmic rays penetrating the atmosphere, the hypothesis says, formation of cloud condensation nuclei was lowered, and the amount of cooling clouds therefore decreased [*Shaviv*, 2003]. Assuming a solar constant S of some 75% of its present value, we see from the energy balance equation (2.2) that in order to maintain a temperature equal to the present day value, $(1 - \alpha)$ must be increased by a factor of $1/0.75$. Assuming a present day planetary albedo of ∼0.3 this explanation thus demands that the planetary albedo is decreased to ∼0.05. This is an unrealistically low value.

Finally the FYS paradox can be resolved by a decrease in the outgoing long-wave radiation R_{out} on early Earth to counteract the dimmer Sun. This is accomplished by an intensified greenhouse effect as a result of increased contents of greenhouse gases. Several agents have been proposed, among

these most importantly carbon dioxide CO_2 and methane CH_4. The exact concentrations of greenhouse gases needed to compensate for the fainter Sun back in time vary from model to model. One scenario, in which a fainter Sun with $S/S_0 = 0.8$ is compensated by greenhouse warming, is with CO_2 concentrations increased by a factor of $\sim$10 and CH_4 concentrations increased by a factor of $\sim 10^4$ as compared to present day values [*Pavlov et al.*, 2000]. Such concentrations, the authors hold, are not unrealistic. This could happen as methanogenic bacteria would have given of CH_4 as a byproduct of their metabolism. This hypothesis of the long-term climate variations primarily determined by changes in greenhouse effect is the path that will be followed in this thesis. The primary focus of our work is related to the effects of CO_2; the explanation of the Faint Young Sun paradox due to methanogenic bacteria and CH_4 is not investigated; in the discussion in chapter 7, howvere, a brief link to the effects of CH_4 is made.

2.1.2 Snowball Earth Events

Although surface temperatures on Earth seem to have been above freezing for most of the time through Earth's history, this is not the entire truth of the climatic evolution of our planet. Various geological evidence exist for the existence of a number of extreme glaciations of the Earth during its $\sim$4.5 Ga history has happened. This evidence strongly indicates that most of Earth's surface was covered in ice and snow during these events, and surface temperatures on Earth in such periods would have been on the order or -50 K [*Hoffman and Schrag*, 2000]. The areal extent of the ice cover is somewhat debated. Some theories suggest that the glaciation was global and ice and snow thus covering Earth's surface from poles to equator—this is termed by the socalled *Snowball Earth*. Other theories suggest that equatorial regions might have had open oceans—this is termed by the socalled *Slushball Earth*. This latter scenario provides life with a habitat to survive such extreme climatic happenings [*Hyde et al.*, 2000]. The estimated temporal spans of these extreme glaciations are, however, small compared to the age of our planet, with some estimated durations on the order of $\sim$10Ma [*Hoffman et al.*, 1998].

There are, as mentioned above, geological evidence of several of such extreme glaciations, see figure 2.1. The first could have occured at $\sim$2.9 Ga in the mid-Archean; this is, however, a less well-established glaciation [*Kasting and Ono*, 2006]. More certain evidence exists for the socalled Palaeoproterozoic glaciations around 2.45–2.2 Ga [*Kopp et al.*, 2005]. This is likely three distinct glaciations, and these seem to appear at the same time as a marked rise in the atmospheric content of oxygen to place, the socalled *Great Oxidation Event*, see e.g. [*Goldblatt et al.*, 2006] and [*Kasting*, 2006]. The latest extreme glaciations are believed to have happened around 750–600 Ma. Here, it seems that up to 4 distinct glaciations took place. These

are the socalled Neoproterozoic glaciations [*Hoffman et al.*, 1998]. Also indicative of these glaciations around 750–600 Ma are large variations in the carbon isotope signal (see below) that indicate that biological production varied between extreme values [*Hoffman and Schrag*, 2000]. In this thesis we will focus our attention on these latest glaciations.

If we assume the FYS paradox from above to be resolved by some of the aforementioned mechanisms, then the existence of such extreme glaciation events poses a new puzzle to palaeoclimatology: The questions are now what could caused them, how were they terminated, and why were they only relatively brief events?

We can imagine different scenarios that explains the occurence of the extreme glaciations. One possibility is, again, that the planetary albedo was temporarily increased by some mechanism which would have caused the glaciation. The cosmic ray–cloud theory, as mentioned in relation to the FYS paradox above, again offers an explanation [*Shaviv*, 2003]. Varations in the cosmic ray flux due to variable star formation rate ion the galaxy are, the theory states, temporally correlated with the appearance of the glaciations. Increased flux of cosmic rays caused cloud cover and thus planetary albedo to increase. Meteorite impacts or extreme volcanic erruptions could likewise be thought to have ejected large amounts of aerosols into the (upper) atmosphere. These could then, as cloud consation nuclei, have caused cloud cover and thus planetary albedo to increase [*Bendtsen and Bjerrum*, 2002].

The other likely explanation of the initiation of the glacations is a natural extension of the idea of the greenhouse effect forming Earth's climate, and this is the path that is followed in this thesis. In this view, some mechanism served to deplete the atmosphere of the greenhouse gases that were responsible for keeping surface temperatures high in the first place. This weakening of the greenhouse effect would then have forced the Earth into the extreme glaciation. For the Neoproterozoic glaciations, this 'some mechanism' responsible for the collapse of the greenhouse atmosphere could, as we shall see in this thesis, be biospheric in origin. As for how the glaciations were terminated in this greenhouse view, there seems to be only one way out of it, namely through the build-up of a CO_2 hothouse. This is pointed out in greater detail later in this thesis.

It should be stressed that the explanations of the palaeoclimatic issues above are subjected to debate. Furthermore, the explanations presented are not always mutually exclusive.

2.2 Evolution of Life

The biosphere is the planet's living organisms. It acts a component of the climate system, interacting with the ocean and atmosphere, as we shall see

in chapter 4. This justifies that climatic history of our planet should be seen together with the biospheric evolution.

Only a few points will have our attention. The first is the timing of the first appearance of life on Earth. *Nisbet and Sleep* [2001] present a nice review on Earth's early life. The earliest geological indications of the presence of life on Earth are from early Archaean ∼3.8 Ga. This somewhat debated line of evidence is based on carbon isotopes in rocks found in Greenland. Fractionation of carbon isotopes is an important indicator of biology at work. In the process of oxygenic photosynthesis, the Rubisco enzyme captures the C from the CO_2 molecule in the surrounding atmosphere/ocean. Rubisco preferentially selects the lighter ^{12}C isotope over the heavier ^{13}C in this process. Organic material is therefore enriched in the lighter ^{12}C isotope, while inorganic carbonate is enriched in the heavier ^{13}C. $\delta^{13}C$ in inorganic carbonate rocks is thus a practical, quantitative measure of the biosphere. When this shows an enrichment in ^{13}C, it is indicative of the presence of life. Less debated isotopic fingerprints of biology are from the Mid-Archaean ∼3.5 Ga. In general, there is strong reasons to believe that microbial life, including photosynthetic plancton, existed in the Mid-Archaean. Methanogens, bacteria that give of CH_4 as a byproduct of their metabolism, could as well have been an important part of the early biosphere, as proposed in e.g. [*Kasting*, 2004].

The second point is the timing of the colonization of land. The Precambrian super-eon and the Phanerozioc eon are separated by the socalled Cambrian explosion at ∼550 Ma. At this point in history, a marked diversification of life is observed from the geological findings. The first shelly fossils dates from this time. There is a temporal correlation between this Cambrian explosion and the Neoproterozoic glaciations mentioned above. Land plants appeared somewhat after this Cambrian explosion. Indisputable fossil evidence of the colonization of land by plants first appears at ∼480–460 Ma, although indications exist for a somewhat earlier colonization at ∼700 Ma [*Heckman et al.*, 2001]. Prior to the colonization of land, life was confined to the ocean. Complex, multicellular life appeared after the Cambrian explosion.

Both of the above points of the biospheric evolution has important implications on climate since it affects the carbon cycle, as we shall see later.

2.3 Outlook and Summary

Let us, before we sum up the above short history of Earth, end this motivation with a brief outlook towards other planets. Surface temperatures on Earth has allowed life to develop and thrive, although large variations have occured. Our planet is the only planet in the Universe known to harbor life. When we look at our closest terrestrial neighbors, Mars and Venus, the *cli-*

matic fate of our planet is also strikingly different. Venus is a hothouse with a mean surface temperature of $\sim$460°C, whereas Mars a freezer with mean temperatures around -50°C. Part of the climatic difference between Earth, Venus and Mars, of course, is simply due to the difference in distance to the Sun. This locates Earth within the habitable zone of the Sun. However, the difference is also attributable to the different fates of the greenhouse effects on the planets. If we turn our attention beyond our own Solar System, several extrasolar planets orbiting distant stars have been found within recent years, and this number will naturally increase as the search continues. The extremely interesting question is whether habitable planets exist somewhere in the Universe, and, ultimately, if some of these planets could be harbouring life? The scientific hope is to be able to perform a spectral analysis on some of the extrasolar planets within a not too distant future, in order to reveal the atmospheric composition on the planets [James F. Kasting, personal communication]. This could serve as a way of detecting life, with the strongest indicators for life being considerable amounts of oxygen or methane (actually perhaps just an atmosphere whose state is far from chemical equilibrium).

Returning to our own planet, the evolution of Earth's climate over geological timescales is dominated by two main puzzles: 1. The fact that surface temperatures were probably similar to, or perhaps even higher than, present day values most of the time, despite a considerably less luminous Sun (the Faint Young Sun paradox), and 2. The existence of few geologically brief extreme glaciations, possibly of global extent (the Slushball/Snowball Earth events). Parallel to this is the evolution of life with life dating far back in Earth's history.

3 Daisyworld

We will now move on to present the other motivating aspect of the current study. This relates to the Daisyworld model of the climate-biosphere relation.

Daisyworld represents a quantitative foundation for the socalled *Gaia* theory. Gaian theory is based on a hypothesis that all parts of the surficial system of Earth, both the living biosphere and its non-living environment (atmosphere, oceans, soil, rocks), interacts to form a complex system that, to some extent, can be viewed as one single organism, Gaia [*Lovelock*, 1991]. Depending on to what extent the biosphere affects its surrounding to its own benefit, different degrees of Gaia can be used, see e.g. the discussions on Gaia by *Volk* [2002]; *Kleidon* [2002]; *Lenton* [2002]; *Kirchner* [2002]. *Weak* Gaia merely states that the biosphere affects its environment, whereas *strong* Gaia holds that the biosphere alters its environment in such a way that it optimizes its own conditions. In any case, Gaian theory sees the history of Earth as a co-evolution of life and its environment, including Earth's climate.[1]

Daisyworld was originally formulated by *Watson and Lovelock* [1983] as a theoretical example of a simple biological system that regulates its environment without Darwinian natural selection. Daisyworld has since been reviewed several times, see e.g. [*Saunders*, 1994; *Lenton*, 1998]. Below, we will present the fundamentals of Daisyworld, redo the calculations of *Watson and Lovelock*, and review it as a conceptual climate-biosphere model. As will be evident, we present some slightly different results and a somewhat different view on the homeostatic effect of the biosphere, as suggested previously. Daisyworld is a natural starting point for doing conceptual modeling

[1] Although Gaian theory can be seen as a strictly scientific discipline, there is a strong glow of philosophy over it. We shall only deal with the scientific part.

of the interactions between climate and biosphere. From a practical point of view, this section will simultaneously serve to introduce the notation of feedbacks within the framework of *model diagrams*, to illustrate the methods of linear stability analysis, and to introduce stochastic dynamics in a simple model.

3.1 Life and Climate on Daisyworld

Daisyworld is an imaginary, terrestrial planet, inhabited by a very simple biosphere, consisting of only two plant species: black and white daisies. These daisies differ only in the color of their flowers. Areas covered with white daisies have a higher albedo and therefore reflect a larger portion of the incoming radiation from the nearby Sun-like star than areas with bare ground. Likewise, areas covered with black daisies have a lower albedo and therefore reflect a smaller portion of the incoming radiation. Thus, the planetary albedo is controlled by the areal extent of daisies. The growth rate of the daisies is determined by the surface temperature of their surroundings. The climate of Daisyworld, as parameterized by the effective temperature of the planet (and thus also the surface temperature), is controlled by the luminosity of the star and the planetary albedo, through the overall energy budget of the planet, which balances the incoming shortwave solar radiation and the outgoing longwave radiation; the greenhouse effect on the planet is assumed to be irrelevant. With the effective temperature set by the planetary albedo, the planetary albedo by the areal extent of daisies, and the growth of the daisies, in turn, by the surface temperature, a simple climate-biosphere feedback mechanism exists on Daisyworld.

3.1.1 Governing Equations

Daisyworld is a simple mathematical model of the coupling between biology and climate. The equations are briefly presented below, please refer to [*Watson and Lovelock*, 1983] for a more detailed motivation of these.

The prognostic variables in Daisyworld are the areal cover of the two types of daisies, a_w and a_b, measured as fractions of the total planetary area, i.e. $a_w, a_b \in [0, p]$, where $p \leq 1$ is the fertile area of Daisyworld. The governing equations for these are written as:

$$\frac{da_i}{dt} = a_i \cdot \left(a_{\text{bare}} \cdot U_{\text{growth}} - \gamma \right), \tag{3.1}$$

where the index i designates the type of daisy: white w and black b. The temporal derivative of the areal cover of daisy of type i, $\frac{da_i}{dt}$, is controlled by the growth rate function U_{growth}, the areal cover of uninhabitated, fertile ground a_{bare} on the planet, plus a constant death rate term γ. The areal cover of uninhabitated, fertile ground a_{bare} depends on the the areal cover of

daisies, a_w and a_b, and the growth rate U_{growth} depends on the local surface temperature of colonized areas, T_{s}^i. The local surface temperature T_{s}^i, in turn, is assumed to depend on the planetary albedo A_{p} and the effective temperature of the planet T_{eff}. A_{p} depends on the areal cover of daisies, a_w and a_b, and lastly T_{eff} is set by the planetary albedo A_{p} and the solar constant S via the global energy balance. The solar constant S is taken to be the forcing model parameter. The uncolonized area a_{bare}, the growth function U_{growth}, the local surface temperatures T_{s}^i, the planetary albedo A_{p}, and the effective temperature T_{eff} are parameterized by the following diagnostic relations:

$$
\begin{aligned}
p &= a_{\text{bare}} + a_w + a_b && (3.2)\\
U_{\text{growth}} &= 1 - \mu(T_0 - T_s)^2 && (3.3)\\
T_{\text{s}}^i &= T_{\text{eff}} + q(A_p - A_i^T) && (3.4)\\
A_{\text{p}} &= a_w A_w + a_b A_b + (1 - a_w - a_b)A_g && (3.5)\\
\sigma T_{\text{eff}}^4 &= \frac{S}{4}\big(1 - A_{\text{p}}\big) && (3.6)
\end{aligned}
$$

In equation (3.2), p is the fertile area of Daisyworld. $\mu > 0$ in equation (3.3) describes the sensitivity of the growth function to surface temperature T_s. This growth function is assumed to be a parabola which has a maximum at $T_s = T_0$ and vanishes at $T_s = T_0 \pm \mu^{-1/2}$. In equation (3.4), A_w^T and A_b^T are 'surface temperature determining albedo parameters' of white daisies and black daisies, respectively, and q describes the degree of heat redistribution on Daisyworld's surface. A_w^T, A_b^T and q are chosen such that regions with white daisies are cold with a temperature *less* than the effective temperature, and regions with black daisies are warm with a temperature *greater* than the effective temperature. A_w, A_b, and A_g in equation (3.5) are the albedos of white daisies, black daisies and bare ground, respectively, and these are chosen such that $A_b < A_g < A_w$. In the global energy balance equation (3.6), σ is the Stefan-Boltzmann constant. The physical and biological constants and model parameters are listed in table A.1 in appendix A.3.

3.1.2 Model Diagram and Feedbacks

A frequently used method to depict the qualitative characteristics of a simple model is by use of a model diagram, or systems analysis diagram, see e.g. [*Beerling and Berner*, 2005] and [*Berner*, 2003]. In figure 3.1, the model diagram for Daisyworld is depicted, showing the variables of the model and their causal relationships.

The arrows in figure 3.1 show the causal relationships within the model. $x \multimap y$ indicates that y is functional dependent of x, except when y is a prognostic variable, in which case the *time derivative* of y, $\frac{\partial y}{\partial t}$, is functional dependent on x. Also indicated at each arrow is the possible sign(s) that $\frac{\partial y}{\partial x}$

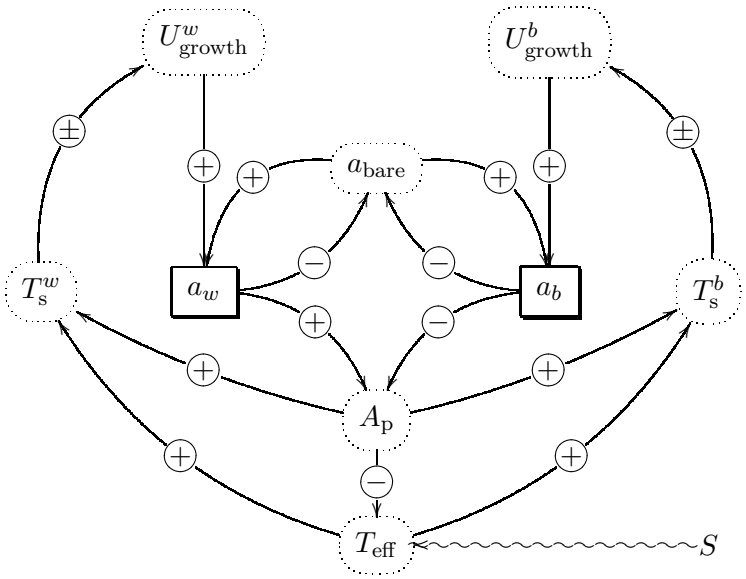

Figure 3.1: Model diagram of Daisyworld. Solid boxes represent prognostic variables, while dotted boxes represent diagnostic variables. Arrows indicate causal relationships between variables (see text for further explanations).

can take on for $a_w, a_b \in [0, p]$ with the model parameters used in [*Watson and Lovelock*, 1983] version I. These are easily computed from equations (3.1)-(3.6).

Each pathway from one prognostic variable to another, when following the direction of the arrows, defines an *interaction* between these. The daisy populations interact both via the uncolonized area, reflecting a biological constraint from competition on resources (here, space), and via the albedo-temperature, reflecting a climatically mediated constraint.

A pathway starting and ending at the same prognostic variable defines a *feedback loop* for the variable. Note that feedbacks, in the sense of being characterized with respect to both stability and sensitivity, are only defined for prognostic variables, see e.g. the discussion of feedbacks in climate theory in [*Bates*, 2007]. The sign of a single feedback loop operating via diagnostic variables can be inferred from the product $\prod_i \frac{\partial y_i}{\partial x_i}$, where i runs over the arrows along the loop. To see this, let us assume that the system resides in a steady state a_j^* such that $\frac{da_j}{dt}\big|_{a_j^*} = 0$. We now pertube one of the daisy covers a_j by a small amount δa_j such that $a_j = a_j^* + \delta a_j$. We then wish to determine the response in a_j due to a given feedback loop in figure 3.1 that operates on a_j via diagnostic variables. A simple Taylor expansion to first order shows that the pertubation $\delta a_j = a_j - a_j^*$ away from the steady state

a_j^* evolves according to:

$$\frac{d(\delta a_j)}{dt} = \frac{da_j}{dt} \approx \frac{da_j}{dt}\Big|_{a_j^*} + \left[\prod_i \frac{\partial y_i}{\partial x_i}\right] \delta a_j = \left[\prod_i \frac{\partial y_i}{\partial x_i}\right] \delta a_j, \tag{3.7}$$

where, again, i runs over the arrows along the feedback loop. The product $\prod_i \frac{\partial y_i}{\partial x_i}$ arises from differentiating according to the chain rule along the loop. The solution to equation (3.7) is easily seen to be

$$\delta a_j(t) = \delta a_j^0 \exp\left(\prod_i \frac{\partial y_i}{\partial x_i} \cdot t\right), \tag{3.8}$$

where δa_j^0 is the intial pertubation at $t = 0$. If $\prod_i \frac{\partial y_i}{\partial x_i} < 0$, then the pertubation falls off exponentially with time and a_j approaches the steady state a_j^*, meaning that the feedback loop is negative. If $\prod_i \frac{\partial y_i}{\partial x_i} > 0$, then the pertubation increases exponentially with time and a_j is forced away from the steady state a_j^*, meaning that the feedback loop is positive. Multiple simple feedbacks loops can combine as either parallel or serial loops.

Let us for simplicity assume that only black daisies exist in order to point out the possible feedbacks in figure 3.1. The black daisies are subjected to a simple negative feedback loop via $a_b \to a_{\text{bare}} \to a_b$, and two parallel climatic feedback loops. The sign of these two feedbacks operating via the albedo-temperature depends on the local surface temperature, i.e. the location in the (a_w,a_b) phase space. This is because of the peaked growth-to-temperature relation, such that $\frac{\partial U_{\text{growth}}}{\partial T_{\text{s}}} > 0$ for $T_{\text{s}} < T_0$ and $\frac{\partial U_{\text{growth}}}{\partial T_{\text{s}}} < 0$ for $T_{\text{s}} > T_0$. For $T_{\text{s}} < T_0$, e.g., the black daisies are subjected to a positive feedback loop via $a_b \to A_{\text{p}} \to T_{\text{eff}} \to T_{\text{s}}^b \to U_{\text{growth}}^b \to a_b$ and a parallell negative feedback loop via $a_b \to A_{\text{p}} \to T_{\text{s}}^b \to U_{\text{growth}}^b \to a_b$. These are reversed for $T_{\text{s}} > T_0$.

To illustrate these feedbacks in words, assume that a small population of black daisy plants has been put on Daisyworld and that the temperature T_{s} is just above the temperature at which the daisies can grow, but still such that $T_{\text{s}} < T_0$. When the daisies reproduce and spread, the increased cover of black daisies means that there is less room for the plants to thrive, which in turn decreases growth rates, causing the cover of daisies to retreat. This is the negative feedback mechanism. However, as the original black daisy population reproduces and spreads, the planetary albedo is lowered, making the effective temperature and subsequently also surface temperatures higher, and hence the growth rate of black daisies increases, causing the cover of daisies to expand. This is the positive feedback mechanism. These mechanism act to change the cover of black daisies with time. When, or if, a state is reached where negative feedbacks dominate positive feedbacks, the cover of daisies settles into a stable steady state.

Equivalent loops exist for white daisies in a Daisyworld inhabited only by white daisies. When both types of daisies are allowed in Daisyworld, more and longer feedback loops arise. As we shall see below, the peaked growth-to-temperature curve, along with the assumptions that black daisies affect climate by warming their surroundings, while white daisies cool their surroundings, are crucial for the homeostasis of Daisyworld.

It should be emphasized that the key to the model behaviour lies in the governing equations (3.1) and the parameterizations (3.2)-(3.6), i.e. the mathematical formulations of the arrows in the model diagram of figure 3.1, and cannot be deduced from the figure alone. Only the signs, and not the magnitudes, of the interactions and feedbacks can be displayed in such a diagram.

3.2 The Homeostasis of Daisyworld Revisited

Let us, using a more quantitative approach than above, examine the response in the system's steady states to an increasing solar luminosity S with time. We will use the model parameter values from the two versions of Daisyworld in [*Watson and Lovelock*, 1983] (see apendix A.3), thus following the path that led them to the homeostatic parable of Daisyworld, for both versions (see also the analysis in [*Saunders*, 1994]). The homeostatitic results of *Watson and Lovelock* [1983] are seen as a (more or less) constant response in effective temperature to the increasing solar luminosity for the biotic planet, or alternatively just as a numerically smaller response for the biotic planet than for the *abiotic* planet.[2]

The task is, for a given solar luminosity, to find the steady states of the system. Let us write the governing equations as:

$$\frac{da_w}{dt} = F_w(a_w, a_b) \tag{3.9}$$

$$\frac{da_b}{dt} = F_b(a_w, a_b) \tag{3.10}$$

The governing equations define a set of autonomous, non-linear, first order ordinary differential equations. The steady states of the system are found by solving $F_w(a_w^*, a_b^*) = F_b(a_w^*, a_b^*) = 0$ for a_w^* and a_b^*. The steady state solutions of Daisyworld can be separated into four different types: the *abiotic* state $a_w = a_b = 0$ is easily recognised as a (trivial) solution. Assuming $a_w > 0$, $a_b = 0$ yields the *white-only biotic* solution, while taking $a_b > 0$, $a_w = 0$ yields the *black-only biotic* solution. Lastly, taking both $a_w > 0$, $a_b > 0$ gives us the *biotic* type of solution. Please see A.3 for further details.

Once the fixed points are established, the stability of these can be found by performing a linear stability analysis. This procedure was outlined in the

[2] In analogy to, e.g., the constant response in the temperature inside the human body to the varying outer conditions.

above discussion of the sign of feedbacks, only in one dimension however. In more dimensions we need to consider the *Jacobian matrix*, see e.g. [*Strogatz*, 1994]. The Jacobian matrix of the system (3.9)-(3.10) is given by:

$$\mathbf{J} = \frac{\partial F_i}{\partial a_j} = \begin{bmatrix} \frac{\partial F_w}{\partial a_w} & \frac{\partial F_w}{\partial a_b} \\ \frac{\partial F_b}{\partial a_w} & \frac{\partial F_b}{\partial a_b} \end{bmatrix}. \tag{3.11}$$

This is computed by inserting the parameterizations (3.2)-(3.6) and finding the deratives using the chain rule. Using the Jacobian matrix (3.11), the governing equations can be linearized around the fixed points. This method is described in appendix A.2.

The stability of a given fixed point in phase-plane, i.e. 2D phase space, can then be inferred from the eigenvalues of the Jacobian matrix evaluated in the fixed point (see again appendix A.2). These eigenvalues are in general complex numbers. Three robust cases exist: If the real parts of both eigenvalues are negative then the fixed point is stable (an attractor or sink). If the real parts of both eigenvalues are positive then the fixed point is unstable (a repeller or source). A saddle has one positive and one negative eigenvalue. In addition to these are two marginal cases: If both eigenvalues are purely imaginary, then the fixed point is a center. Finally, if at least one eigenvalue is zero, then the fixed point is non-isolated. The characterisation of the stability of a fixed point from linearization is only problematic for the marginal cases. As long as the linearization predicts the fixed point to belong to one of the robust stability cases, then the fixed point really *does* belong to this case.

Fixed points in the phase-plane can be classified into different types, characterising the geometry of the trajectories in phase-plane near the fixed point: nodes (purely real eigenvalues), spirals (complex eigenvalues with non-vanishing real parts), saddle points, stars, and degenerate nodes occur among the robust stability cases. Centers and non-isolated fixed points are the marginal stability cases. The characterisation of the type of a fixed point from linearization of the original system can be corrupted from small nonlinear terms. However, as long as the linearization predicts a node, a spiral or a saddle, then the fixed point of the original system really *is* a node, a spiral or a saddle.

3.2.1 Daisyworld I

In the following, we will use the model parameters values of the first version of Daisyworld, the one also depicted in figure 3.1. Figure 3.2 shows the phase portrait for three values of solar luminosity S/S_0, S_0 being some reference luminosity. The arrows sketch the phase space velocity field $(\frac{da_w}{dt}, \frac{da_b}{dt})$ from equation (3.1). Filled circles indicate stable nodes, open circles unstable nodes, and open squares saddle points. The solid lines connecting unstable

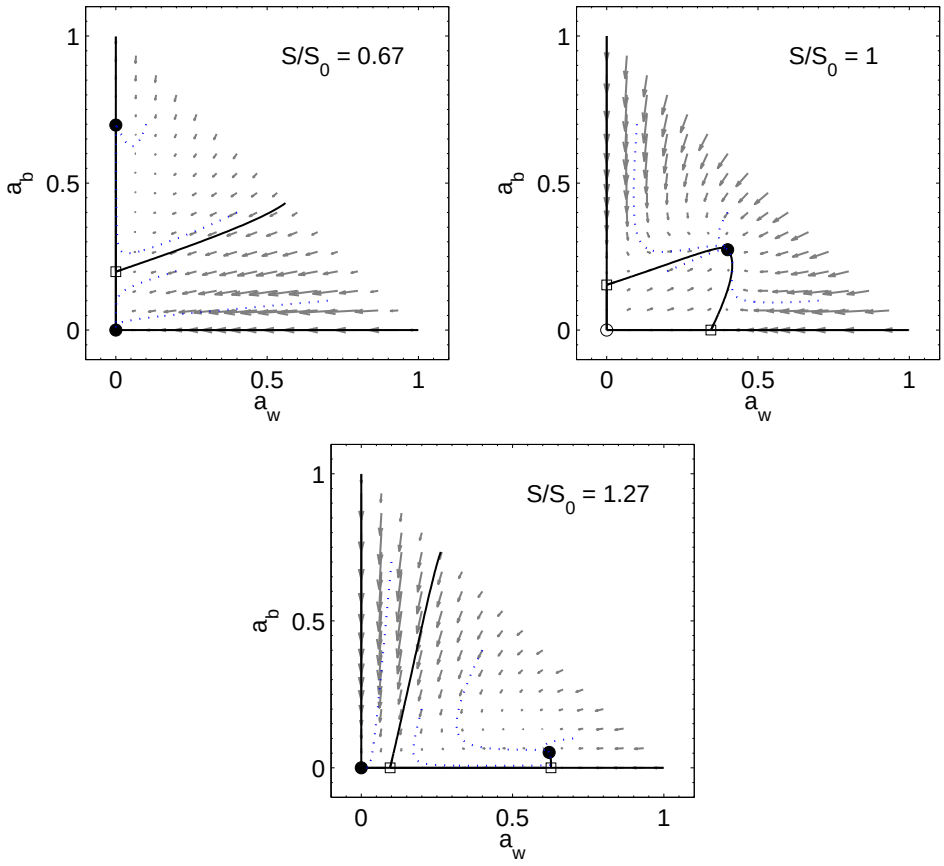

Figure 3.2: Phase portrait of Daisyworld I for three values of S/S_0. The gray arrows sketch the phase space velocity field. The steady states are indicated by markers: Filled circles correspond to stable nodes, open circles to unstable nodes, and open squares to saddle points. Also shown are the trajectories for four random initial conditions (dotted blue lines), and the heteroclinic trajectories (solid black lines).

nodes or saddle points with stable nodes are *heteroclinic trajectories*. These separate the phase space into basins of attraction. The dotted, blue lines sketch trajectories for four random initial conditions.

The response in steady state daisy population when varying the solar luminosity is shown in figure 3.3. Here, the steady state areal cover of the daisies is plotted as function of solar constant S/S_0 for $S/S_0 \in [0.5, 1.7]$. The four panels corresponds to the different types of steady state solution as indicated: no daisies, white-only, black-only, and both types of daisies. Looking at the upper right plot, we see that for low solar luminosities S/S_0, no black-only solution exists. This is because temperatures are too cold due to the small value of S/S_0. When increasing S/S_0, a saddle-node bifurcation is seen to occur, giving birth to a stable (the upper solid line) and an unstable

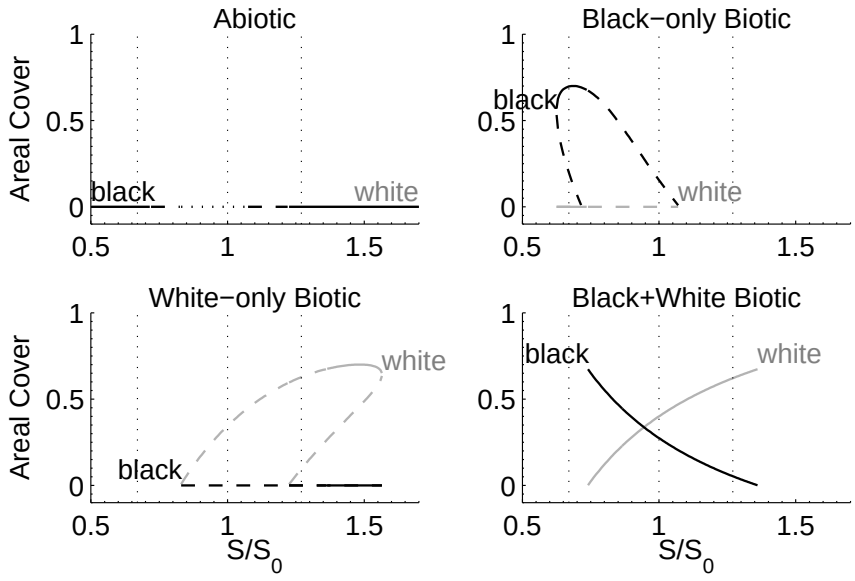

Figure 3.3: Steady state areal cover of daisies as function of solar luminosity for Daisyworld I. Each panel corresponds to the indicated type of solution. The vertical, dotted lines indicate the plots in figure 3.2.

(the lower dotted line) black-only solution. Now a relatively large cover of warming black daisies is capable of making the planet warm enough for the plants to thrive, in spite of the low solar luminosity. As S/S_0 is increased, the stable fixed point evolves into a saddle point, as the full biotic solution is born. However, since the stable manifold coincides with the a_b-axis in phase space, it is possible for the system to reside in the state as long as no white daisies are introduced (i.e. all initial conditions $a_b > 0$, $a_w = 0$ will end up here). This state is maintained by a still smaller and smaller cover of black daisies as S/S_0 increases. Eventually, S/S_0 becomes too high for the black daisies to thrive and still keep temperatures within their limits, and the stable black-only state disappears. A similar bifurcation pattern is seen for the white-only solution in the lower left plot, only now the bifurcations takes places as S/S_0 is *decreased*. This change is simply due to the reversed effect of the white daisies on the planetary albedo, as compared to the black daisies. White daisies are favored by high solar luminosities, since their color can *cool* the planet to habitable temperatures, whereas black daisies are favored by low solar luminosities, since they can *warm* the planet to habitable temperatures. The upper left plot shows that the stability of the abiotic solution changes as S/S_0 varies and other steady states appear. The lower right plots shows that for a large range of S/S_0, a stable steady state exists where both white and black daisies can thrive together.

Now, from these daisy populations, the associated effective temperature T_{eff} can directly be computed. The resulting bifurcation diagram is seen in figure 3.4, showing the steady state T_{eff} as function of S/S_0. This figure

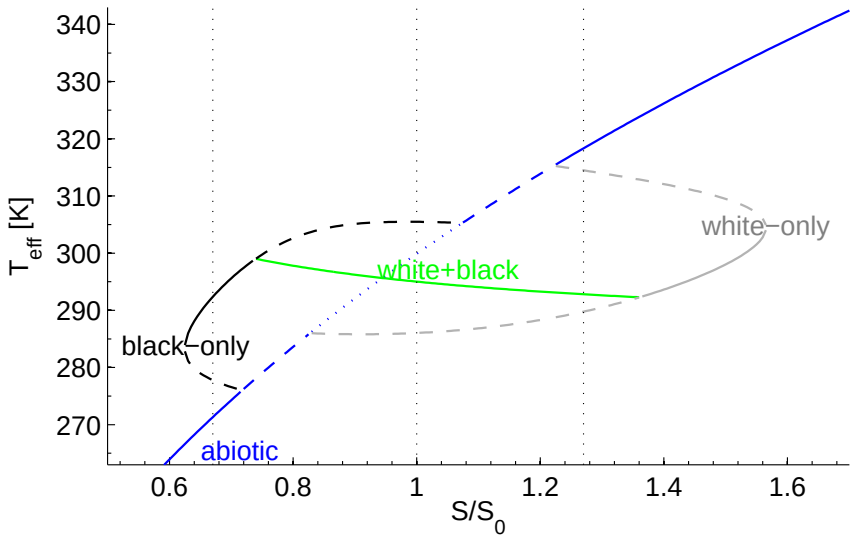

Figure 3.4: Steady state effective temperature as function of solar luminosity S/S_0 for Daisyworld I. The vertical, dotted lines indicate the plots in figure 3.2.

shows the same bifurcations as in the plots of figure 3.3. The blue curve corresponds to the abiotic solution in the upper left plot in figure 3.3, the gray curves correspond to the white-only solution in the lower left plot in figure 3.3, the black curves correspond to the black-only solution in the upper right plot in figure 3.3, and finally the green curve corresponds to the full biotic solution in the lower right plot in figure 3.3

It is now interesting to look at the slope of the curves $\partial T_{\text{eff}}/\partial(S/S_0)$ in figure 3.4. This is a good, first quantitative measure of homeostasis, since this exactly measures the response in effective temperature to changes in solar luminosity. The homeostatic effect on climate of the daisies is then clearly seen as the fact that the absolute value of the slope, $|\partial T_{\text{eff}}/\partial(S/S_0)|$, is, for most values of S/S_0, smaller for the inhabited planet than for the life-less planet. This is true for both the habitable black-only planet (upper black curve), the habitable white-only planet (lower white curve), and the black+white planet (green curve). For the latter, the effective temperature is actually seen to *decrease* in response to the increasing solar luminosity.

The results shown in figure 3.4 are similar to those found in [*Watson and Lovelock*, 1983], except at two points. First is the existence of a black daisy steady state (black line) in the interval $0.62 < S/S_0 < 0.66$. This

solution is not found by the method used by *Watson and Lovelock* [1983].[3] This part of the black-only biotic solution is of particular interest since the response in steady state temperature to an increase in solar constant is actually *larger* than for the abiotic solution, as measured by $|\partial T_{\text{eff}}/\partial(S/S_0)|$ This is in somewhat contradiction with the notion of a purely homeostatic effect of the daisies on the climate of Daisyworld, although, admittedly, is does not change the general picture much. Secondly, both the lower, black-only saddle point branch and the upper, white-only saddle point branch are not shown in [*Watson and Lovelock*, 1983], but since the axis of the non-vanishing variable coincides with the unstable manifold in both cases (as opposed to the upper black-only and the lower white-only branches where it coincides with the stable manifold as mentioned above), these states are not habitable, see also figure 3.2.[4]

3.2.2 Daisyworld II

Now, let us turn to the other version of Daisyworld as described in [*Watson and Lovelock*, 1983]. In Daisyworld II, the darkening effect of the black daisies is changed to a whitening effect, trying to mimic the formation of convective clouds over the warm, black daisies. All other model details are left unaltered. *Watson and Lovelock* [1983] found that only black daisies could flourish in such a world, still with a homeostatic effect on climate. In figure 3.1, the change from version I to version II amounts to a change of sign of the arrow from a_b to A_{p}. The web of feedbacks in figure 3.1 is then, so to speak, symmetric around a central, vertical line between the two types of daisies, but only in signs, not in amplitude. Intuitively, one would therefore expect the two types of daisies to exhibit somewhat similar behaviour. As demonstrated below, it is indeed possible for white daisies to thrive in this version, leading to bistability of Daisyworld II for a range of solar luminosities.

Following the same procedure as in the section above, figure 3.5 shows the phase portrait for three values of S/S_0. Solving for steady state daisy populations when varying the solar luminosity yields the results in figure 3.6. From these, the bifurcation diagram in figure 3.7 is generated, showing the steady state effective temperature as function of solar luminosity. Again, we focus on figure 3.7. The full biotic stable node branch in Daisyworld I (figure 3.4) is seen to have disappeared in Daisyworld II; only a saddle point branch exists in a narrow interval of S/S_0. Also, the saddle-node bifurcation associated with the black-only solution is seen to be oriented in the same way as the saddle-node bifurcation associated with the white-only solution. We note that only the abiotic solution and the lower, stable black-

[3] One would expect their figure 1b to depict a hysteresis loop similar to the one in their figure 1c if the system had also been solved for decreasing solar luminosity.

[4] The results presented here are similar to the results found by *Saunders* [1994].

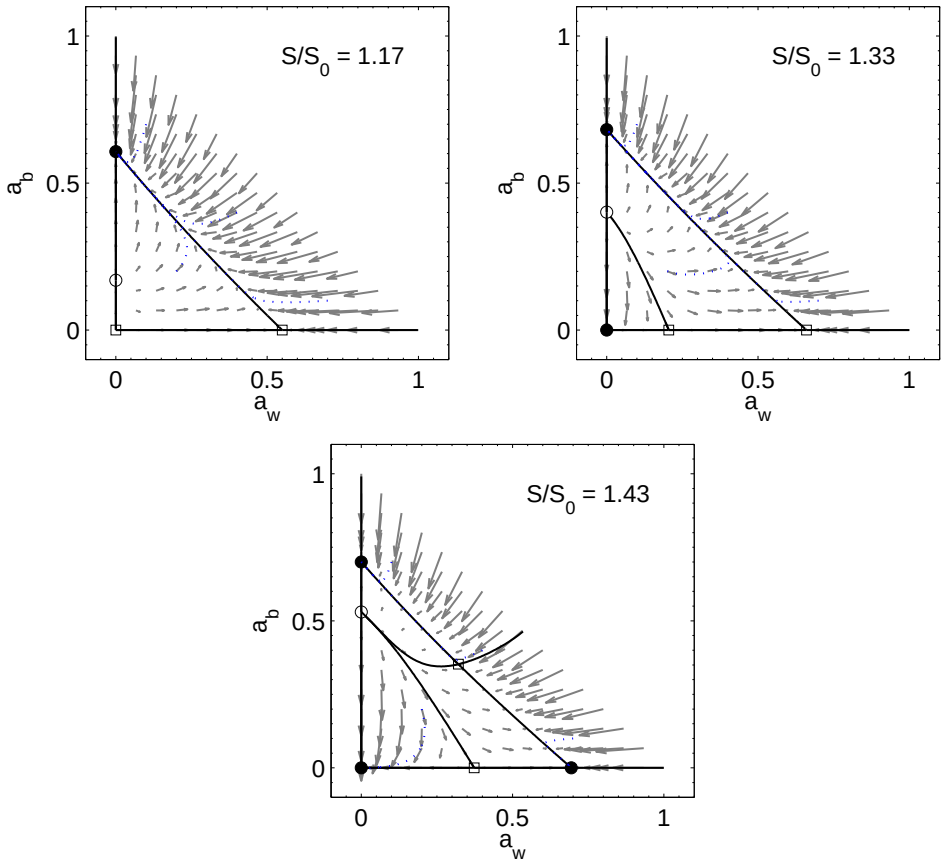

Figure 3.5: Phase portrait of Daisyworld II for three values of S/S_0. The gray arrows sketch the phase space velocity field. The steady states are indicated by markers: Filled circles corresponds to stable nodes, open circles to unstable nodes, and open squares to saddle points. Also shown are the trajectories for four random initial conditions (dotted blue lines), and the heteroclinic trajectories (solid black lines).

only solution are found by the methods used in [*Watson and Lovelock*, 1983]. For the black-only solution, the upper branch is unstable. For the white-only solution, the upper, saddle point branch is not relevant, with the same reasoning as above. However, it is indeed possible for a system comprised of only white daisies to reside in the lower, saddlepoint/stable node branch. The (norm of the) slopes of both biotic curves are in general smaller than the slope of the abiotic, thus still supporting the homeostatic effect of the biosphere as suggested in [*Watson and Lovelock*, 1983]. However, for a range of solar luminosities $1.36 \lesssim S/S_0 \lesssim 1.50$, both the white-only steady state and the black-only steady state are stable (as well as the abiotic state), as is also seen in the lower plot of figure 3.5. The system is thus biotic *bistable*.

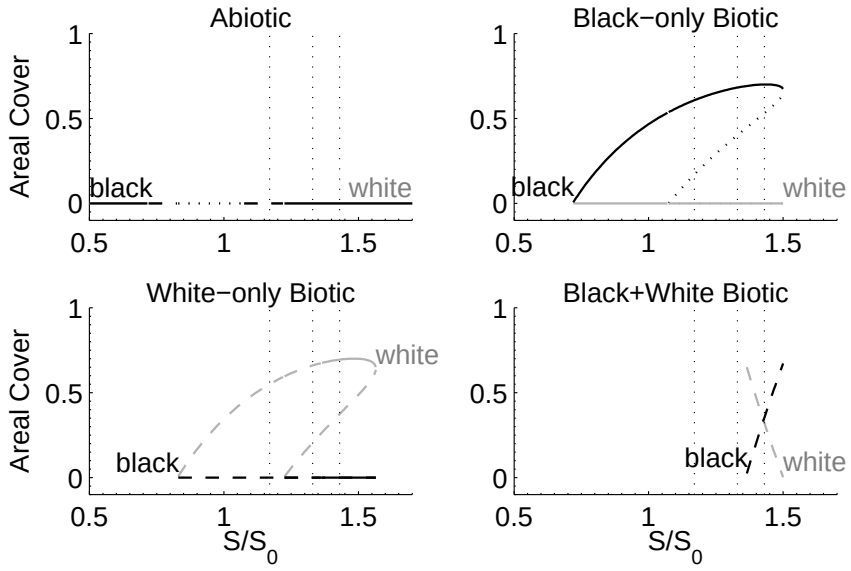

Figure 3.6: Steady state areal cover of daisies as function of solar luminosity for Daisyworld II. Each panel corresponds to the indicated type of solution. The vertical, dotted lines indicate the plots in figure 3.5.

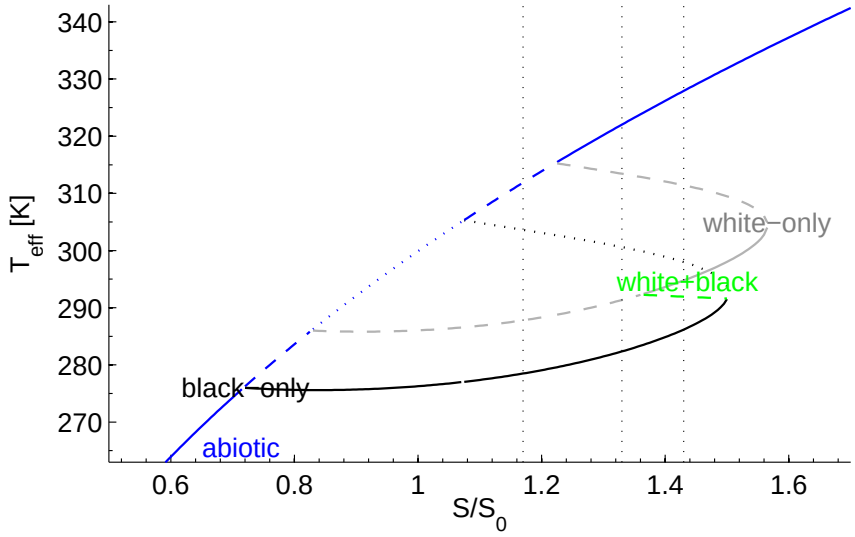

Figure 3.7: Steady state effective temperature as function of solar luminosity S/S_0 for Daisyworld II. The vertical, dotted lines indicate the plots in figure 3.5.

This means that transitions between the two biotic states are possible if the system is subjected to suitable pertubations. A jump between the two biotic

states is associated with a change in effective temperature of up to ∼9K. Such transitions between states are not considered in [*Watson and Lovelock*, 1983], but it surely would be a non-homeostatic phenomenon in Daisyworld. This is discussed in greater detail below.

Also, it obviously seems problematic to claim that the white daisies fail in this modified version of Daisyworld, because they are 'distinctly less fit' than black daisies, as is postulated in [*Watson and Lovelock*, 1983]. White daisies could indeed thrive well in Daisyworld II; the outcome in [*Watson and Lovelock*, 1983] is a mere result of the procedure used to solve the system.

3.3 Discussion of Daisyworld

The critism to Daisyworld as a conceptual climate-biosphere model points in two directions: Firstly, we can critize its conclusions. Secondly, we can critize its assumptions. This is done below.

3.3.1 Bistability and Noise-induced Transitions

When accepting the model assumptions and accepting it as a conceptual model of interactions between climate and life, the homeostatic conclusions drawn by *Watson and Lovelock* [1983] are still somewhat disputable, as outlined above. This is most prominent for the biotic bistability of Daisyworld II, i.e. the existence of both a stable white-only and a stable black-only steady state for luminosities $1.36 \lesssim S/S_0 \lesssim 1.50$. The bistability makes transitions between biotic states possible for luminosities within this range, jumps that are associated with considerable changes in temperature. Such transitions can be induced by noise from both internal and external short-term processes that have not been directly included in the model.

We can envision this by use of the formalism that will be introduced in the next chapter 4. This is based on the Langevin equation (4.2). Let us assume a luminosity of $S/S_0 = 1.43$. To the governing equations (3.1) for a_w and a_b, we then add a white noise term $\sigma\eta$. A realisation of this pertubed system is shown in figure 3.8. On the left, the areal cover of daisies a_w and a_b are plotted as function of time, and on the right, the resulting effective temperature T_{eff} as function of time is sketched. The governing equations have been pertubed by a white noise $\sigma\eta(t)$, where the noise η is assumed to be (normal) Gaussian distributed, and the intensity taken to be $\sigma = 0.5$. This transient model run is performed by numerical integration of the white-noise pertubed governing equations using a fourth order Runge-Kutta scheme. For $t \lesssim 500$, the planet is dominated by black daisies, and T_{eff} fluctuates around the equilibrium state $T_{\text{eff}} \approx 286\,\text{K}$. At $t \approx 500$, the transition takes place, and for $t \gtrsim 500$, the planet is dominated by *white* daisies, with T_{eff} fluctuating around the equilibrium state $T_{\text{eff}} \approx 295\,\text{K}$.

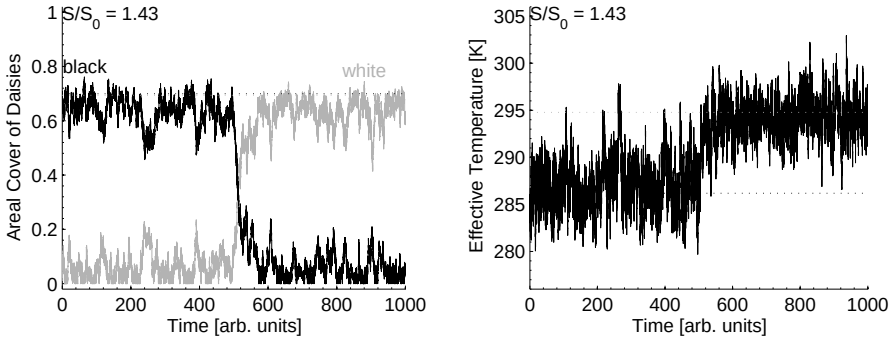

Figure 3.8: A realisation of the pertubed governing equations using a Gaussian white noise for $S/S_0 = 1.43$ in Daisyworld II. Left: Areal cover of daisies a_w (solid gray) and a_b (solid black) as function of time. Also shown, with dotted lines, are the steady state one-species areal covers. Right: Effective temperature T_{eff} as function of time. Also shown, with dotted lines, are the steady state single-daisy effective temperatures.

In figure 3.9, the corresponding trajectory in phase space for the realisation is sketched. The gray line shows the trajectory $(a_w(t),a_b(t))$. Also shown are contour lines of the effective temperature as function of a_w and a_b, and the three steady state solutions. The system sets out from the black-only steady state in the upper left part of phase space, and ends up in the lower right part around to the white-only steady state.

Two points deserves attention. Firstly, before the transition occurs, the black daisies seem to fluctuate around a value slightly less than the steady state value, as seen in figure 3.8. This is because the white daisies fluctuate around a value *larger* than the steady state at zero, since the noise can not pertube the value below this value, only above. This influences the growth of black daisies negatively. And vice versa *after* the transition.

Seccondly, figure 3.8 shows that the transition is more prominent in a_w and a_b than in T_{eff}, as measured by the signal-to-noise ratio. Refering to figure 3.9 this is better understood (see also the phase portrait in the lower plot of figure 3.5). The heteroclinic trajectories that connect the biotic saddlepoint (only shown in figure3.5) with the two stable biotic nodes are, of course, parallel to the unstable eigendirection of the saddle point. This is also the slowest eigendirection of the saddle point. The stable eigendirection, which is then the fastest, is perpendicular to this. This is why the transition takes place along these heteroclinic trajectories; when the system is pertubed it will, so to speak, be dragged onto this line and then slowly pushed away from the saddle point towards one of the stable nodes (a steady state is approached along the slowest eigendirection). For the transition to occur, the noisy pertubations must overcome the slow push away from the

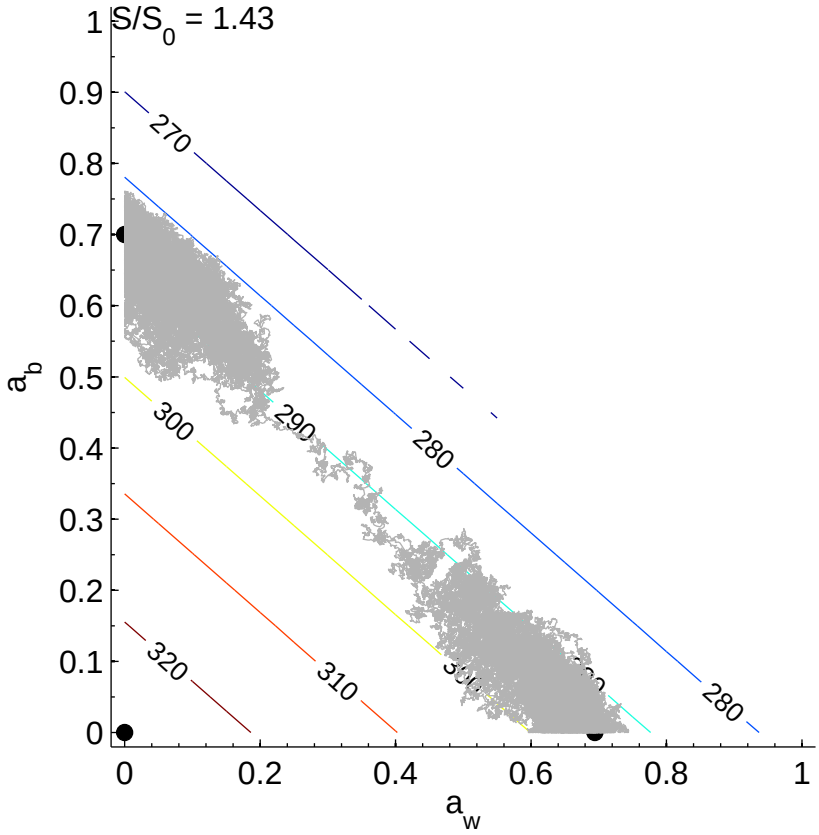

Figure 3.9: Phase space trajectory of a noise-induced transition in Daisyworld II for $S/S_0 = 1.43$. Also shown are contour lines of the effective temperature (in K) and the three stable steady states (filled circles).

saddle point (this could be illustrated by a potential formulation). This path between the two stable biotic nodes is seen to be nearly perpendicular to the gradient in effective temperature T_{eff}, and T_{eff} is therefore only changed modestly during the transition, whereas a_w and a_b change appreceably.

So, from where does the noise that induces the transistion originate? The noise could be initiated on the level of the biosphere, e.g. by variations in nutrient cycles, thereby pertubing daisy growth, or by introducing a new species with a different trait as is done in [*Lenton*, 1998]. The transition could as well be initiated on the climatic level, i.e. in the existing limiting growth factor of the model: a change in the temperature by some new, external factor could drive the system into a different state. This clearly signifies the need to resolve the climatic behaviour in a better way. As we shall see later, this new climate factor should be the greenhouse effect. In any case, this above is a non-homeostatic effect of life.

3.3.2 Planetary Albedo as Biosphere-Climate Coupling

Watson and Lovelock view Daisyworld as a parable, and not a realistic model of our planet. What, then, could be done to make the model more realistic, while still keeping it simple?

In Daisyworld, the interaction between the life and climate operates through albedo properties of different species and their influence on the planetary albedo. It is fair to say that this mechanisms is very unlikely to be responsible for the main features of Earth's climatic evolution over geological timescales, such as solving the Faint Young Sun paradox. This has several strings: Firstly, the daisy mechanism is problematic due to the simple fact that indisputable fossil evidence of plants on the continents first appears at ∼480–460 Ma [*Heckman et al.*, 2001]. The mechanism would then have to be related to oceanic biology. Secondly, the planetary albedo is heavily controlled by a range of other quantities, most importantly clouds, extent of ice and snow, land-ocean distribution, etc. Thirdly, the effective temperature of our planet is not only determined, to a first order, by the planetary albedo, but also by the strength of the greenhouse effect, as determined by the content of greenhouse gases in the atmosphere. As mentioned in chapter 2, if the planetary albedo were to hold the key to the Faint Young Sun paradox, a back-of-the-envelope calculation shows that the 70% reduction in solar luminosity would require a planetary albedo of $A_p \sim 0$ in order to maintain a surface temperature as today, everything else being equal. Although possible, it seems unlikely. If instead we allow the content of CO_2 and CH_4 in the atmosphere to change while keeping the planetary albedo constant, a similar result is reached for much more likely changes in these greenhouse gases.

3.4 Summary

Daisyworld serves as a mathematical foundation for Gaian theory. It is a simple example of a hypothetical biosphere-climate model, in which the biosphere influences the climate. This influence is in most respects a stabilizing, homeostatic effect. As pointed out, however, some details in the model's homeostatic behaviour lack proper treatment, particularly the biotic bistability. In the end, Daisyworld leaves room for improvements on the task of doing more realistic modelling of the interactions betwen climate and biosphere. In the following part of the thesis, an alternative approach is presented.

4 Climate Theory

This chapter presents an introduction to some of the important characteristics and mechanisms of the climate system. These are presented in both qualitative and quantitative contexts. This will serve to motivate the formalism introduced later in the modelling part. First the climate system is defined and different models of the climate system briefly described. After this, the simple energy balence model of the climate is described, followed by a brief qualitative introduction to the carbon cycle, and lastly the biospheric component of climate system is described with focus on the interactions between climate and biosphere.

4.1 The Climate System

The word 'climate' of a given location is often referred to as a temporal average (and perhaps variability) of the weather at that location over some specified periode (e.g. 30 years). Here, weather designates the state of the atmosphere at a given location and time, and involves quantities such as temperature, humidity, precipitation, wind, cloudiness etc.

The climate *system*, however, is traditionally said to consist of five components [*Harvey*, 2000]: atmosphere, oceans, cryosphere (ice and snow), lithosphere (crust, soil, rock etc.), and biosphere (living organisms), in contrast to the one-component definition above. These five components interact with each other through a variety of physical, chemical and biological processes, that let energy and mass flow between them. In addition to these interactions, the climate system is subjected to a number of external forcings, or mechanisms, of which the most important is the input of solar radiation. In this way, the word 'climate' refers to the state of the entire climate system, and climate studies, in their broadest sense, are concerned

with the description and understanding of this system. This is also known as the *Earth System*.

4.2 Models of the Climate System

Models of the climate system come in a great variety of complexity. The complexity of a climate system model is primarily determined by the number of included variables, and the number and nature of the processes and mechanisms that govern the behaviour of the variables. At the top level, GCMs (General Circulation Models) solve the dynamical equations for the atmosphere and oceans numerically: the Navier-Stokes equation on the rotating Earth, the continuity equation, the equation of state, and the thermodynamic equation. This can be coupled to models of other parts of the Earth system to form one single model of the climate system. At the other end of the spectrum we find the simple or conceptual models. This is the regime that we will be working in. Here, the number of variables and processes are kept at a minimum. This makes calculations easier and the model more transparent to draw conclusions from.

4.2.1 Spatial Resolution

The spatial resolution of the variables plays an important role for climate system models as well—both from a physical point of view, and also when it comes to computational complexity. In GCMs, the numerical calculations are performed on three-dimensional spatial grids. In the simplest spatial approach, the components of Earth's climate system, i.e. the atmosphere, oceans, cryosphere and lithosphere, are treated as simple boxes (the biosphere is spatially integrated into these). This is the approach that we will be using. Such a model is spatially zero-dimensional, and all quantities are specified as spatial averages for the box. For the 'real-world' physical observable $O(x, y, z)$ defined in three spatial dimensions (x,y,z), the box model approach considers the spatial mean $\bar{O}$:

$$\bar{O} = \langle O(x, y, z) \rangle_{xyz} = \frac{1}{V} \iiint_{\text{box}} O(x, y, z) \, \mathrm{dx} \, \mathrm{dy} \, \mathrm{dz}. \tag{4.1}$$

where $V = \iiint \mathrm{dx} \, \mathrm{dy} \, \mathrm{dz}$ is the volume of the box. For two-dimensional quantities, such as fluxes into or out of the box, similar spatial averages are carried out over the relevant surface of the box. Things become more complicated when we consider products (or higher order or non-linear terms) of more variables. Then we need to take the mean of the product which in general is not equal to the product of the means, and additional terms must then be parameterized.

4.2.2 Temporal Resolution

Processes within the climate system occur over many different typical timescales, and the temporal resolution of the climate model thus also plays an important role. Large scale variations in the atmosphere, such as the passing of a low-pressure over Denmark, take place with a typical timescale ranging from days to weeks. Variations in the oceans, such as currents, occur with typical timescales from years to centuries. Variations in ice-sheets occur with typical timescales up to millenia. The long-term carbon cycle operates on timescales ranging from hundreds of thousands of years and up, as we shall see below in section 4.4.2.

This span of timescales, covering several orders of magnitude, pose a fundamental challenge to the modelling of the climate system: In this thesis, we wish to model the behaviour of the climate system on geological timescales, i.e. $\sim 10^5$ years and up. We know, however, that many processes exist within the system that operate over timescales much smaller than this, and including these makes the model less transparent and computationally very expensive. One way out of this is through *separation of timescales* [*Ditlevsen*, 2004, chap. 11]. Say we wish to model the behaviour of a given climate variable O and we know that this is governed by processes operating on long timescales τ_1 and subjected to fluctuations from other processes operating on short timescales $\tau_2 \ll \tau_1$. The trick is now to treat the fluctuations from the short timescale processes as noise when writing the governing equation:

$$\frac{dO}{dt} = F(O) + \sigma\eta. \tag{4.2}$$

Here, the first term on the right-hand-side captures the long-term processes while the last term represent an independent white noise $\eta(t)$ with intensity σ, arising from the short-term processes. Equation 4.2 is a simple form of what is known as a *Langevin* equation. This was used in the treatment of the Gaian Daisyworld in chapter 3.

4.3 The Energy Balance Model

In the following, we will let the state of the planet's climate be described by one single variable, the surface temperature T_s of the planet. All other variables and processes within the climate, i.e. the general circulation within the atmosphere and oceans, the precipitation and evaporation, the snow and ice cover, the cloud cover, the surface albedo, and so on, must then be parameterized by T_s. This energy balance model is thus a simple model of the entire non-living part of the climate-system. This type of climate model is inspired by the work of Bodyko and Sellers, who independently introduced such models several decades ago, see e.g. [*Hartmann*, 1994] for a later treatment. In their original formulations, however, a latitudinal

dependence of surface temperature was included, making the models one-dimensional. We shall for the purpose of simplification hold on to the zero-dimensionality.

In the energy balance model, we wish to account for the fluxes of energy into and out of the planet. Designating these fluxes by R_{in} and R_{out}, respectively, and by letting C term the heat capacity of the planet, the rate of change in temperature T_s is given by

$$C\frac{dT_s}{dt} = R_{\text{in}} - R_{\text{out}}, \tag{4.3}$$

where t is time and C the heat capacity of the climate system. Below, the two terms on the right-hand-side of this intuitively simple energy balance equation are explained seperately. The heat capacity C of the climate system in (4.3) describes the thermal inertia of the climate system, and can be approximated by

$$C = \left\langle \int c_p \rho \mathrm{dz} \right\rangle_{xy}, \tag{4.4}$$

where the spatial average $< \ldots >$ is carried out over the horizontal surface over which the radiative fluxes are distributed. The oceans make up the bulk of the planetary heat capacity.

4.3.1 Incoming Shortwave Radiation and the Planetary Albedo

Let us look at the first term on the right hand side of (4.3). The flux of energy received by Earth, of course, originates from the Sun, which is fueled by nuclear fusion of hydrogen into helium, taking place in the stellar interiors. (We neglect the minute geothermal contribution of $\sim$0.8Wm^{-2} to the energy budget of Earth's surface system.) The solar radiation hitting the top of Earth's atmosphere resembles the blackbody emission spectrum for a temperature of $\sim$6000 K, the temperature in the lower surface layers of the Sun, and peaks at a wavelength of $\sim$500nm, see e.g. [*Salby*, 1996].

The total flux of radiant energy at one astronomical unit AU away from the Sun, the average Sun–Earth distance, when integrated over wavelength, is about 1370 Wm^{-2} today, a quantity referred to as the *solar constant* S. Changes in the Sun's activity cause variations in the solar constant. The most extreme variation is the 70% increase in S over the history of the Sun, as mentioned in chapter 2. The variations in S associated with the 11 year sunspot cycle are much smaller and of order 0.1%. Variations in the eccentricity of Earth's orbit around the Sun also affect the global annual mean energy flux that Earth receives (this is one of the socalled Milankovich cycles).

As the photons of the solar radiation pass through the atmosphere, absorption by different molecules in Earth's atmosphere changes the observed spectrum at the planetary surface from the one at the top of atmosphere.

Most importantly, oxygen and ozone cut off much of the UV part of the spectrum, whereas carbon dioxide and water vapor cut off much of the IR part.

A significant part of the solar radiation hitting the top of Earth's atmosphere is reflected back to space on its way down to the surface, thereby reducing the incoming flux of energy. This is expressed by the *planetary albedo* α_p. The albedo of Earth is the ratio of the part of the incident flux of solar radiant energy that is reflected back to space, to the total incident flux of solar radiant energy. Using this, we thus have the following expression for the *incoming shortwave radiation* R_{in}, or ISR:

$$R_{\text{in}} = \frac{S}{4}(1 - \alpha) \tag{4.5}$$

The factor of 1/4 arises from the ratio of the cross-sectional area of Earth, over which the incident solar radiation is shed, to the surface area of Earth, over which the energy is distributed.

The task is now to determine an expression for the albedo as function of surface temperature T_s. Reflection of sunlight back to space takes place both from the atmosphere, due to clouds, and from Earth's surface. The planetary albedo is a result of both cloud and surface properties of the planet. Today, Earth's planetary albedo is ∼0.3. Clouds do not only cool the Earth by lowering R_{in} through the increase in albedo, but they also warm the Earth by lowering R_{out} through the greenhouse effect, as described below. The combined result of these counteracting effects depends on the height of the clouds and on the state of the surrounding atmosphere. Different planetary surfaces have different albedos. Some typical albedos are listed in table 4.3.1 These values are strongly dependent on the specific surface

Surface	Albedo	Surface	Albedo
forest	0.05–0.10	granite	0.30–0.35
grass	0.05–0.30	sand	0.20–0.40
snow	0.6–0.9	soil	0.05–0.30
urban areas	0.05-0.20	ocean[a]	0.03–0.4

Table 4.1: Typical albedos of various surfaces. *a* is from [*Jin et al.*, 2004], the remaining from `http://scienceworld.wolfram.com/physics/Albedo.html`.

at hand and the incident angle. It is a fact, however, that the albedo of snow and ice is markedly greater than the albedo of soil, forest, rocks etc. The planetary albedo depends on the amount and the distribution of the different surfaces of the planet. Changes in the land-ocean distribution thus affects the planetary albedo. The parameterization of the planetary albedo by temperature, most importantly however, must express the fact that the amount of ice and snow varies in response to temperature (disregarding

the more uncertain reponse in clouds). When the global mean temperature falls, snow cover, ice sheets and glaciers on land, along with sea ice on the ocean expand in areal extent, all other things being equal, covering up surfaces that was previously bare land or ocean. Since ice and snow have higher albedos than land and ocean, this changes the planetary albedo, making the planet brighter. All other things being equal, this increase in planetary albedo would in turn decrease the incoming shortwave radiation and thus the global mean temperature. This loop of processes is termed the *ice-albedo feedback mechanism*. This is a positive feedback loop since it enhances the initial pertubation. In the simplest approach this dependence of planetary albedo upon surface temperature can be implemented by a piecewise linear relation for the dependence of the planetary albedo upon surface temperature [*Ditlevsen*, 2005]:

$$\alpha_p(T_s) = \begin{cases} \alpha_i & \text{for} \quad \mathrm{T_s} \leq \mathrm{T_i} \\ \frac{(T_f - T_s)\alpha_i + (T_s - T_i)\alpha_f}{T_f - T_i} & \text{for} \quad \mathrm{T_i} < \mathrm{T_s} < \mathrm{T_f} \\ \alpha_f & \text{for} \quad \mathrm{T_s} \geq \mathrm{T_f} \end{cases} \tag{4.6}$$

For surface temperatures below some lower threshold $T_i \approx -10°\mathrm{C}$, the planet is completely covered in ice and the plantery albedo therfore equal to that of ice, while for temperatures above some upper threshold $T_f \approx 20°\mathrm{C}$, the planet is completely ice-free and the plantery albedo therefore equal to that of ocean/land/clouds. For surface temperatures $T_i < T_s < T_f$ between these limits, the planetary albedo is assumed to vary linearly between the albedo of ice and bare ocean/land.

4.3.2 Outgoing Longwave Radiation and the Greenhouse Effect

Let us now turn to the second term on the right hand side of equation (4.3). The spectrum of the emitted radiation from Earth, as observed from space, resembles that of a blackbody with a temperature of ∼288K, the average surface temperature on Earth, which corresponds to a wavelength of maximum intensity of $\sim 10\mu$m, see e.g. [*Salby*, 1996]. This resemblence is true, however, only in the part of the spectrum known as the *atmospheric window* $\sim$8–12μm. Significant parts of the spectrum are influenced by absorption by various molecules in the atmosphere, including water vapor, carbon dioxide, methane and ozone, among others. These gases are known as *greenhouse gases*. Those parts of the spectrum correspond to emission spectra at significantly lower temperatures, corresponding to higher levels in the atmosphere. When the emission spectrum is integrated over wavelength, we end up with the *outgoing longwave radation* R_{out}, or OLR, the flux of radiant energy emitted to space. The parameterization of OLR by temperature is not trivial. In the following, three approaches are described.

If the planet was a perfect blackbody with surface temperature T_{eff}, the emitted flux of energy would, according to the Stefan-Boltzmann law, simply be σT_{eff}^4, where σ is the Stefan-Boltzmann constant. However, due to the presence of the atmosphere and its content of greenhouse gases, Earth is not a perfect blackbody. The emissivity g measures, so to speak, the deviation of the planet from a perfect blackbody. Using this, the OLR can be written as

$$R_{\text{out}} = \sigma g T_{\text{eff}}^4. \tag{4.7}$$

One then needs to determine how the emissivity g depends on temperature, which, via the chain rule, translates into determining how the emissivity depends on greenhouse gas content, and how the grenhouse gas content depends on temperature.

An alternative way to formulate the OLR, still expressing the same physical phenomena, is by direct use of the *greenhouse temperature* $T_g = T_s - T_{\text{eff}}$, defined as the difference between the Earth's surface temperature and the effective blackbody temperature of the planet T_{eff} [*Ditlevsen*, 2005]. In this way, we write:

$$R_{\text{out}} = \sigma T_{\text{eff}}^4 = \sigma (T_s - T_g)^4. \tag{4.8}$$

The effective, or blackbody, temperature of Earth is the temperature of the atmosphere at the level from which the OLR effectively originates (the optical depth of the atmosphere). Since, on Earth, this emitting level is located on the order of $\sim$3 km above the surface, and the atmospheric lapse rate is approximately $-10\,\text{K}\,\text{km}^{-1}$, the greenhouse temperature of our planet is on the order $\sim$30 K. Using the parameterization of the OLR in equation (4.8), the greenhouse effect can be expressed directly by letting the greenhouse temperature depend on the content of greenhouse gases in the atmosphere $T_g = T_g([\text{H}_2\text{O}], [\text{CO}_2], [\text{CH}_4], \ldots)$, where [GHG] denotes the concentration of some greenhouse gas. From a physical perspective, this dependence can be understood by the following: All other things being equal, increasing the content of a given greenhouse gas makes the atmosphere more opaque for longwave radiation, and hence the radiative height of the OLR is increased. Since the tropospheric temperature profile has a negative lapserate, i.e. temperature decreases with height, this decreases the effective temperature T_{eff}, and the greenhouse temperature T_g increases.

An alternative parameterization of the OLR by temperature can be used in simple energy balance models, and this is also the approach that will be used in this thesis. Here, the OLR is linearized with respect to surface temperature T_s. This is done to implement the atmospheric water vapor effects. It can be shown that the saturation water vapor pressure e_s in an atmosphere overlying an ocean varies with temperature T according to:

$$\frac{d \ln e_s}{dT} = \frac{L}{R_v T^2}. \tag{4.9}$$

This is the *Clausius-Clapeyron* equation, where L is the latent heat of evaporation, and R_v the water vapor gas constant. It can further be shown that the solution to (4.9) can be approximated by an exponential increase in e_s with temperature, and thus also an exponential increase in the specific humidity in the atmosphere. To put it very simple then: Increasing the temperature, increases the content of water vapor. And since water vapor is a greenhouse gas, this decreases the OLR. All other things being equal, this decrease in the OLR, in turn, would increase the temperature further. This is the socalled *water vapor* feedback loop. This is a positive feedback loop. It turns out, that an easy way to capture the dependence of OLR upon temperature is by letting the OLR vary linearly with surface temperature T_s, instead of the fourth-order power law as dictated by the Stefan-Boltmann law [*Hartmann*, 1994]. In this way, we simply write:

$$R_{\text{out}} = A_0 + B_0(T_s - T_0), \tag{4.10}$$

where T_0 is the offset in surface temperature around which the OLR is linearized. Numerical values are, e.g., $T_0 = 0°\text{C} = 273.15\,\text{K}$, $A_0 = 209\text{Wm}^{-2}$ and $B_0 = 1.9\text{Wm}^{-2}\text{K}^{-1}$.

The three parameterizations (4.7), (4.8) and (4.10) of how the OLR depends on temperature should of course be equivalent. If we make a Taylor-expansion of e.g. (4.8) to first order around T_0, we find

$$R_{\text{out}}(T_s) \approx \sigma(T_0 - T_g)^4 + 4\sigma(T_0 - T_g)^3(T_s - T_0) + \ldots, \tag{4.11}$$

where $T_0 - T_g$ is the effective temperature corresponding to the surface temperature around which the expansion is made. To have the parameterizations equivalent, we must identify the first term on the right-hand-side $\sigma(T_0 - T_g)^4$ with the constant A_0 in (4.10) and the last term $4\sigma(T_0 - T_g)^3$ with B_0 in (4.10).

We have endorced the effects of water vapor as a greenhouse gas in the OLR parameterization in (4.10), but we still need to implement the greenhouse effect from well-mixed greenhouse gases. The radiative effects of wellmixed greenhouse gases have been subject of much research due to the anthropogenically induced increases. This has lead to the concept of the *radiative forcing* associated with a given change in concentration of greenhouse gas, defined as the difference in irradiance between the pre-industrial atmosphere and an atmosphere with altered concentration of greenhouse gas (actually, one differentiates between instantaneous and adjusted radiative forcings). Our modelling focus of this thesis is on carbon dioxide, so in the following we will content ourselves to implement the effects of CO_2. We can include the radiative effects of CO_2 by letting R_{out} decrease logarithmically with atmospheric mixing ratio of carbon dioxide fCO_2, cf. *Myhre et al.* [1998]. This captures a slow saturation of absorption bands as fCO_2

increases. Expanding the OLR expression in equation (4.10) by such a CO_2 term yeilds:

$$R_{\text{out}} = A_0 + B_0\big(T_s - T_0\big) - A_{\text{CO}_2} \ln\left[\frac{f\text{CO}_2}{f\text{CO}_2^0}\right]. \tag{4.12}$$

where $f\text{CO}_2^0$ is the offset in CO_2 mixing ratio around which the radiative forcing as computed. The radiative modelling of *Myhre et al.* [1998] suggest $A_{\text{CO}_2} = 5.35\text{Wm}^{-2}$ with $f\text{CO}_2^0 = 280$ppmv as the pre-industrial CO_2 mixing ratio. More complicated functions of $f\text{CO}_2$ can be used for the OLR expression, by use of more full-blown radiative-convective models. However, since the scope of this thesis is conceptual modelling, we shall stick to the simple expression.

4.4 Cycles of Matter

The energy budget of our planet is affected by various matters within the climate system. Water and carbon are important factors for climate, as stressed above. How these can be exchanged between the components of the climate system is briefly described below.

4.4.1 The Hydrological Cycle

Water appears as both greenhouse gas, cloud, ocean and ice and snow in the climate system. The behaviour of water within the climate system is described by the *hydrological cycle*. The hydrological cycle is concerned with the flow of water, in all its forms, between the different reservoirs within the climate system. This flow primarily takes place between the ocean and the atmosphere, but also the cryosphere plays an important role. It involves evaporation from the oceans, sublimation from the ice masses, condensation, cloud formation, precipitation, and river runoff from continents as some of the primary processes. The importance of water, as seen from a climatologist's point of view, has three aspects, cf. [*Pierrehumbert*, 2002]. 1: It serves as an important way of transporting energy in the atmosphere (the latent energy transport: evaporation, air-parcel transport, condensation). 2: It affects the global radiation balance through clouds, water vapor and ice-cover. 3: It influences the carbon cycle through the silicate weathering and thus the atmospheric CO_2. Our focus is on points 2, described above, and 3, which is delt with below.

4.4.2 The Long-term Carbon Cycle

Carbon acts as greenhouse gas in the form of CO_2 and CH_4. The behaviour of carbon within the climate system is described by the *carbon cycle*. Our focus is on CO_2. The important controller of atmospheric carbon dioxide on

timescales of order hundreds of thousands of years and longer is the *long-term carbon cycle* Below, the qualitative main features of the long-term carbon cycle are briefly described, see e.g. *Berner* [1998; 2003; 2005]; *Kasting and Catling* [2003]. A quantitative formulation of this is postponed to the model presentation in chapter 5. The long-term carbon cycle is concerned with carbon exchanges between rocks and the surficial system, including the atmosphere, oceans, biosphere and soils. The processes within this cycle all have characteristic timescales, i.e. reservoir residence times, ranging from hundreds of thousands of years and up.

The long-term carbon cycle differs from the conventional carbon cycle that deals with carbon fluxes within the surficial system alone and operates on much shorter timescales, ranging up to thousands of years [*Harvey*, 2000, ch. 2.4]. The long-term carbon cycle can be subdivided into two subcycles, depending on what pathway the carbon takes from the surface system to the rocks: the *organic carbon* cycle and *carbonate-silicate* cycle. These are depicted in figure 4.1, with the organic carbon cycle to the left and the carbonate-silicate cycle to the right. These are described below.

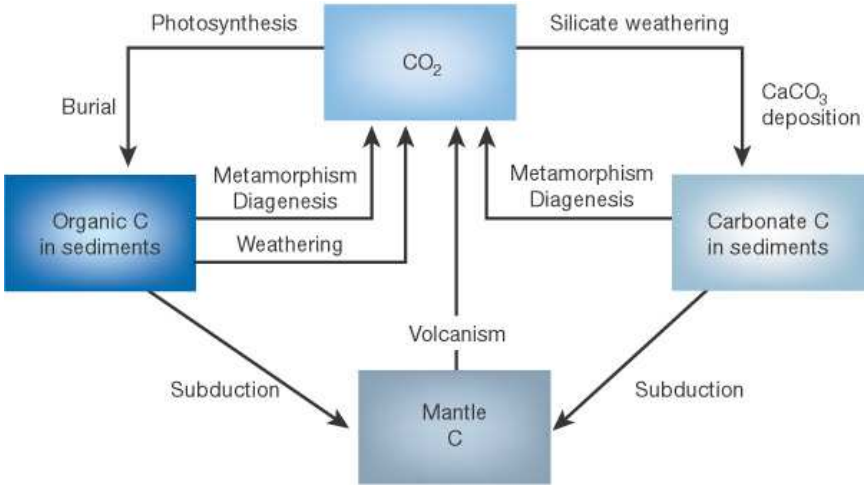

Figure 4.1: A schematic illustration of the long-term carbon cycle. The organic carbon subcycle relates to the left part, and the carbonate-silicate subcycle to the right part. The figure is from [*Berner*, 2003].

The organic carbon cycle is concerned with the exchange of organic carbon in sediments and carbon dioxide in the atmosphere–ocean system. It can be summarized by the generalized reaction

$$CO_2 + H_2O \leftrightarrow CH_2O + O_2,$$

which involves several intermediate steps. Going from left to right, it represents the burial in sediments of biologically produced organic carbon CH_2O by global net photosynthesis (the upper left arrow in figure 4.1). The global net photosynthesis represents the net excess of photosynthesis over respiration, the reverse process, and is found as photosynthesis minus the respiration. Going from right to left, the reaction represents the oxidative weathering of previously burried organic carbon CH_2O, which is exposed to the atmosphere by erosion on the continents (the middle left arrows in figure 4.1)—the burning of fossil fuels by humans today is an increase of this process.

The carbonate-silicate cycle is concerned with the exchange of carbonate carbon in the sediments and carbon dioxide in the atmosphere–ocean system. It can be summarized by the generalized reactions

$$\begin{aligned} CO_2 + CaSiO_3 &\leftrightarrow CaCO_3 + SiO_2 \\ CO_2 + MgSiO_3 &\leftrightarrow MgCO_3 + SiO_2. \end{aligned}$$

These reactions are also known as the Urey reactions, and involves several intermediate steps. Going from left to right, silicate weathering on land, followed by a transport to the ocean by rivers and subsequent carbonate deposition on the ocean floor by dead shelly organisms take carbon from the atmosphere–ocean system to the sediments (the upper right arrow in figure 4.1). Going from right to left, metamorphism and diagenesis (changes in crystallisation of the rock, or some other physical or chemical property of the rock) bring carbon from the sedimentary rocks back to the atmosphere–ocean system (the middle right arrows in figure 4.1).

Silicate weathering works as a sink of atmospheric carbon dioxide. The weathering rate depends on both temperature and partial pressure of carbon dioxide. As described below in section 4.5.2, biology also affects weathering rates through several mechanimsms. The temperature dependence of weathering rates has two parts [*Kasting and Catling*, 2003]. Most important is the indirect effect that operates through the hydrological cycle: both the chemical reaction rate of weathering on land and the transport of weathering products to the ocean increase as precipitation rates increase; the rate of precipitation, in turn, increases with surface temperature. The direct temperature effect is due the increase in chemical reaction rates with temperature. As a result of these effects, weathering is enhanced at higher temperatures. The dependence of weathering rates upon CO_2 partial pressure is perhaps less well-determined, although present.

Lastly, both the organic carbon cycle and the carbonate-silicate cycle are closed as the lithospheric plates are subducted into the deeper, partially molten asthenosphere as a result of plate-tectonics. From here, volcanism

brings the carbon back to the atmosphere as CO_2 is outgassed (the lower arrows in figure 4.1).

The silicate-carbonate cycle in itself holds a negative feedback loop for climate on long timescales, due to the temperature dependence of silicate weathering [*Walker et al.*, 1981]: Imagine that the Earth resides in a steady state with respect to temperature and CO_2. An increase (decrease) in surface temperature, would increase (decrease) weathering rates and thereby diminish (enhance) the greenhouse effect by drawing out (pumping in) atmospheric carbon dioxide, and this would thus decrease (increase) the surface temperature, all other things being equal. The effects of this feedback loop and how this fits into the FYS paradox and the snowball Earth events is further discussed in chapters 5 and 7.

4.5 The Biosphere

In the following, a quantitatively description of the biosphere as a component in the climate system is introduced, and a qualitative overview of the long-term interactions between the climate and biosphere is given.

4.5.1 Models of the Biosphere

In biology, population ecology studies the structure and dynamics of populations [*Sharov*, 1996]. Here, quantitive models with varying complexity of the 'population system' are setup and studied. A population system includes, besides the population itself, resources (food, space, etc.), enemies (predators, diseases, etc.), and environment (air/water/soil temperature, composition, etc.). A simple model of a population M_{bio} is motivated by a logistic growth:

$$\frac{dM_{\text{bio}}}{dt} = \Big[\big(M_{\max} - M_{\text{bio}}\big)U - \lambda\Big] M_{\text{bio}}. \tag{4.13}$$

Here, t is time, $M_{\max}$ a carrying capacity, U the growth rate, and λ the death rate of the population (actually we should take $\lambda = 0$ to reach the original Verhulst equation [*Sharov*, 1996]). In (4.13), the last term in the brackets on the right-hand-side, λ, expresses that the number of dying population members per time is proportional to the population size. The first term in the brackets expresses that the growth of the population likewise increases proportionally to its size, but is also limited by the size due to struggle for resources.

In this thesis we are concerned with the biology that affects the long-term carbon cycle, as described below. This is, as we shall see, related to all oceanic and continental photosynthesizing biology, responsible for producing a surplus of organic carbon that can be burried in sediments, and large vascular plants on land, responsible for enhancing silicate weathering rates.

The population M_{bio} in equation (4.13) thus refers to this carbon cycle affecting biosphere in a very broad sense.

4.5.2 Climate-Biosphere Interactions

The biosphere and climate interact as components of the Earth system. A great variety of processes comprise the web of links between these components. Below, the two directions are treated seperately.

Climatic Effects on Biology

The biosphere is influenced by the state of the climate as this defines the environment of the biology. In our simple approach, with climate prescribed by the surface temperature T_s, this is a result of the fact, that the growth rate of any given species is dependent on the temperature of the environment in which the species grows. It is fair to assume that any species can only exist in a limited range of temperatures. Within this range of tolerable temperatures, the growth rate of the species will presumeably always have a preferred temperature, where the growth of this species is optimal, leading to a socalled 'peaked growth-temperature curve', as also used in the Daisyworld model [*Watson and Lovelock*, 1983]. More formally, we should include that growth rates of most species is not only dependent on the surface temperature, but rather a result of parameters such as soil moisture for land plants, availability of nutrients for both land and marine biota, and the atmospheric composition, mainly CO_2 levels, which is a direct result of the biota itself.

Biological Effects on Climate

Reffering to the energy balance equation (4.3) and the expressions (4.5) and (4.12) for the ISR and OLR, respectively, biology can affect climate in two ways: It can influence the planetary albedo α_p, and it can influence the atmospheric content of greenhouse gases.

Planetary albedo On land, the albedo coupling between the biosphere and climate expresses the fact that areas covered with vegetation in general has a lower albedo than bare land. Referring to the albedo values in table 4.3.1, we see that forrest has $\alpha = 0.05$–0.1 and grass $\alpha = 0.05$–0.3, whereas, e.g., granite has $\alpha = 0.3$–0.35 and sand $\alpha = 0.2$–0.4. In the ocean, the effect is more subtle, and actually of opposite sign. Here, oceanic phytoplancton is believed to influence the formation of cloud condensation nuclei by production of dimethyl sulfide (DMS), thereby affecting the cloud cover and thus the albedo [*Hartmann*, 1994, chap. 9]. This latter coupling is non-trivial and probably more speculative. As we saw in chapter 3, the albedo effect is the very essence of the Daisyworld model [*Watson and Lovelock*, 1983]. As

was also argued, this effect is probably less relevant on the long timescale compared to the following effect that operates through the greenhouse gas content in the atmosphere, when we consider the conceptual modelling of climate-biosphere interactions over long timescales.

Atmospheric composition and greenhouse gases An important effect of biology on climate is related to the atmospheric content of greenhouse gases. The biota heavily influences the composition of the atmosphere, affecting the levels of oxygen, carbon dioxide, methane, water vapor etc [*Lenton*, 1998]. For simplicity, we shall in this thesis examine only the effects of CO_2 as a long-term feedback mediator from the biota to climate. This is relevant since CO_2 acts as an important greenhouse gas. The long-term changes in the atmospheric content of CO_2 is governed by the long-term carbon cycle. As pointed towards above, biology enters the long-term carbon cycle primarily two places: The burial of organic carbon and the enhancement of silicate weathering.

OrganicCarbon Burial The biosphere is directly responsible for the burial of organic carbon, as outlined in section 4.4.2 above. The burial is not necessarily only related to oxygenic photosynthesis. The amount of organic material that avoids decomposition, and thus gets burried in the sediments, could depend on the biological origin of the carbon, however. Carbon burial takes place on land as well as in the ocean.

Silicate Weathering The biosphere accelerates silicate weathering rates through several mechanisms. This involves rootlet secretion of organic acids, decomposition of organic litter into acids, enhancement of precipitation rates due to plant recirculation of water, and the ability of roots to stop the soil from eroding, thereby retaining water in the soil [*Berner*, 2005]. From field studies, these effects have been reported to result in an increase in weathering rates by a factor of approximately 2–10 [*Berner*, 2005]. These mechanisms, however, are all related to terrestrial, vascular plants (especially large vascular plants with extensive root systems). Weathering rates during the Precambrian supereon, with life confined to the oceans, were not subject to these mechanisms and thus unaffected by biospheric changes.

4.6 Summary

This concludes the introduction to the climate system. In the following chapter, the simple energy balance, the long-term carbon cycle, and the biospheric growth model will be employed to set up a simple coupled model of the climate-biosphere system.

5 A Simple Model: Setup

The climate and the biosphere of our planet are components of the Earth system, and affect each other through various processes on various timescales. In this chapter we present a conceptual model of long-term interactions between climate and life. Focus will be on the biotic influence on the atmospheric composition and content of greenhouse gases, as stressed in section 4.5.2. We will, for simplicity, consider only carbon dioxide CO_2. The prime target of the model is to discern the possible long-term biospheric effects on climate. Also, the Faint Young Sun paradox and the possible Snowball Earth events still serve as bright objectives of our wandering in the dark.

5.1 Description of Components

Ideally, we could try to implement all aspects of the Earth system in our climate-biosphere model. In reality, the challenge is to make reasonable assumptions, to focus on the important mechanisms, while leaving the less important ones out. By doing this, we construct a model, intended as a simplified representation of the Earth system. We will draw upon the theory presented in chapter 4. The modelling work of several other, e.g. [*Caldeira and Kasting*, 1992; *Lenton*, 1998; *Tajika*, 2003; *Goldblatt et al.*, 2006], will also serve as inspiration as we build our model.

Climate: Surface temperature T_s

We wil describe the climate of the planet by the spatially mean surface temperature T_s. The rate of change of T_s is governed by the global energy balance of the planet, given by the difference in incoming and outgoing

radiative fluxes R_{in} and R_{out}, respectively:

$$c\frac{dT_s}{dt} = R_{\text{in}} - R_{\text{out}}, \tag{5.1}$$

where c denotes the heat capacity of the climate system, setting the timescale for changes in T_s, as determined by (4.4).

R_{out} is determined using the Stefan-Boltzmann law, and must include the greenhouse effect. We will only account for the greenhouse effect of H_2O and CO_2; the atmospheric content of other greenhouse gases are treated as being constant (see below). We do this by letting R_{out} vary linearly with surface temperature to express the water vapor feedback due to the increase in water vapor saturation pressure with temperature according to the Clausius-Clapeyron relation, and logarithmically with atmospheric mixing ratio of carbon dioxide $f\text{CO}_2$ to capture a slow saturation of absorption bands as $f\text{CO}_2$ increases:

$$R_{\text{out}}(T_s, f\text{CO}_2) = \text{A}_0 + \text{B}_0\big(\text{T}_\text{s} - 273.15\big) - \text{A}_{\text{CO}_2} \ln\left[\frac{\text{fCO}_2}{\text{fCO}_2^0}\right]. \tag{5.2}$$

We will take the temperature linearization coefficient $B_0 = 1.9\text{Wm}^{-2}\text{K}^{-1}$ and scale A_0 to present day T_s using pre-industrial CO_2. For the CO_2 dependence, radiative modelling of *Myhre et al.* [1998] suggest $A_{\text{CO}_2} = 5.35\text{Wm}^{-2}$ with $f\text{CO}_2^0 = 280\text{ppmv}$ as the offset pre-industrial CO_2 mixing ratio.

R_{in} is determined by the luminosity S of the Sun, and the planetary albedo α_p:

$$R_{\text{in}}(T_s) = \frac{S}{4}\Big(1 - \alpha_p(T_s)\Big). \tag{5.3}$$

The planetary albedo α_p depends on the surface temperature through the ice-albedo feedback mechanism, expressing the change in areal extent of ice and snow with temperature. This is implemented by the following relation:

$$\alpha_p(T_s) = \alpha_1 - \alpha_2 \tanh\left(\frac{T_s - T_{\text{ice}}}{\Delta T_{\text{ice}}}\pi\right), \tag{5.4}$$

where α_1, α_2, T_s and ΔT_{ice} are model parameters. α_1 and α_2 are chosen from equating the albedo of the cold Earth $T_s \ll T_{\text{ice}}$ to that of a fully glaciated planet, $\alpha_{\text{ice}} = 0.62$, and the albedo of the warm Earth $T_s \gg T_{\text{ice}}$ to that of a fully *de*glaciated planet, $\alpha_{\text{free}} = 0.30$, cf. [*Hartmann*, 1994, chap. 9]. This yields $\alpha_1 = \frac{\alpha_{\text{ice}}+\alpha_{\text{free}}}{2} = 0.46$ and $\alpha_2 = \frac{\alpha_{\text{ice}}-\alpha_{\text{free}}}{2} = 0.16$. We will take the transition from the ice-covered to the ice-free planet to occur around $T_{\text{ice}} = 5°\text{C}$ and with a width of $\Delta T_{\text{ice}} = 15\,\text{K}$ (the norm of the argument of tanh in (5.4) is π for $T_s = -10°\text{C}$ and $T_s = 20°\text{C}$). The parameterization is shown in figure 5.1. Compared to the piecewise linear parameterization presented in [*Ditlevsen*, 2005; 2004, chap. 9], it is distinguished by a smooth, yet swift, transition between the glaciated and the deglaciated state (also, it has a

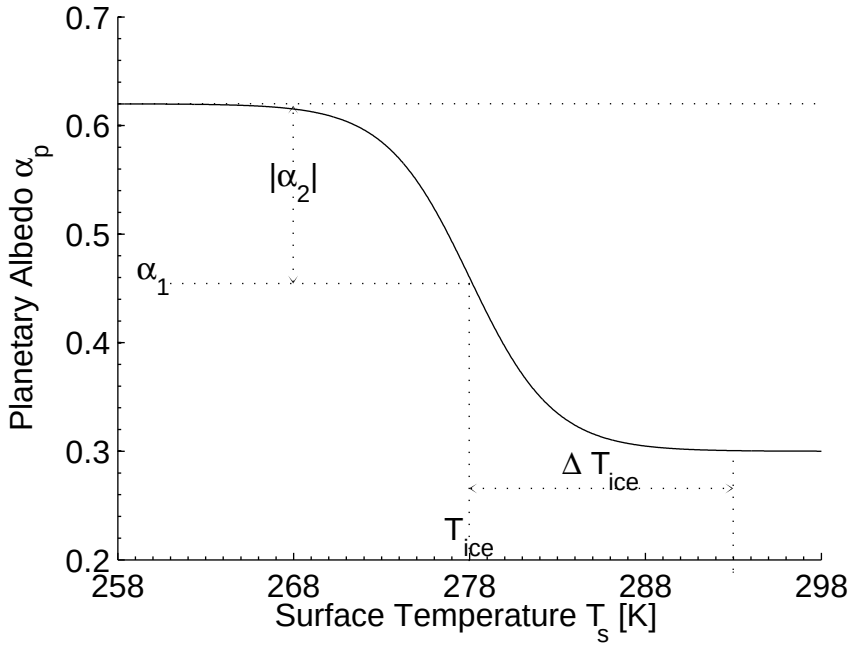

Figure 5.1: Planetary albedo as function of surface temperature for the model.

continous derivative). All other controllers of the planetary albedo, such as clouds and land-ocean distribution, i.e. palaeogeography, are considered constant. Particularly, biologically (Daisyworld-like) mechanisms, like the darkening by green plants or brightening by DMS producing plancton are neglected.

The climate model is scaled to yield a steady state surface temperature for $T_{\mathrm{PD}} = 15°\mathrm{C}$ for present day solar constant $S = S_0$ and pre-industrial $f\mathrm{CO}_2 = 280\mathrm{ppmv}$. This is done by adjusting the OLR linearization constant such that $A_0 = S_0/4(1 - \alpha(T_{PD})) - B_0[T_{PD} - 273.15)]$, yielding $A_0 = 209.9\mathrm{Wm}^{-2}$.

Biosphere: Biomass M_{bio}

The biosphere on the planet, envisioned to inhabit both ocean and continents, is described by the relative size of the total biomass M_{bio}, measured as fraction of present day total biomass. We will assume M_{bio} to be governed by a logistic growth model [*Sharov*, 1996]:

$$\frac{dM_{\mathrm{bio}}}{dt} = \Big[\big(M_{\max} - M_{\mathrm{bio}}\big)U - 1\Big]M_{\mathrm{bio}}. \tag{5.5}$$

Here, $M_{\max}$ is the bearing capacity. The death rate, stemming from the last term in the parenthesis, is assumed constant, while the growth func-

tion U must express the change of environmental hospitality with surface temperature:

$$U(T_s) = U_0 \exp\left(-\frac{(T_s - T_{\rm bio})^2}{2\sigma_{\rm bio}^2}\right). \tag{5.6}$$

The Gaussian dependence on T_s captures that the biological activity works best at an optimal temperature $T_{\rm bio}$, and declines for more extreme temperatures, as specified by the variance $\sigma_{\rm bio}$, see figure 5.2. The biosphere

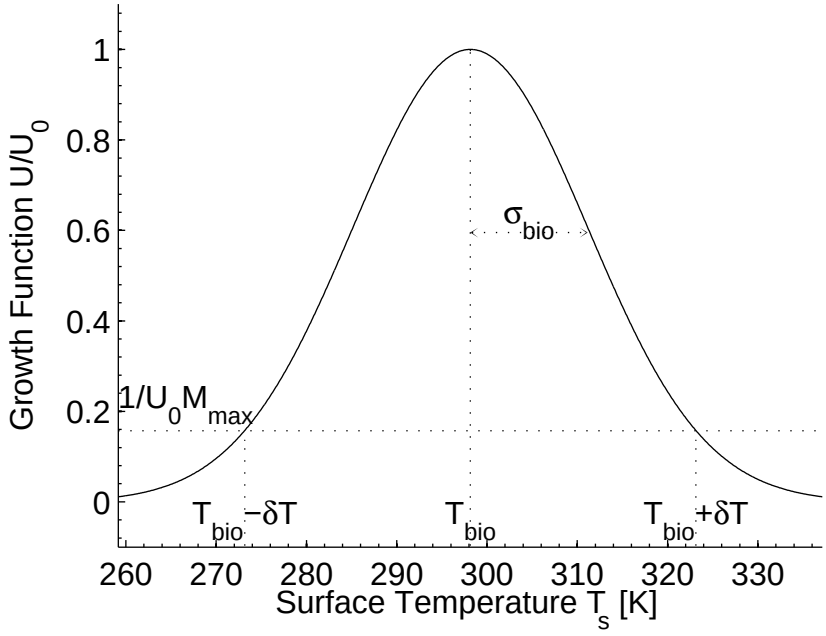

Figure 5.2: Growth rate for the biosphere in units of U_0 as function of surface temperature T_s (solid line). The biosphere can exist for $T_s \in [T_{\rm bio} - \delta T, T_{\rm bio} + \delta T]$. This interval is indicated by vertical dotted lines.

persists temperatures within the range $[T_{\rm bio} - \delta T, T_{\rm bio} + \delta T]$ with $\delta T = \sigma_{\rm bio}\sqrt{2\ln[U_0 M_{\rm max}]}$. Outside this temperature range, equation (5.5) with (5.6) inserted has no steady state solutions with $M_{\rm bio} > 0$, see figure 5.2. The growth function is assumed independent of fCO_2; CO_2 fertilization/starvation effects, as in e.g. [*Caldeira and Kasting*, 1992; *Franck et al.*, 2006], are not included.

This biospheric model is completely in line with Daisyworld [*Watson and Lovelock*, 1983] with a similar peaked growth-to-temperature curve for biology. However, we have left behind the concept of multiple competitive species. Instead focus has been put on a more realistic treatment of the processes that make up the biosphere-climate interactions, namely the atmospheric content of CO_2.

We will take $T_{\rm bio} = 25°\mathrm{C}$ and $\sigma_{\rm bio} = 13°\mathrm{C}$ and assume $\delta T = 25°\mathrm{C}$ such that the biosphere can thrive for temperatures within $0°\mathrm{C} < \mathrm{T_s} < 50°\mathrm{C}$. By demanding a steady state solution of $M_{\rm bio} = 1$ for present day $T_{\rm PD} = 15°\mathrm{C}$ we can determine the remaining parameters, yeilding $U_0 \approx 5.00\,\mathrm{yr}^{-1}$ and $M_{\rm max} \approx 1.27$, where the timescale in U is chosen to be years. This yields a modest increase in biomass of $M_{\rm bio} \approx 1.1$ for optimal growth temperature $T_{\rm bio}$.

Carbon cycle: $f\mathrm{CO}_2$

We will consider a planetary atmosphere with a composition similar to the present day Earth. In this atmosphere, however, we will only consider variations in the content of CO_2. We will take the atmospheric content of CO_2 to be governed by a simple geological carbon cycle, (im)balancing the long-term sinks and sources as described in chapter 4. The source stems from volcanism V (formally including the input from the oxygenic weathering of buried organic carbon, and from the thermal decomposition of carbonates in the lithosphere by diagenesis and metamorphism). The sinks stem from organic carbon burial $B_{\rm orgC}$ and silicate weathering $W_{\rm sil}$. In a simple approach, we can take:

$$\mu \frac{d(f\mathrm{CO}_2)}{dt} = V_0 - W_{\rm sil} - B_{\rm orgC}, \tag{5.7}$$

where μ is the total atmospheric load. Earth's atmosphere today contains $\sim 1.773 \cdot 10^{20}$ moles cf. *Goldblatt et al.* [2006], of which ∼78% is nitrogen and ∼21% is oxygen. We will simply treat the total load as constant and disregard the effects from variations in other atmospheric constituents.

The burial rate of organic carbon, the last term on the right-hand-side of equation (5.7), is assumed to vary linearly with $M_{\rm bio}$; this is the simplest approach, when no a priori knowledge is at hand.

$$B_{\rm orgC}(M_{\rm bio}) = \beta N_{\rm PP} M_{\rm bio}. \tag{5.8}$$

Here, $N_{\rm PP}$ is the *Net Primary Production* of organic carbon from photosynthesis. We will take $N_{\rm PP} = 3.75 \cdot 10^{15} \mathrm{mol\,yr}^{-1}$ [*Goldblatt et al.*, 2006]. The β parameter is the burial fraction, i.e. the ratio of the organic carbon that is burried in the sediments to the total organic carbon produced as NPP, and we will use $\beta = 4.1 \cdot 10^{-4}$, inferred from [*Goldblatt et al.*, 2006].

The silicate weathering rate $W_{\rm sil}$, the second term on the right-hand-side of equation (5.7), depends on both the surface temperature, the biomass and the CO_2 mixing ratio. We will take $W_{\rm sil}$ to increase exponentially with T_s, due to a direct effect through increased chemical reaction rates and an indirect effect through the intensified hydrological cycle, and to obey a power-law dependence on $f\mathrm{CO}_2$. Furthermore, $W_{\rm sil}$ is assumed to increase

linearly with $M_{\rm bio}$, which is again the simplest approach. Thus:

$$W_{\rm sil}(T_s, M_{\rm bio}, f{\rm CO_2}) = {\rm W_0} \exp\left(\frac{\rm T_s - T_{sil}}{\Delta {\rm T_{sil}}}\right) \left[\frac{\rm fCO_2}{\rm fCO_2^0}\right]^{\rm n} \left(1 + \Omega {\rm M_{bio}}\right) \quad (5.9)$$

We will, inspired by [*Tajika*, 2003], use a $f{\rm CO_2}$ scaling exponent of $n = 0.4$ and a biospheric enhancement factor of $\Omega = 4$. The latter is a reasonable estimate of the effects of complex multicellular life, i.e. land plants, normally quoted to enhance weathering by a factor of 2–10, as mentioned in 4. A somewhat less temperature sensitive parameterization is assumed as compared to the original work of *Walker et al.* [1981] since we are primarily concerned with effects of the biology. We shall assume a T_s exponential parameter of $\Delta T_{\rm sil} = 40\,{\rm K}$.

The volcanic input V_0, the first term on the right-hand-side of equation (5.7), is treated as a constant external process without any functional dependencies.

The W_0 parameter is found by equating $W_{\rm sil}(288{\rm K}, 1, 280{\rm ppm})$ to the estimate of present day silicate weathering of $6.65 \cdot 10^{12} {\rm mol\,yr^{-1}}$ [*Tajika*, 2003]. Finally, the carbon cycle model is scaled to yield a steady state for pre-industrial $f{\rm CO_2} = 280{\rm ppm}$, and present day surface temperature $T_{\rm PD} = 15^\circ\,{\rm C}$ and biomass $M_{\rm bio} = 1$. This is done by adjusting the volcanim output, yeilding $V = \beta N_{\rm PP} + W_{\rm sil}^{\rm PD} = 8.19 \cdot 10^{12}\,{\rm mol\,yr^{-1}}$.

5.2 Equations, Diagram and Parameters

The governing equations of the model (5.1), (5.5) and (5.7) represent a coupling of an energy balance model for the surface temperature, a logistic growth model for the biosphere, and a long-term carbon cycle for the atmospheric CO_2 mixing ratio, respectively. These are supplemented by the parameterizations of the ISR (5.3) through the planetary albedo (5.4), the greenhouse effect through OLR (5.2), the biospheric growth function (5.6), the silicate weathering rate (5.9) and the carbon burial rate (5.8). For clarity the full set of governing equations is written below:

$$c\frac{dT_s}{dt} = \frac{S}{4}\left[1 - \left(\alpha_1 - \alpha_2 \tanh\left[\frac{T_s - T_{\rm ice}}{\Delta T_{\rm ice}}\pi\right]\right)\right] - \left(A_0 + B_0\left(T_s - 273.15\right) - A_{\rm CO_2} \ln\left[\frac{f{\rm CO_2}}{f{\rm CO_2^0}}\right]\right) \quad (5.10)$$

$$\frac{dM_{\rm bio}}{dt} = \left[\left(M_{\rm max} - M_{\rm bio}\right) U_0 \exp\left(-\frac{(T_s - T_{\rm bio})^2}{2\sigma_{\rm bio}^2}\right) - 1\right] M_{\rm bio} \quad (5.11)$$

$$\mu\frac{f{\rm CO_2}}{dt} = V_0 - W_0 \exp\left(\frac{T_s - T_{\rm sil}}{\Delta T_{\rm sil}}\right)\left[\frac{f{\rm CO_2}}{f{\rm CO_2^0}}\right]^n \left(1 + \Omega M_{\rm bio}\right) - \beta N_{\rm PP} M_{\rm bio} \quad (5.12)$$

This is a dynamical system, comprised of a set of three coupled autonomous (no explicit t dependence in the governing equations), first-order (no higher order derivative with respect to t), ordinary (no partial derivatives), nonlinear differential equations.

The qualitative characteristics of the model are captured in the diagram in figure 5.3. It sketches the model variables and causal relations between these. This can be compared to the model diagram of Daisyworld in figure 3.1. Time t is the independent variable; the model has no spatial resolution.

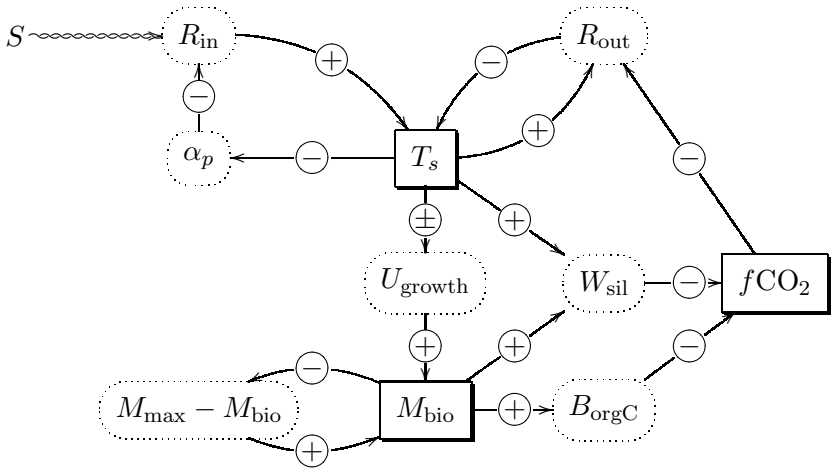

Figure 5.3: Model diagram of the simple Earth system. Solid boxes represent prognostic variables, while dotted boxes represent diagnostic variables. Arrows indicate causal relationships between variables. See also figure 3.1 for comparison with Daisyworld.

The prognostic, dependent variables are the surface temperature T_s, the biospheric size M_{bio}, and the atmospheric mixing ratio of carbon dioxide $f\text{CO}_2$ (solid boxes). These are linked by the diagnostic dependent variables (doted boxes). The arrows in figure 5.3 sketch a web of feedback mechanisms between the variables. The planetary albedo α_p in the incoming shortwave radiation R_{in}, and the outgoing longwave radiation R_{out} determines T_s. R_{out} is also affected by $f\text{CO}_2$, thus relating T_s to $f\text{CO}_2$. The biological growth function U shows that M_{bio} depends on T_s. M_{bio} is again also affected by M_{bio} itself. The weathering rate W_{sil} and the burial rate B_{orgC} shows that $f\text{CO}_2$ increases with M_{bio}. Also, the weathering rate W_{sil} depends on T_s, thus relating $f\text{CO}_2$ to T_s. The solar constant S is taken as the external, forcing parameter. All other processes within the Earth system, such as volcanism (influencing $f\text{CO}_2$), clouds (influencing T_s), palaeogeographic continental-oceanic distribution (influencing both T_s and $f\text{CO}_2$), atmospheric load and composition (influencing $f\text{CO}_2$) are treated as constants. It is left to the reader to match the different pathways to the governing equations (5.10)-(5.12).

Some points deserve attention, regarding the model diagram in figure

5.3. First of all, the many pathways might seem somewhat confusing. It should be stressed that the primary intention with the diagram is to give an overview of how the model works on a more general level. Also, the signs are somewhat misleading. The sign of, e.g., the arrow from T_s to α approaches zero for high/low temperatures compared to T_{ice}, since the derivative of $\tanh(x - x_0)$ tends to zero for $|x/x_0| \gg 1$ Furthermore, the choice of which variables are prognostic, and which are diagnostic, is of course made by the modellor; nature does not necessarily make the same destinction. Also, for a given pathway, the number of intermediate steps through diagnostic variables is somewhat arbitrary. To understand the behaviour of the model, one should rather turn to the governing equations (5.10)-(5.12).

The governing equations and the parameterizations of the model are accompanied by several model parameters that need to be specified by reasonable physical, biological, and chemical assumptions. The choice of these parameters have been outlined above, and their values are summarized in table 5.1, along with some physical constants. To yield a steady state at present (T_s,M_{bio},$f\text{CO}_2$) the least well-constrained parameters have been scaled, as determined from observations or other models, although the choice of which parameters to scale and which to fix is somewhat arbitrary. Of these are Ω and β of special interest to us, since they control the biospheric influence on CO_2 and thus climate. Ω controls the biotic enhancement of the silicate weathering, rate and β controls the burial rate of organic carbon.

5.3 Summary

This finalizes the setup of the conceptual model of long-term interactions between climate and life with focus on the atmospheric content of CO_2. It has three parts: an energy balance model for the surface temperature T_s, a logistic growth model for the biosphere M_{bio}, and a long-term carbon cycle for the atmospheric CO_2 mixing ratio. A relevant question might now be as to how this model differs from the motivating Daisyworld. Firstly, in the above simple model, we have left the Daisyworldian idea of the colour of the biology and its influence on the planetary albedo as the biosphere-climate mediator. In addition, we have improved the treatment of the climatic component of the Earth system by implementing the ice-albedo and greenhouse effects. The treatment of the biospheric component has been more or less left unaltered, as compared to Daisyworld, although the inclusion of multiple species in the model has been dropped.

Parameter	Value	Description	Reference
σ	$5.67 \cdot 10^{-8}\ Wm^{-2}K^{-4}$	Stefan-Boltzmann constant	
S_0	$1,370\ Wm^{-2}$	Solar constant	
c	$1.20 \cdot 10^{10}\ JK^{-1}m^{-2}$	Planetary heat capacity	
a_1	0.46	Albedo parameter	
a_2	0.16	Albedo parameter	
T_{ice}	5°C	Temperature offset of albedo	
ΔT_{ice}	15 K	Temperature width of albedo	
A_0	$209.9\ Wm^{-2}$	OLR offset	scaled
B_0	$1.9\ Wm^{-2}K^{-1}$	OLR linearization coefficient T_s	
A_{co_2}	$5.31\ Wm^{-2}$	OLR coefficient CO_2	[*Myhre et al.*, 1998]
$f{\text{CO}_2}^0$	$280 \cdot 10^{-6}$	pre-industrial $f\text{CO}_2$	[*Myhre et al.*, 1998]
U_0	$5.00\ \text{yr}^{-1}$	Biotic max growthrate	scaled
$M_{\max}$	1.27		scaled
T_{bio}	25°C	Biotic optimal temperature	
σ_{bio}	13 K	Biotic growth variance in temperature	
μ	$1.77 \cdot 10^{20}$ mol	Present atmospheric load	[*Goldblatt et al.*, 2006]
V_0	$8.19 \cdot 10^{12}\ \text{mol yr}^{-1}$	Volcanic CO_2 outgassing rate	scaled
W_0	$1.03 \cdot 10^{12}\ \text{mol yr}^{-1}$	Offset sil. weathering rate	[*Tajika*, 2003]
n	0.4	$f\text{CO}_2$ scaling exp. for sil. weath.	[*Tajika*, 2003]
ΔT_{sil}	40 K	temperature sensitivity for sil. weath.	scaled [*Walker et al.*, 1981]
T_{sil}	285 K	temperature offset for sil. weath.	[*Walker et al.*, 1981]
Ω	5	biotic enhancement of sil. weath.	[*Tajika*, 2003]
N_{PP}	$3.75 \cdot 10^{15}\ \text{mol yr}^{-1}$	Net Primary Productivity	[*Goldblatt et al.*, 2006]
β	$4.1 \cdot 10^{-4}$	Organic carbon burial fraction	[*Goldblatt et al.*, 2006]

Table 5.1: Parameters and constants of the model.

6 A Simple Model: Results

A conceptual model of the long-term climate-biosphere interactions was outlined in the previous chapter. The model focusses on the atmospheric content of carbon dioxide as the important coupling between climate and biology. The model couples an energy balance model for the surface temperature T_s, a logistic growth model for the biosphere M_{bio}, and a long-term carbon cycle for the atmospheric carbon dioxide mixing ratio $f\text{CO}_2$. In this chapter, we present the results of the model. First, the steady state solutions of each of the components are analyzed separately. Then, as the primary results of the model, we compute the full model's response in steady states to variations in the forcing parameter, taken to be the increasing solar constant. After this we move on to present the perspectives of these results; Firstly in relation to the homeostasis of Daisyworld, and secondly within the framework of the palaeoclimatic observations: The Faint Young Sun paradox and global glaciations.

6.1 Steady States of the Components

The surface temperature T_s, the biospheric size M_{bio}, and the atmospheric CO_2 mixing ratio are treated separately below. The model parameter values in table 5.1 are used, unless otherwise stated.

6.1.1 Surface Temperature

In the energy balance equation (5.10), the rate of change in surface temperature $\frac{dT_s}{dt}$ is seen to be a function of T_s (from R_{in}) and $f\text{CO}_2$ (from R_{out}). Let us, by means of the radiative balance, investigate the importance of the greenhouse effect from CO_2, i.e. the influence of $f\text{CO}_2$ on T_s, in the model.

The radiative balance in figure 6.1 sketches R_{in} and R_{out} as function T_s for three different values of $f\text{CO}_2$. The curve of ISR of course mirrors

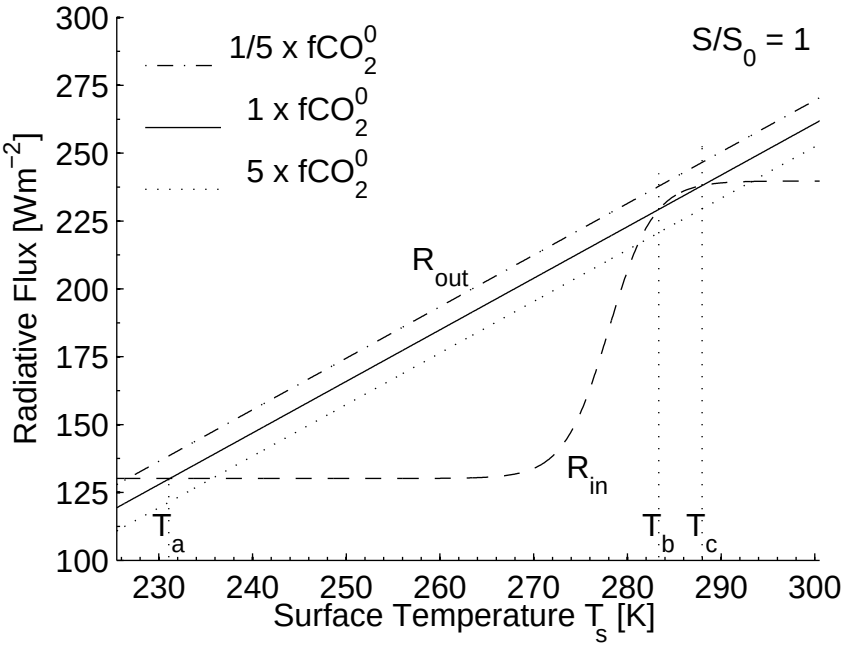

Figure 6.1: Incoming shortwave radiation R_{in} and outgoing longwave radiation R_{out} as function of surface temperature T_s for $S = S_0$ and three different values of CO_2 mixing ratio.

the planetary albedo dependence on temperature via the ice-albedo mechanism: For low surface temperatures, compared to $T_{\text{ice}} = 275$, the snow and ice-cover is large and the ISR therefore small, while for high surface temperatures the snow and ice-cover is small and ISR therefore high. Let us look at the curve for present day, actually pre-industrial, $f\text{CO}_2$ (solid line). The steady state surface temperatures, fulfilling $\frac{dT_s}{dt} = 0$, are found where $R_{\text{in}} = R_{\text{out}}$. As seen, there are three steady states: a glaciated planet with $T_s = T_a$, a deglaciated planet with $T_s = T_c$ and a partially glaciated planet with $T_s = T_b$. The stability of the steady states can be seen from the crossing of the ISR and OLR curves. Assume that the planet resides in the warm steady state where $R_{\text{in}} = R_{\text{out}}$ corresponding to $T_s = T_c$, and assume that we pertube T_s by some small amount $\delta T > 0$. As seen from the figure, R_{out} would then increase more than R_{in}, i.e. $R_{\text{out}} > R_{\text{in}}$ and hence $dT_s/dt < 0$, which would cause T_s to decrease towards $T_s = T_c$. A pertubation $\delta T < 0$ would likewise cause R_{out} to *decrease* more than R_{in}, i.e. $R_{\text{out}} < R_{\text{in}}$ and hence $dT_s/dt < 0$, which would cause T_s to *increase* towards $T_s = T_c$. This means that the steady state corresponding to $T_s = T_c$ is *stable*. Similar

reasoning shows that $T_s = T_a$ is also stable, while $T_s = T_b$ is unstable. This can also simply be deduced from the fact that we have three steady states on the line of which the right-most is an attractor. The only possible way to coherently arrange the two other steady states is by having the middle as a repeller and the left-most as an attractor. In this simple model, we identify present day Earth with the warm state corresponding to $T_s = T_c$.

When $f\mathrm{CO}_2$ is increased, R_{out} decreases in accordance with (5.2), and this changes the crossing of the ISR and OLR curves in figure 6.1. The structural effects on T_s by varying $f\mathrm{CO}_2$ is thus clearly seen from the radiative balance. We can solve (5.10) for steady state surface temperature as function of CO_2 mixing ratio. The results are depicted in figure 6.2. This

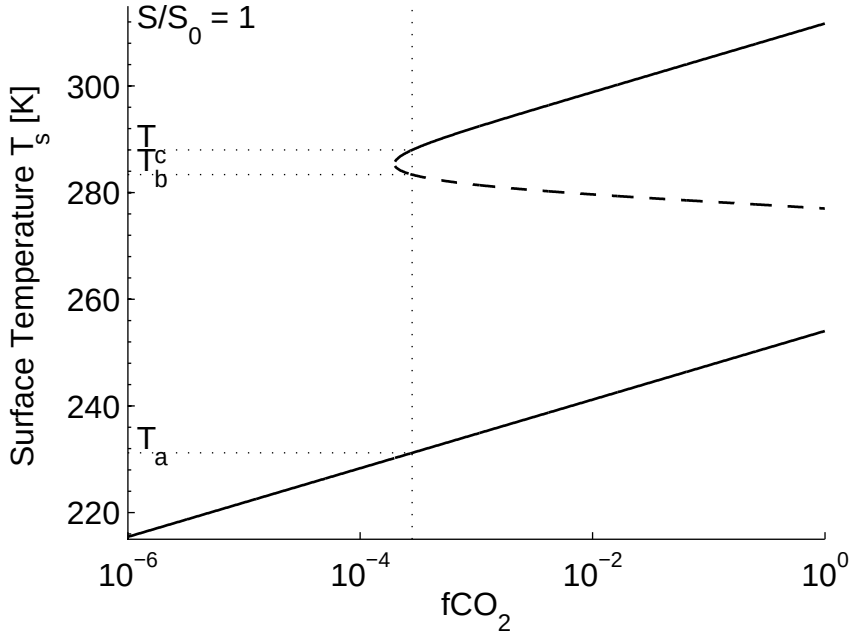

Figure 6.2: Steady state surface temperature T_s as function of CO_2 mixing ratio The full lines represent stable states, the dashed unstable states.

shows a (part of a) hysteresis loop (we have excluded the physically meaningless part with $f\mathrm{CO}_2 > 1$). The upper-most stable branch corresponds to the warm stable state, the lower-most to the cold stable state, and the middle to the unstable state. Multiplying pre-industrial $f\mathrm{CO}_2$ by a factor of 5 results in a modest warming by $\sim$5 K in the upper branch.

6.1.2 Biology

The logistic equation (5.11) for M_{bio}, is easily solved for steady states as function of T_s. This gives rise to two types of solutions: the *abiotic* $M^*_{\mathrm{a}} = 0$

for all T_s, and the *biotic*

$$M_{\rm b}^* = M_{\rm max} - U(T_s)^{-1} = M_{\rm max} - \frac{\exp\left(\frac{(T_s - T_{\rm bio})^2}{2\sigma_{\rm bio}^2}\right)}{U_0}, \qquad (6.1)$$

defined, i.e. positive, for $T_s \in [T_{\rm bio} - \delta T, T_{\rm bio} + \delta T]$ with $\delta T = \sigma_{\rm bio}\sqrt{2\ln(M_{\rm max}U_0)}$. These solutions are depicted in figure 6.3. The biotic solution has a maxi-

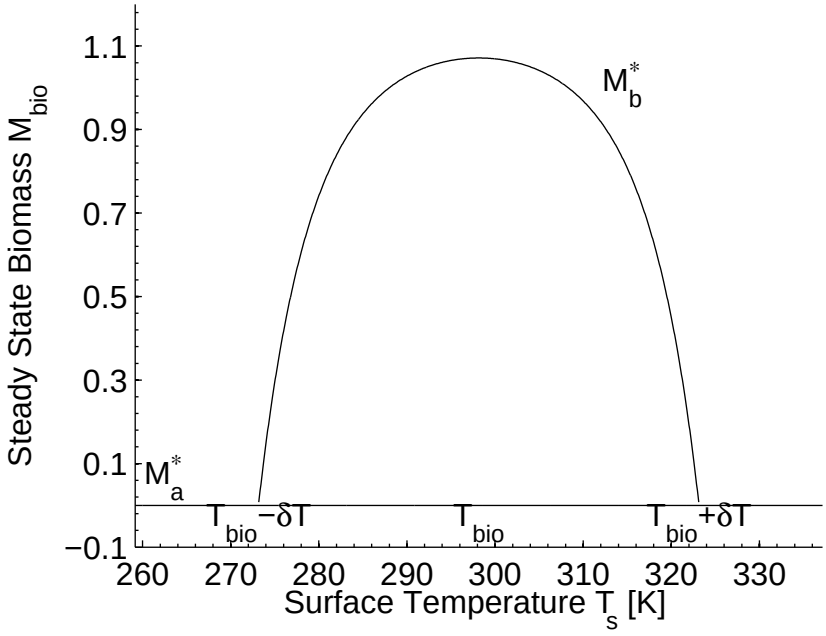

Figure 6.3: Steady state biospheric size $M_{\rm bio}$ as function of surface temperature T_s. Shown are both the abiotic $M_{\rm a}^*$ and the biotic solution $M_{\rm a}^*$.

mum of ∼1.1 when surface temperature equals the optimal growth temperature $T_{\rm bio}$.

6.1.3 Atmospheric Carbon dioxide

The carbon cycle equation (5.12) that governs the atmospheric CO_2 mixing ratio can likewise be solved for steady state $f\mathrm{CO}_2$ as function of T_s and $M_{\rm bio}$. This yields:

$$f\mathrm{CO}_2^* = \mathrm{fCO}_2^0 \left[\frac{\mathrm{V} - \beta \mathrm{N_{PP}} \mathrm{M_{bio}}}{\mathrm{W}_0 \exp\left(\frac{\mathrm{T_s} - \mathrm{T_{sil}}}{\Delta \mathrm{T_{sil}}}\right)\left[1 + \Omega \mathrm{M_{bio}}\right]}\right]^{\frac{1}{\mathrm{n}}} \qquad (6.2)$$

This relation is shown in figure 6.4, where contour lines of the steady state carbon dioxide mixing ratio $f\mathrm{CO}_2$ is drawn as function of surface temperature and biospheric size. We see that high surface temperatures and large

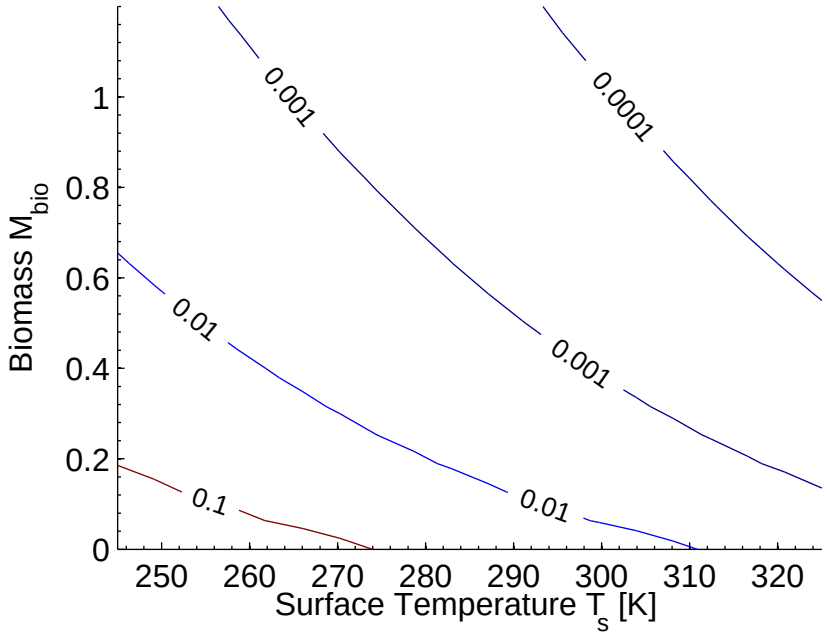

Figure 6.4: Contour lines of the steady state CO_2 mixing ratio as function of surface temperature T_s and biospheric size M_{bio}.

biomasses are associated with low contents of CO_2. This is due to the fact that silicate weathering increases with surface temperature and biomass, and carbon burial increases with biomass.

6.2 Response to Increasing Solar Luminosity

In the following, the coupled model is investigated within the same context as Daisyworld. We thus wish to determine the response in steady states of the model to the increasing solar luminosity, as held by the FYS paradox.

Let us first discuss the timescales of the model. The three variables of the model T_s, M_{bio} and fCO_2 are associated with somewhat different timescales. With the chosen model parameters, M_{bio} responds fast to pertubations, compared to T_s and the even slower fCO_2. A typical timescale for T_s can be estimated from $\tau_T \sim c\Delta T/\Delta R$ where c is the heat capacity of the climate system, ΔR is a typical radiative forcing, and ΔT a typical temperature variation. First we need to estimate the heat capacity c of the climate system. The ocean is the main contributor to c. We can therefore estimate c from oceanic values of the heat capacity $c_p \sim 4 \cdot 10^3 \text{Jkg}^{-1}\text{K}^{-1}$, the density $\rho \sim 1 \cdot 10^3 \text{kgm}^{-3}$ and some mean scale height $H \sim 3 \cdot 10^3 \text{m}$ according to equation (4.4). This yields $c \sim 1.2 \cdot 10^{10} \text{JK}^{-1}\text{m}^{-2}$. If we then use $\Delta R \sim 4\text{Wm}^{-2}$ and $\Delta T \sim 4\,\text{K}$ as typical values associated with a dou-

bling of atmospheric CO_2, we end up finding a typical timescale for T_s of $\tau_T \sim 1.2 \cdot 10^{10}\text{s} \sim 4 \cdot 10^3\text{yr}$. Likewise is the typical timescale for $f\text{CO}_2$ estimated from $\tau_{\text{CO}_2} \sim \mu\Delta f\text{CO}_2/\Delta\text{F}$, where μ is the atmospheric loading, $\Delta f\text{CO}_2$ the variation in $f\text{CO}_2$, and ΔF the difference between sinks and sources of CO_2. By using $\mu \sim 10^{20}\text{mol}$, and taking $\Delta f\text{CO}_2 \sim 3 \cdot 10^{-4}$, corresponding to a doubling of CO_2, and $\Delta F \sim 10^{11}\text{mol}\,\text{yr}^{-1}$, corresponding to a $\sim$5 % change in carbon burial rates, we find a typical timescale for $f\text{CO}_2$ of $\tau_{\text{CO}_2} \sim 3 \cdot 10^5\text{yr}$. All this does not changes the steady state calculations, but it does affect from where in phase space the stable fixed points are approached if the system is pertubed away from these, and how long time this process takes. This will thus normally happen with fast adjustment of M_{bio}, slow adjustment of T_s, and even slower adjustment of $f\text{CO}_2$.

Now, let us move on to determine the response in steady states of the full model to the varying solar luminosity. As a first step, we must determine the steady states of the model for a given solar constant S/S_0, i.e. the surface temperature ${T_s}^*$, biospheric size ${M_{\text{bio}}}^*$, and atmospheric carbon dioxide mixing ratio ${f\text{CO}_2}^*$ fulfilling $\frac{dT_s}{dt}\big|_* = \frac{dM_{\text{bio}}}{dt}|_* = \frac{d(f\text{CO}_2)}{dt}|_* = 0$. This gives us three equations in three unknowns. The governing equations are only weakly coupled (2 of the 6 off-diagonal entries in the Jacobian are zero), and the system is thus relatively simple to solve implicitly, as sketched above. The steady states of the full model are, from a graphically point-of-view, found as the intersections of the planes that span the three separate steady state solutions in (T_s,M_{bio},$f\text{CO}_2$) phase space. Starting with the logistic equation (5.11) for M_{bio}, this is solved for steady states as function of T_s, giving rise to the abiotic and the biotic solutions. These steady state solutions for M_{bio} are then inserted into the carbon cycle equation (5.12) for $f\text{CO}_2$, which is then solved for steady state $f\text{CO}_2$ as function of surface temperature T_s. Finally, these steady state solutions for $f\text{CO}_2$ are inserted into the energy balance equation (5.10) for T_s. We thus end up with the task of finding the roots of a function of one variable T_s, which is approached by a numerical method (bisection).

Let us depict graphically how these roots are found. The radiative balance for present day $S = S_0$ is shown in figure 6.5. The dashed line shows the ISR (5.3) as function of surface temperature. The solid lines shows the OLR (5.2) as function of surface temperature, when the steady state solutions for M_{bio} and $f\text{CO}_2$ are inserted. Here, the black curve corresponds to the *abiotic* solution and the blue curve corresponds to the *biotic* solution. Looking at the solid black curve in the figure, we see that the abiotic OLR still varies linearly with T_s. This is because $f\text{co}_2/\text{fco}_2^0 \sim \exp(-\text{T}_\text{s}/\text{n})$ for the abiotic $f\text{CO}_2$ solution, as seen from equation (6.2), and $R_{\text{out}} \sim \ln(f\text{co}_2/\text{fco}_2^0)$, as seen from equation (5.2). Looking at the solid *blue* curve in the the figure, we clearly see the effect of the biology. For $T_s \in [T_{\text{bio}} - \delta T, T_{\text{bio}} + \delta T]$ with $\delta T = \sigma_{\text{bio}}\sqrt{2\ln(U_0 M_{\max})}$, the biosphere draws down $f\text{CO}_2$, which is seen as the bulge on top of the OLR-curve for the biotic solution. This effect

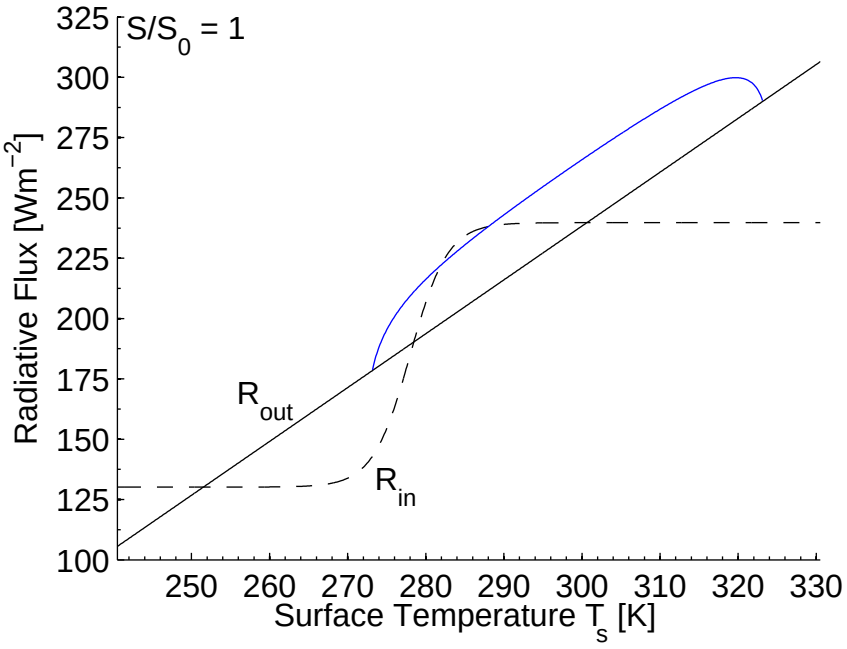

Figure 6.5: Incoming solar radiation R_{in} and outgoing longwave radiation R_{out} as function of surface temperature T_s for present day $S = S_0$ when inserting the steady state solutions for M_{bio} and $f\text{CO}_2$.

should be contrasted with Daisyworld, where the biosphere changes the *ISR* instead: black daisies would appear as a bulge on top of the ISR-curve, and white daisies as a bulge *below* the ISR-curve. Again, the steady states are found where the incoming and outgoing radiations balance, i.e. $R_{\text{in}} = R_{\text{out}}$. Varying the solar constant simply amounts to scaling the ISR-curve, while keeping the OLR-curves fixed. Finally, to find the steady state $f\text{CO}_2$ and M_{bio}, we simply insert the computed steady state surface temperature T_s in the steady state expressions (6.1) and (6.1) above.

The next step is to determine the stability of the fixed points in (T_s,M_{bio}, $f\text{CO}_2$) phase space. This can be done by a linear stability analysis, as a more stringent formulation of the arguments above, when examining the stability of T_s. This procedure was outlined in chapter 3 in connection with the two dimensional Daisyworld model (see also appendix A.2). Again we need to consider the Jacobian matrix $\mathbf{J}$ of the system (5.10)–(5.12):

$$\mathbf{J} = \frac{\partial F_i}{\partial x_j} = \begin{bmatrix} \frac{\partial F_T}{\partial T_s} & \frac{\partial F_T}{\partial M_{\text{bio}}} & \frac{\partial F_T}{\partial f\text{CO}_2} \\ \frac{\partial F_M}{\partial T_s} & \frac{\partial F_M}{\partial M_{\text{bio}}} & \frac{\partial F_M}{\partial f\text{CO}_2} \\ \frac{\partial F_f}{\partial T_s} & \frac{\partial F_f}{\partial M_{\text{bio}}} & \frac{\partial F_f}{\partial f\text{CO}_2} \end{bmatrix}, \tag{6.3}$$

where the functions $F_T(T_s, M_{\text{bio}}, f\text{CO}_2)$, $F_M(T_s, M_{\text{bio}}, f\text{CO}_2)$, and $F_f(T_s, M_{\text{bio}}, f\text{CO}_2)$

are given by the left-hand-sides of equations (5.10), (5.11) and (5.12), respectively. The stability is found from the three eigenvalues of the Jacobian matrix (6.3). The stability classifications presented in chapter 3 are easily extended to the three-dimensional phase space of the current model.

So, with the procedures for finding the steady states of the full model for a given solar luminosity, and the procedure for determining their stability in place, we are now ready to move on. Solving the model for steady states while varying S/S_0 by repeating the process described above yields the bifurcation diagram shown in figure 6.6. The plot sketches the steady state surface temperature T_s as function of solar luminosity S/S_0. In the

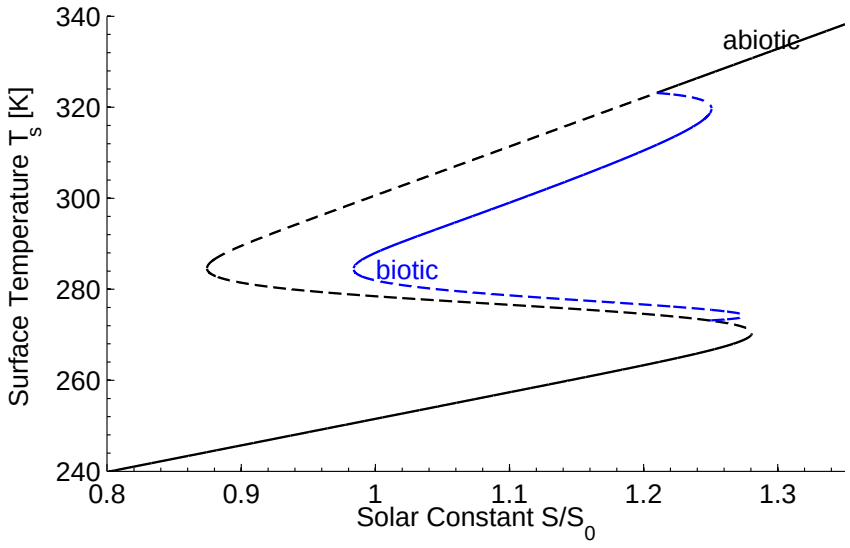

Figure 6.6: Steady state surface temperature T_s as function of solar luminosity S/S_0.

bifurcation diagrams in figure 6.7, the corresponding steady state biospheric size M_{bio} and atmospheric mixing ratio of carbon dioxide $f\text{CO}_2$ are shown as function of solar luminosity S/S_0. Note that the plots show the response in the projection of the fixed points onto each of the three axes that span the three-dimensional phase space (T_s,M_{bio},$f\text{CO}_2$). The stability is in all plots indicated by the line type: Solid lines correspond to attractors, dotted lines to repellers, and dashed lines to saddles. A few numerical integrations of the governing equations, using slightly pertubed steady states values as intial conditions, have been carried out to check the stabilities.

First we consider the *abiotic* response. Let us first focus on figure 6.6, showing the steady state T_s as function of S/S_0. With *black* is shown the steady state T_s for a uninhabited planet. Again, this shows a typical hysteresis loop. For low solar luminosities $S/S_0 \lesssim 0.87$, only the cold, fully

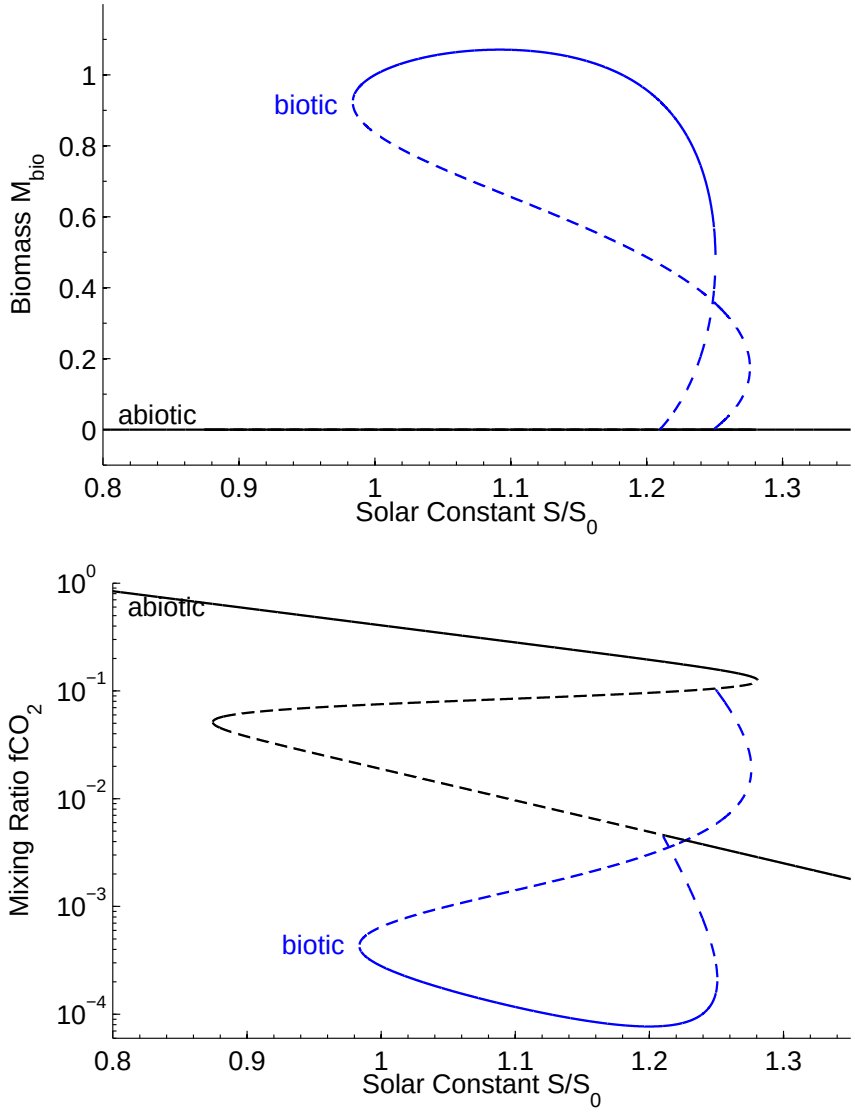

Figure 6.7: Steady state biospheric size $M_{\rm bio}$ (top) and atmospheric mixing ratio of carbon dioxide $f\mathrm{CO}_2$ (bottom) as function of solar luminosity S/S_0.

glaciated state exists (lower solid black line), while for high solar luminosities $S/S_0 \gtrsim 1.28$, only the warm, ice-free state exists (upper dashed/solid black line). In between these values, both the cold and the warm state exist, separated by an saddle, temperated, partially ice-covered state (middle dashed black line). The warm state is a saddle for $S/S_0 \lesssim 1.21$ and an attractor for $S/S_0 \gtrsim 1.21$. The saddle branch is only unstable towards pertubations in $M_{\rm bio}$, not in T_s and $f\mathrm{CO}_2$. This means that all initial con-

ditions with $M_{\rm bio} = 0$ can end up in this state (as well as in the stable cold abiotic state). The temperated, partially ice-covered saddle branch is also unstable towards pertubations in T_s. The upper and lower branches are straight lines because for sufficiently high and low surface temperatures the planetary albedo is practically constant:

$$\alpha_p \approx \alpha_1 \pm \alpha_2 \quad \text{for} \quad \begin{cases} T_s < T_{\rm ice} - \Delta T_{\rm ice} \\ T_s > T_{\rm ice} + \Delta T_{\rm ice} \end{cases}$$

and equation (5.10) thus reduces to a linear relation between T_s and S. Now, turning to figure 6.7, the corresponding steady state atmospheric mixing ratio of carbon dioxide $f{\rm CO}_2$ is shown as function of solar luminosity S/S_0 in the lower plot. The response in $f{\rm CO}_2$ is seen to be, so to speak, the inverse of the T_s response. This is a consequence of the fact that the logarithm of $f{\rm CO}_2$ in the steady state decreases linearly with T_s, as seen from equation (6.2) when inserting $M_{\rm bio} = 0$.

Let us then turn to the *biotic* response. Moving back to figure 6.6, the *blue* line shows the steady state T_s as function of S/S_0 for the biotic solution. Focussing on this, it shows several saddle-node bifurcations. As S/S_0 is increased from 0.85, a stable, warm biotic branch (upper solid curve) and an saddle, temperated, partially ice-covered biotic branch (lower dashed curve) appear at $S/S_0 \approx 0.98$. At $S/S_0 \approx 1.21$ a warm saddle branch appears (upper dashed curve), as the biotic state regains its stability. This disappears at $S/S_0 \approx 1.25$ in a saddle-node bifurcation. Also at $S/S_0 \approx 1.25$ a colder saddle branch is born (lower dashed curve), disappearing again at at $S/S_0 \approx 1.27$. The appearance of these bifurcations are naturally understood from the radiative balance plot in figure 6.5. Now returning to figure 6.7, these characteristics are also seen. Here, in the upper plot, we see that for the biotic branch (upper solid blue curve) we have $0.5 \lesssim M_{\rm bio} \lesssim 1.1$ with a maximum around $S/S_0 \approx 1.1$, where $T_s = T_{\rm bio}$. The corresponding response in $f{\rm CO}_2$ is a reduction by $\sim$2 orders of magnitude (lower solid blue curve), as compared to the corresponding warm abiotic saddle branch (lower dashed/solid black curve).

6.3 Perspectives

Using the model results above, let us now draw some perspectives to the motivating factors of this study. Firstly, we shall discuss the effects of biology on climate in relation to the hypothesized Gaian homeostasis in Daisyworld. Secondly, we will look at parallels between the model results and the palaeoclimatic observations.

6.3.1 Biospheric Effects on Climate

To answer whether this model supports a biospheric stabilization of climate or not, let us focus on the upper, stable *biotic* branch, and the upper stable/saddle *abiotic* branch in figure 6.6 (as mentioned below, the lower branch is less suited to draw conclusions from). The blue curve shows that a stable inhabited planet exists for $0.98 \lesssim S/S_0 \lesssim 1.25$, and in this regime, the planet has a surface temperature $T_s \in [284, 320]$ K. The black curve shows that the warm, uninhabited planet exists for $S/S_0 \lesssim 0.87$, and in this regime, the planet has a surface temperature $T_s \gtrsim 284$. As is seen in figure 6.6, the slope of the two curves $\frac{\partial T_{\text{eff}}}{\partial S/S_0}$ for $0.98 \lesssim S/S_0 \lesssim 1.25$ are practically equal. This is important, since it rules out the distinct homeostatic effect of the biosphere as in Daisyworld. Indeed, the biotic branch is practically parallel to the corresponding abiotic branch, only shifted $\sim$13 K. This demonstrates that in this model the effect of the the planetary biosphere is a cooling of the planet by some 13K, as compared to a planet without life. This is a direct result of the removal of CO_2 from the atmosphere due the enhancement of silicate weathering and carbon burial.

Although the curves are parallel, the range of solar luminosities S/S_0 with stable surface temperatures within habitable limits $T_{\text{bio}} \pm \delta T_{\text{bio}}$ are quite different for the two states: $0.87 \lesssim S/S_0 \lesssim 1.21$ for the abiotic and $0.98 \lesssim S/S_0 \lesssim 1.25$ for the biotic solution. This window in solar luminosity with temperatures within habitable limits is thus narrower ($\Delta(S/S_0) \approx 0.27$ for the biotic solution, and $\Delta(S/S_0) \approx 0.34$ for the abiotic) and shifted towards higher luminosities (the center of the window is about 1.12 for the biotic solution and about 1.04 for the abiotic) with biology present. The fact that this window is narrower with biology present actually argues for a *destabilizing* effect of the biology on climate. These results should be contrasted to the results of Daisyworld in chapter 3. Take, for instance, the response in effective temperature of Daisyworld inhabited by white daisies only. As sketched in figures 3.4 and 3.7 showing the effective temperature as function of Daisysun luminosity in the two versions of Daisyworld, the range of luminosities with temperatures within habitable limits of white daisies is clearly larger with the daisies present (the gray curve) than without the daisies (the blue curve) for both versions. This is, again, expressing the biological stabilization of climate in Daisyworld.

The above conclusions are structurally in agreement with the model work of *Lenton* [1998], who shows a slightly larger change in temperature of $\sim$20 K between the biotic and the abiotic state for $S/S_0 = 1$.

6.3.2 Palaeoclimatic Implications

Let us in the following try to draw some perspectives from the results by asking ourselves how they fit into the palaeoclimatic puzzles of Earth? It

should firstly be emphasized that the exact numerics of the above results should perhaps not be given too much weight. This is a simple model. Model results and assumptions in general are discussed further in chapter 7. The values of the steady state solutions depend on the assumed model parameters, but the overall structure does not. This should be adressed by a sensitivity study, in which we examine how variations in the model parameters affect the results. Such a sensitivity study of the effects of the two biological parameters Ω and β, that control the weathering and burial rates, is outlined in 7.1. Silicate weathering is enhanced by land plants, not by e.g. oceanic cyanobacteria. When relating the model results to geological observations, we should therefore primarily focus on times where land plants are believed to have existed.

Snowball Earth Geological evidence supports the occurence of geologically brief extreme glaciations, perhaps of global extent. One of these events is the Neoproterozoic glaciations about $\sim$650 Ma ago. Such a Snowball Earth is obviously a possible outcome of our simple model since the fully glaciated state exist and is stable for $S/S_0 \lesssim 1.4$ as seen in figure 6.6. But how such a state could be entered and, perhaps more importantly, rather quickly left, deserves some attention. Let us briefly touch upon this in light of the simple model.

To this end, we redraw the results shown in figure 6.6 in a slightly different way by showing the corresponding temporal response in surface temperature when letting the solar constant evolve according to equation (2.1). This is depicted in figure 6.8, showing the steady state T_s as function of time before present. As seen in the figure, in the period between 1.7 Ga BP and 0.2 Ga BP there is no biotic steady state, whereas both the stable abiotic Snowball Earth state and the saddle abiotic warm state exist. A Snowball Earth event could thus be seen as a transient jump from the warm saddle branch to the cold stable branch, and back again in this regime of S/S_0 (this is possible since, as we shall see, the cold branch is perhaps not stable at all). This jump could be initiated by the biosphere. Still referring to the figure 6.8, assume that the system has been brought to reside in the warm abiotic state at $t = 700$ Ma, i.e. without the weathering and burial enhancing biology present. This is indicated by the star in the figure. Imagine now that the biosphere is born at $t = 700$ Ma. At this point temperatures *does* allow biology to thrive, but no biotic steady state solution exist. Thus, biology will draw down atmospheric CO_2 and thereby T_s to such a degree that the system inevitably is forced into the cold, Snowball Earth state, which is the only stable state at this time. This, of course, results in the extinction of the biosphere.

Such a scenario is depicted in figure 6.9. It shows the results of a transient model run, where the governing equations (5.10)–(5.12) have been numer-

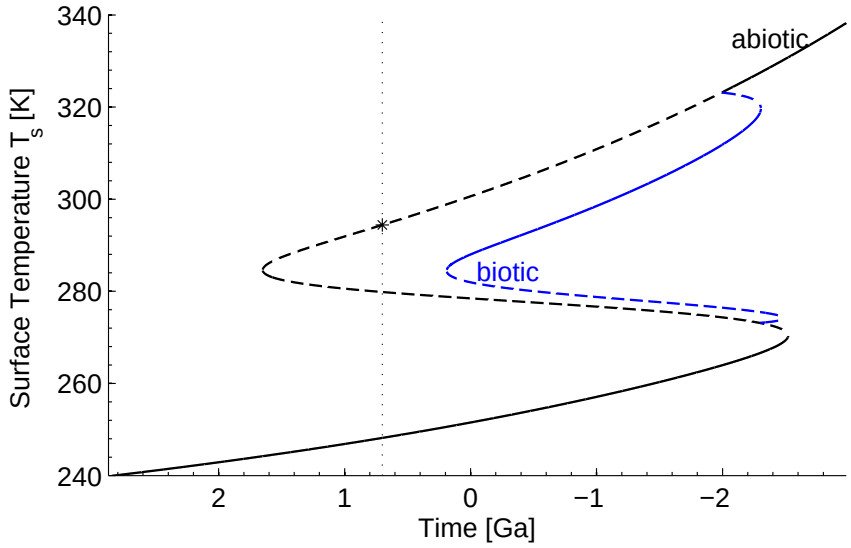

Figure 6.8: Steady state surface temperature T_s as function of time before present.

ically integrated forward in time using a simple Runge-Kutta scheme with the model parameters in table 5.1 and the increasing solar luminosity as given by the relation (2.1). The system starts out from the warm, stable abiotic state with $T_s = 295\,\mathrm{K}$, $M_{\mathrm{bio}} = 0$ and $f\mathrm{CO}_2 = 3 \cdot 10^{-2}$ at $t = 0$, assuming $S/S_0 = 0.943$ which corresponds to $\sim$700 Ma ago. We see that (T_s,M_{bio},$f\mathrm{CO}_2$) are unchanged untill $t = 200\,\mathrm{ka}$. At $t = 200\,\mathrm{ka}$ we pertube the biomass so that $M_{\mathrm{bio}} = 0.01$. M_{bio} then immediately grows up to a value of about 1. This forces $f\mathrm{CO}_2$ to start declining, and thus also T_s starts declining. At $t \approx 375\,\mathrm{ka}$, the system jumps to the cold, glaciated state. T_s is then no longer within habitable limits, and M_{bio} therefore vanishes. $f\mathrm{CO}_2$ then slowly increases towards stable levels, with the increase in T_s following behind (see also appendix A.4 where a plot of the same model run is shown for longer periode of integration).

But how, then, is this stable Snowball Earth state left? As mentioned below, one could argue that we have probably underestimated the decline in weathering in cold climates in our model to such a degree that the Snowball Earth state is actually unstable. A planet with surface temperatures much lower than present, and with snow and ice covering continental areas, and a hydrological cycle close to shut-down, will have weathering rates close to zero. With weathering shut off, volcanism would serve to fill the atmosphere with CO_2. After sufficient time, the greenhouse effect warms the planet enough to abruptly melt the ice-cover (this timespan is on the order of 10 million years, as estimated from present day volcanic outgassing rate and the amount of CO_2 needed to sustain sufficiently warm temperatures,

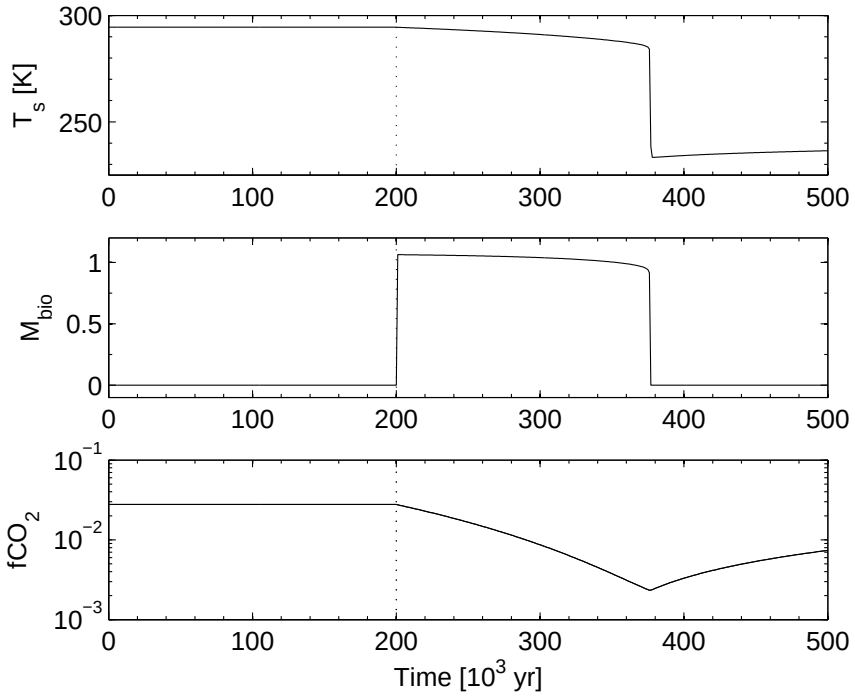

Figure 6.9: Surface temperature (top panel), biomass (middle panel) and carbon dioxide mixing ratio (bottom panel) as function of time for a transient model run initiated from the stable warm abiotic state at $S/S_0 = 0.943$ which corresponds to $\sim$700 Ma ago. At $t = 200$ ka we set $M_{\rm bio} = 0.01$. This ultimately forces the transition to the cold state at $t \approx 375$ ka.

$p\mathrm{CO}_2 \sim 0.3$ bar, cf. [*Kasting and Catling*, 2003]). This would create a temporary CO_2 hot-house untill the weathering again depletes the CO_2 to buffer the volcanism, and we are back where we started. It should be stressed that this scenario of how to escape the Snowball Earth demands a more proper treatment of the radiative effects of CO_2 than presented here, since $f\mathrm{CO}_2$ can not support high enough temperatures to escape Snowball Earth, as seen in figure 6.2. Contamination of the ice, e.g. from volcanic dust, and its decrease of the planetary albedo could ease this thawing process, as could also increased contents of other greenhouse gases such as methane.

FYS paradox As for the Faint Young Sun paradox we note again from figure 6.8 that for before ~ 1.7 Ga ago, only the cold, fully glaciated state exists. This contrasts with the geological evidence, supporting that through most of the time back to $\sim$3.5 Ga, Earth has indeed been warm and inhabitable, and only subjected to extreme glaciations a few times. As pointed towards above, a purely abiotic CO_2 mechanism operating through the dependence of

silicate weathering upon temperature (and the hydrological cycle) has been proposed, see e.g. [*Walker et al.*, 1981]. In a simple formulation [*Ditlevsen*, 2005], this builds on the fact that for a completely ice-covered Earth, the hydrological cycle is more or less completely switched off. In the present model, this means that for surface temperatures $T_s \lesssim T_{\text{ice}} + \Delta T_{\text{ice}} = -10°\text{C}$, we should take $W_{\text{sil}} = 0$ in equation (5.12). Below this threshold temperature, the CO_2 in the atmosphere is governed solely by the input from volcanism, since volcanism is not influenced by the planetary freeze-over; the biological carbon burial is inactive in this temperature regime, too. When T_s falls below $-10°\text{C}$, $f\text{CO}_2$ will climb towards higher levels, slowly increasing surface temperatures. This switches weathering back on and temperatures should rise to levels where weathering buffers the volcanic input [*Ditlevsen*, 2005] (the $f\text{CO}_2$ dependence complicates things in the current model a bit). In figure 6.6, this should cause the lower abiotic Snowball Earth branch, where $T_s < -10°\text{C}$, to disappear, and instead a warmer, non-steady state branch would appear. This is a geochemically mediated thermostat for surface temperatures on Earth [*Ditlevsen*, 2005]. As we shall briefly touch upon in the next chapter, however, it seems that the CO_2 levels needed to compensate for the fainter Sun are inconsistently high when compared to geological observations [*Rye et al.*, 1995]. This means that some other solution to the FYS paradox must be found.

6.4 Summary

A simple Earth system model has been outlined above, focusing on the long-term coupling between climate and biosphere through the content of atmospheric carbon dioxide.

This highly simplified model points, despite its simplicity, towards an important long-term biospheric regulation of the the planetary climate. This originates in a well-established biotic draw-down of atmospheric CO_2 related to enhancement of silicate weathering and carbon burial rates. For a wide range of solar constants S/S_0 this causes a cooling of the planet by some 13 K, as compared to the uninhabited planet. The range of S/S_0 with habitable surface temperatures is shifted towards higher luminosities by the biosphere, and the width of this range somewhat narrower, as compared to the uninhabited planet. Our model is a step towards more realism as compared to the parable of Daisyworld, in which a homeostatic effect of the biosphere on the climate is seen as a result of a more speculative biospheric control of the planetary albedo. Our model does not show this homeostasis; This, then, seems not to be a generic property of the life-climate connection.

The model supports a possible biospheric explanation for the occurence of Snowball Earth events. The Neoproterozoic glaciations could be results of biospheric weathering enhancement associated with an early colonization

of land, although this remains somewhat speculative. The model poses no biospheric solution to the FYS paradox. In order to explain the apparant ice-free climate of the early Earth, in spite of a fainter Sun, as a result of life, the warming effect of a methane producing early biosphere is a better candidate in light of this simple model.

7 Discussion

In the preceeding two chapters, a conceptual climate-biosphere model was first presented, and the results of this model then computed and put into the perspectives of biotic homeostasis and palaeoclimatology. In this chapter we firstly discuss the assumptions upon which the model is build. Secondly, the validity of the model results and thus the implied perspectives are discussed. At the end, an extension of the conceptual modelling of climate-biosphere interactions over geological timescales is very briefly suggested, focussing on the effects of methane. This last point serves as a suggestion for further work in the field.

7.1 Parameters of the Model

Let us firstly touch upon the importance of the model parameters. The model is characterized by a considerable number of model parameters, as is evident from table 5.1. The choice of these have been motivated by various physical, biological and chemical reasoning and assumptions. Two points deserve attention in this context: Firstly, we have aimed at keeping the number of less-constrained model parameters at a minimum—i.e. avoiding to introduce some parameter out of the blue. Secondly, uncertainties on the model parameters, and how these propagate into the model behaviour and results, should be addressed. Let us content ourselves to focus on the effects of the two biological parameters Ω and β, that control the silicate weathering and organic carbon burial rates, respectively, in the long-term carbon cycle.

$\underline{\Omega}$ In appendix A.5 is shown the results when using a somewhat smaller enhancement factor of silicate weathering of $\Omega = 2$, and a somewhat

larger value of $\Omega = 10$ compared to the value of $\Omega = 5$ in table 5.1, with all other parameters unchanged. These values are the extreme values reported earlier. In the bifurcation diagrams we see that the stable biotic solution does not change considerably in any of the variables T_s, M_{bio} and $f\text{CO}_2$ between the two Ω values. This is because the model is scaled to yield a steady state for present day biotic conditions. The abiotic solution is, however, affected by a change in Ω: Decreasing the biotic enhancement factor Ω of silicate weathering increases the abiotic weathering rate (due to the scaling of W_0), which in turn decreases the steady state abiotic $f\text{CO}_2$, and thus T_s. At $S/S_0 = 1$ the difference in T_s between the stable biotic state and the saddle abiotic state is $\sim$20 K for $\Omega = 10$, and $\sim$10 K for $\Omega = 2$. This should be compared to the difference in T_s between the stable biotic state and the saddle abiotic state of $\sim$13 K for $\Omega = 5$. Although the numerical values do change, it is fair to say that the *overall structure* of the solutions does not change much.

$\underline{\beta}$ In appendix A.5 is also shown the results when varying the organic carbon burial fraction β. Here, we have simply multiplied the value of $\beta = 4.1 \cdot 10^{-4}$ in table 5.1 by a factor of 5 and 1/5, with all other parameters unchanged. This results in a change of the bifurcation diagrams similar to the one described above. The stable biotic solution does not change considerably in any of the variables T_s, M_{bio} and $f\text{CO}_2$ between the two β values, whereas the biotic solution does. Now, decreasing the burial fraction β decreases the volcanic outgassing rate V (due to the scaling of the model), which in turn decreases the steady state abiotic $f\text{CO}_2$, and thus T_s. At $S/S_0 = 1$ the difference in T_s between the stable biotic state and the saddle abiotic state is $\sim$15 K for $\beta = 5\beta_0$, and $\sim$10 K for $\beta = \beta_0/5$. Again, we dare to say, however, that there are only little changes with respect to the overall structure.

7.2 Assumptions of the Model

In the following, the foundation of the conceptual climate-biosphere model is discussed by outlining some of the most important assumptions. We will thus try to act as the Devil's advocates on the model.

General assumptions Our simple Earth system model is subjected to several assumptions. The choice of which assumptions and simplifications are made is important, since this limits the application and thus sets the usability of the model. A chain is not stronger than its weakest link, and this undoubtedly also applies to any model of the Earth system.

The spatial zero-dimensionality is the first simplification, since the variables we are examining actually are given as two- or three-dimensional quan-

tities, as the surficial extent of ice and snow, and the surface temperature. The first dimension to include should be latitude. The solar insolation is non-uniformly distributed with the polar regions receiving less than the tropical regions. This is essentially what drives most of the atmospheric circulation, and contributes to the oceanic thermohaline circulation. The second dimension should be the vertical.

Regarding the temporal resolution, we have performed a separation of timescales and focused on mechanisms of interaction on the order of hundred of thousands years of years, and then parameterized the short-term mechanisms. Short-term variability of quantities is thus neglected. This could be implemented by using the approach in the analysis of Daisyworld section 3.3.1. Here, the governing quations of the system were supplemented by a stochastic noise-term.

Climate We have parameterized the state of all the (non-living) components of the climate by the global mean surface temperature T_s. This means that the state of the ocean, atmosphere and ice-caps is assumed to be given as a function of T_s. This is of course a crude simplification. The surface temperature is assumed to be determined by a simple energy balance of the planet. The parameterizations of the OLR and the ISR in this energy balance are important for the model. For the OLR, we have assumed very simple dependencies upon H_2O and fCO_2 based on extrapolation of relations perhaps way beyond legitimate limits. Also, for the ISR, the planetary albedo depends on atmospheric composition, due to scattering and absorption in the atmosphere. These effects on the radiative balance call for a more sophisticated radiative-convective model (RCM).

Biosphere We have parametrized the biosphere by a relative global mean biomass, endorcing all biology, and this was assumed to be governed by a logistic growth model. The link from the climate to the biosphere, operating through the dependency of the growth function upon surface temperature only, is of course a crude simplification of the limiting factors for biology: Energy (light and wavelength), food, water, enemies, nutrients etc. We have excluded the effects from CO_2 fertilization/starvation on the net primary production. Furthermore, several model parameters were introduced to scale the model.

Carbon cycle The atmospheric CO_2 mixing ratio has been taken to be governed by a simple long-term carbon cycle model. In this, we have disregarded the effects from variations in other atmospheric constituents, although we compute fCO_2 to vary many orders of magnitude. The organic carbon burial rate has, somewhat arbitrarily, been assumed to increase linearly with biomass. The silicate weathering rate has furthermore been as-

sumed less temperature dependent than normally quoted, and the volcanism treated as constant. The chosen CO_2 dependence is also uncertain [*Tajika*, 2003]. A partitioning of the CO_2 reservoir between ocean and atmosphere is not made.

Now, one might ask whether this simple Earth model is anything more than some artificial system completely out of touch with reality? Can we use such a simple model at all, knowing that it is subjected to a long list of erroneous assumptions? I believe we can, yes.[1]. We should, however, only use it with caution, especially when it comes to the exact numerical results, since these depend on the chosen values of the model parameters.

7.3 Comparison with Observations

A sound scientific study presents a test of a given theory, or model, against some data, from which the model can be either accepted or rejected by some level of certainty. In the following we shall try to outline such a test of the results of the model. This discussion relates firstly to the numerical results, i.e. the temperature, CO_2 and biomass as function of solar luminosity. Let us repeat the quantitative results of the model and compare these to observational indications. This should be based on examination of data records, e.g. of $\delta^{13}C$ and $\delta^{18}O$ measurements, that can be used to infer biomass and temperature back in time. The content of atmospheric CO_2 can be inferred from e.g. palaesols, that are portions of ancient soils (see apendix A.1).

In figure 6.6 we saw that steady state surface temperatures on Earth should be $T_s \lesssim 245\,\mathrm{K}$ for $S/S_0 \lesssim 0.87$, i.e. Earth is uninhabited and a fully glaciated Snowball, and $T_s \gtrsim 330\,\mathrm{K}$ for $S/S_0 \gtrsim 1.28$, i.e. Earth is uninhabited and dessert-like. Referring to figure 6.7, the corresponding atmospheric CO_2 mixing ratio should be $f\mathrm{CO}_2 \gtrsim 10^{-1}$ for $S/S_0 \lesssim 0.87$ and $f\mathrm{CO}_2 \lesssim 10^{-3}$ for $S/S_0 \gtrsim 1.28$. Such low values for prehistoric T_s for $S/S_0 \lesssim 0.87$, corresponding to $\sim$1.7 Ga years ago, contradict with the Faint Young Sun paradox, cf. section 2.1.1. The extremely high $f\mathrm{CO}_2$ values for $S/S_0 \lesssim 0.87$ are furthermore unrealistic and contradicts with indications from palaesol data, supporting $f\mathrm{CO}_2$ values $\lesssim$100 times present day values at $S/S_0 = 0.8$ [*Rye et al.*, 1995] (see appendix A.1).

Within the region $0.87 \lesssim S/S_0 \lesssim 1.28$ two possible types of steady state solutions exist for Earth, see again figures 6.6 and 6.7. For the *abiotic* solutions, surface temperature exhibits bistability: a glaciated state exist with $245\,\mathrm{K} \lesssim \mathrm{T_s} \lesssim 270\,\mathrm{K}$ and $f\mathrm{CO}_2 \gtrsim 10^{-1}$, and a de-glaciated state with $285\,\mathrm{K} \lesssim \mathrm{T_s\,K} \lesssim 330\,\mathrm{K}$ and $10^{-3} \lesssim f\mathrm{CO}_2 \lesssim 10^{-2}$. Again, the glaciated

[1] For the same reason that people living before the 16^{th} century could navigate on the oceans by use of maps that held the Earth was flat

state has extremely high values of fCO_2. As pointed towards above, this stable Snowball Earth is unrealistic. In this range of solar luminosities, the *biotic* type of solutions also exists for $0.98 \lesssim S/S_0 \lesssim 1.25$. In this region, the stable solution biomass varies within $0.5 \lesssim M_{\text{bio}} \lesssim 1.1$ with a maximum around $S/S_0 \sim 1.1$. This means that the system only has stable states with biology present after ∼200 Ma ago. This timing is somewhat different from the estimated colonization of land ∼480–460 Ma ago. This biotic state has surface temperature $285\,\text{K} \lesssim T_s \lesssim 320\,\text{K}$ and mixing ratio $10^{-4} \lesssim fCO_2 \lesssim 10^{-3}$ which are of course reasonable values simply due to the fact that the model has been scaled to present day conditions. The surface temperature is some 13 K less than the non-glaciated abiotic state, and the carbon dioxide mixing ratio ∼2 orders of magnitude smaller.

As shown above, several of the results are rather problematic when compared to observations. As such, this should lead us to question the validity of this Earth system model. Regarding the exact values of the above quantitative results, one should, however, only draw strict conclusions with precautions, since this *is* a conceptual model. It is my believe that the model can still be used to draw more qualitative conclusions from. As we saw in section 6.3.2, we are led to draw two conclusions:

One is related to palaeoclimatology. The Neoproterozoic Snowball Earth events at ∼650 Ma, just prior to the Cambrian explosion, could be initiated by an early colonization of land by fungi and plants at ∼700Ma, as indicated by molecular clocks [*Heckman et al.*, 2001], although this remains somewhat speculative since indisputable fossil evidence first appears at ∼480–460 Ma. This land colonization would have caused CO_2 to decline due to the increase in weathering and burial rates, and thus led Earth into an extreme glaciation. Such a biospheric initiation of a Snowball Earth is obviously a highly non-homeostatic effect of life. It should be stressed that our results are not revolutionary news in the field; rather, our work represents an understanding of this mechanism within the framework of a simple model. The timing of the initiation of biology in the model is somewhat off compared to observations, as stressed above. This still does not change the conclusion that an initiation of biology before the climate-biosphere system has a stable biotic steady state, i.e. before solar luminosity is high enough, could force the system into a Snowball Earth. However, the termination of the Snowball Earth event is not captured by the model.

In this connection, it should also be mentioned that another, related but non-biological, explanation of the initiation of the Neoproterozoic Snowball Earth is related to the break-up of a super-continent, positioned towards the warmer and moister equatorial regions. This continental positioning in itself would serve to increase global weathering rates [*Tajika*, 2003]. Also, with the darker ocean towards polar regions and the brighter continents towards equatorial regions, the planetary albedo would be relatively high and thus favor a planetary cooling. See also the alternative explanations in chapter

2.1.2.

The other qualitative result is of more philosophical nature, namely that the model does *not* support a biospheric stabilization of climate, when considering the response to a varying solar luminosity, as has been alluted to in Daisyworld. On the contrary, the range of solar luminosities with temperatures within habitable limits is narrower for a planet with biology present than for a planet *without*. How could such a hypothesis be tested? Well, one way could be to look at conditions on other planets. Such a test is of course somewhat problematic, since we only have a limited number of planets to examine, and only one of these is inhabited. At the moment, the hypothesis is thus hard to falsify. We can only wait for the discovery of more planets with life...

The big question is whether the above results could be representative for conditions on Earth? Is this all there is to say about the long-term effects of biosphere-climate coupling: the biosphere draws down fCO_2 by about 2 orders of magnitude and thereby lowers the surface temperature by some 13 K, as compared to an abiotic planet? Well, surely life has changed the environment on Earth in dusins of other ways. But when investigating the effects of the enhancement of silicate weathering and carbon burial, then this is a primary effect in the real world, although the numbers are perhaps not exact.

7.4 Outlook

We end this chapter by returning to the The Faint Young Sun paradox. As previously stressed, a likely solution to this problem is through increased content of greenhouse gases in the atmosphere. However, CO_2 seems not to be the entire solution. Methane could be a likely candidate for the missing part of the solution, see e.g. [*Pavlov et al.*, 2000]. CH_4 is a potent greenhouse gas and, highly important in the current context, the content of CH_4 in the atmosphere is related to biology [*Kasting and Siefert*, 2002; *Kasting and Ono*, 2006; *Kasting*, 2005]. This is due to methanogenic bacteria that give of CH_4 as a byproduct of their metabolism. Today, such bacteria are found in oxygen-free settings, such as inside the guts of a cow. However, on an Earth with low atmospheric oxygen levels before $\sim$2.3 Ga, such bacteria could have flourished the planet [*Nisbet and Sleep*, 2001; *Kasting*, 2004].

In the simple model above, only the content of CO_2 in the atmosphere was allowed to change. Implementing the radiative effects of CH_4 is therefore an obvious choice when trying to extend our simple biosphere-climate model with focus on the atmospheric composition. This calls for a much more sophisticated biogeochemical modelling to compute the atmospheric content of CH_4, involving also O_2 and H_2.

As shown above, the biospheric effects of CO_2 is a depletion and hence a

planetary cooling. The biospheric effects on CH_4, on the contrary, is source-like, and hence a planetary *warming*. This would thus seem to pose a somewhat stabilizing effect of the climate-biosphere coupling. The Palaeoproterozoic glaciations at $\sim$2.3 Ga, accompanying the Great Oxidation Event, could be the the result of a collapse of such a methane greenhouse [*Kasting*, 2006; *Goldblatt et al.*, 2006]. This collapse could be a direct effect of the biospheric invention of oxygenic photosynthesis [*Kopp et al.*, 2005].

The concept of the biospheric control of atmospheric composition is a key component of Gaian theory [*Watson and Lovelock*, 1983; *Lenton*, 1998]. To some extent, Gaian theory is simply the study of the global biogeochemical cycles [*Volk*, 2002]. As such, setting up such a model is still a pursue of Gaian ideas...

7.5 Summary

In the preceeding two chapters, a simple Earth system model was first setup and the response of this to an increasing solar luminosity then computed. In the above, the assumptions of the model was first outlined, emphasizing that the model is indeed simple. We saw that the results naturally depends on the assumed model parameters. This was followed by an attempted validation of the numerical model results. From this we were led to conclude that the model can only be used as an indicator of more general patterns.

8 Conclusion

The aim of this thesis has been to investigate the interactions between climate and biosphere over geological timescales using a conceptual modelling approach.

The study has been motivated from two different sides: An observational and a modelling part. The observational motivation stems from geological evidence, indicating that surface temperatures on Earth has been within habitable limits for most of our planet's $\sim$4.6 Ga history, in spite of considerably less luminous younger Sun (the Faint Young Sun paradox), and only for a few geologically briefer periods has Earth been subjected to extreme glaciations (the Snowball Earth events). These contrasting phenomena are both likely related to variations in the greenhouse effect of our planet, and these variations, in turn, are likely results of the biological influence on the atmospheric composition. The modelling motivation stems from the Gaian Daisyworld model, advocating for a strongly stabilizing effect of biology on climate.

Two primary steps have been taken, concerning the understanding of the interactions of climate and biology from simple models. Firstly, the Gaian Daisyworld was reviewed. Here, the purely homeostatic effect of biology on climate was challenged, and it was shown that the model actually exhibits climatic bistability due to the presence of biology. Also, the underlying assumptions of Daisyworld as a conceptual climate-biosphere model were critizised.

Secondly, as the most important result of this thesis, a conceptual model of the climate and biosphere, operating through the atmospheric content of CO_2, was set up and analyzed. In this simple model, the biosphere was found to draw down CO_2 levels by some 2 orders of magnitude as a result of the biotic enhancement of silicate weathering and organic carbon burial,

resulting in a cooling of the planet by about 13 K for a wide range of solar luminosities, as compared to an uninhabited planet. We found that the range of solar luminosities with habitable surface temperatures is shifted towards higher luminosities by the biosphere, and the width of this range is somewhat narrower, as compared to an uninhabited planet.

The Gaian homeostatic effect of the biosphere on climate is not a property of this simple model. Furthermore, the model points towards a possible biotic origin of the Neoproterozoic extreme glaciations, although this remains somewhat speculative. As such, the model can be seen as a first step towards more realism, as compared to the parable of Daisyworld. Our simple model poses no biospheric solution to the Faint Young Sun paradox. In order to explain the mostly ice-free climate of early Earth, in spite of a fainter Sun, as a result of life, the warming effect of a methane producing early biosphere is an obvious candidate in light of this simple model.

The simple model presented in this thesis is, in its nature, only suggestive of the exacts numerics. And it surely is to go too declare the Neoproterozoic Snowball Earth events fully explained by such a simple model. For this, our model is subjected to far too many simplifications and assumptions. Nevertheless, it is our believe that it points towards actual and important long-term interactions between climate and biosphere.

A Appendix

A.1 Nomenclature

This section briefly describes some names and concepts of the thesis.

The geological timescale Eons separate Earth's history into four: The Hadean (∼4.5–3.8 Ga), the Archaean (∼3.8–2.5 Ga), the Proterozoic (∼2.5–0.55 Ga), and the Phanerozoic eon (from ∼0.55 Ga an onwards). The Precambrian super-eon covers the Hadean, the Archaean, and the Proterozoic eons. Eons are subdivided into eras, eras into periods, and periods into epochs. Often used prefixes are Palaeo (early or old), Meso (mid or middle), and Neo (late or new).

Ga, Ma and ka The convention on the geological time scale is: 1 Ga = 1 Giga-anni = 10^9 years, 1 Ma = 1 Mega-anni = 10^6 years, and 1 ka = 1 kilo-anni = 10^3 years. "Before present", or BP, is often left out and taken to be implicit.

GHG Greenhouse gas

OLR Outgoing Longwave Radiation.

ISR Incoming Shortwave (Solar) Radiation.

δ^{13}C Carbon isotope ratio. Used as proxy-indicator of biology.

δ^{18}O Oxygen isotope ratio. Used as temperature proxy.

FYS paradox Faint Young Sun paradox.

Snowball/Slushball Earth Extreme glaciation of the Earth. In the Snowball Earth hypothesis, the planet is completely covered in ice. In the Slushball Earth hypothesis, the planet is only partially covered in ice. In this thesis, we refer to extreme glaciations as Snowball Earth events, but this should not be taken too strict.

Palaeosols Preserved portions of ancient soil, now found as fossils. Several findings of fossil soils, dated to originate in the period from 2.75 to 2.2 Ga BP, have been examined for various chemical constituents, among these siderite ($FeCO_3$). For siderite to be present in the soils of an, at that time, anoxic Earth sufficiently high soil CO_2 partial pressures at the time of formation are needed. The fact that none of these palaesol findings contain siderite is taken as evidence for an atmospheric CO_2 partial pressure below this limit at 2.75–2.2 Ga BP.

A.2 Analysis of a 2D System

Linearization

In the following, the technique of linearization of a two-dimensional system is outlined, see e.g. [*Strogatz*, 1994]. We will consider the following system of equations

$$\begin{aligned} \dot{x} &= f(x,y) \\ \dot{y} &= g(x,y), \end{aligned} \tag{A.1}$$

where the dot denotes differentiation with respect to time. Assume that the system (A.1) has a fixed point in $(x,y) = (x^*, y^*)$, meaning that

$$f(x^*, y^*) = g(x^*, y^*) = 0. \tag{A.2}$$

We will consider small pertubations away from the steady state by defining $x' = x - x^*$ and $y' = y - y^*$. We next compute the temporal derivative of this pertubation, first for the x-component:

$$\begin{aligned} \dot{x'} &= \dot{x} \\ &= f(x^* + x', y^* + y') \\ &= f(x^*, y^*) + \frac{\partial f}{\partial x}\Big|_* x' + \frac{\partial f}{\partial y}\Big|_* y' + O\big((x')^2, (y')^2, x'y'\big) \\ &= \frac{\partial f}{\partial x}\Big|_* x' + \frac{\partial f}{\partial y}\Big|_* y' + O\big((x')^2, (y')^2, x'y'\big), \end{aligned} \tag{A.3}$$

where the partial derivatives are evaluated in the fixed point (x^*, y^*). Here we have first used the definition of x' twice, then made a Taylor-expansion

around the fixed point, and lastly used equation (A.2). A similar calculation for the y-component yields

$$\dot{y'} = \frac{\partial g}{\partial x}\Big|_* x' + \frac{\partial g}{\partial y}\Big|_* y' + O\big((x')^2, (y')^2, x'y'\big). \tag{A.4}$$

If we neglect the qudratic terms in (A.3) and (A.4) we thus arrive at the following linearized system:

$$\begin{pmatrix} \dot{x'} \\ \dot{y'} \end{pmatrix} = \begin{pmatrix} \frac{\partial f}{\partial x} & \frac{\partial f}{\partial y} \\ \frac{\partial g}{\partial y} & \frac{\partial g}{\partial y} \end{pmatrix}_{(x^*,y^*)} \begin{pmatrix} x' \\ y' \end{pmatrix}. \tag{A.5}$$

This set of equations can thus be used to approximate how small pertubations away from the fixed point (x^*, y^*) will evolve. The matrix on the right-hand-side is the Jacobian matrix evaluated in the fixed point:

$$\mathbf{J} = \begin{pmatrix} \frac{\partial f}{\partial x} & \frac{\partial f}{\partial y} \\ \frac{\partial g}{\partial y} & \frac{\partial g}{\partial y} \end{pmatrix}_{(x^*,y^*)} \tag{A.6}$$

Classification of Stability

Next, let us consider how the above can be used to understand the dynamics of the original system (A.1) from the linearized system (A.5) and the Jacobian matrix $\mathbf{J}$ in (A.6). For this we will now define the vector $\mathbf{x}'(t) = \big(x'(t), y'(t)\big)$ and seek solutions to (A.5) on the form

$$\mathbf{x}'(t) = e^{\lambda t}\mathbf{v}. \tag{A.7}$$

Here, $\mathbf{v} \neq \mathbf{0}$ is some constant vector and λ a scalar that need to be determined. Inserting this in (A.5) we arrive at

$$\lambda e^{\lambda t}\mathbf{v} = \mathbf{J}e^{\lambda t}\mathbf{v}. \tag{A.8}$$

By cancelling the common factor of $e^{\lambda t}$ we get the eigen-equation:

$$\mathbf{J}\mathbf{v} = \lambda\mathbf{v}. \tag{A.9}$$

Thus, the solution (A.7) exists if $\mathbf{v}$ is an eigenvector of $\mathbf{J}$ with corresponding eigenvalue λ. Such a *eigensolution* moves in phase space along the eigenvector $\mathbf{v}$ with a speed (and direction) given by the eigenvalue λ.

To take the stability analysis further, we must compute the eigenvalues and eigenvectors of the Jacobian $\mathbf{J}$. The eigenvalues are found from the characteristic equation of $\mathbf{J}$.

$$\det(\mathbf{J} - \lambda\mathbf{I}) = 0, \tag{A.10}$$

where **I** is the identity matrix. The solutions of this can, by simple manipulations, be shown to yield:

$$\lambda = \frac{\tau \pm \sqrt{\tau^2 - 4\Delta}}{2}, \tag{A.11}$$

where τ and Δ denotes the trace and the determinant of the Jacobian **J**, respectively. From these eigenvalues, the stability of the fixed point (x^*, y^*) can then be characterized. The eigenvectors describe the geometry of phase space close to the fixed-point.

A.3 Daisyworld

This section contains some additional material on the Daisyworld model.

Constants and Parameters

The used constants and parameters are listed in table A.1. The model is

Parameter	Description	Value I (II)
σ	Stefan-Boltzmann constant	$5.67 \cdot 10^{-8}\ Wm^{-2}K^{-4}$
S_0	Daisysun Solar constant	$3.668 \cdot 10^{3}\ Wm^{-2}$
p	areal extent of fertile ground	1
γ	death rate of daisies	$0.3\ s^{-1}$
T_0	optimal temperature for daisy growth	22.5°C
μ	temperature sensitivity for daisy growth	$3.265 \cdot 10^{-3}\ K^{-2}s^{-1}$
A_w	albedo of white daisies	0.75
A_b	albedo of black daisies	0.25 (0.80)
A_g	albedo of bare ground	0.50
A_w^T	'T-albedo' of white daisies	0.75
A_b^T	'T-albedo' of black daisies	0.25
q	surface heat exchange linear. coefff.	$20\ K$

Table A.1: Variables and constants of Daisyworld. Only the value of A_b changes from version I to version II. Values are equivalent to the values used in [*Watson and Lovelock*, 1983].

investigated by setting $S = s \cdot S_0$ and varying s in $[0.5, 1.7]$. By choosing different values for the model parameters, the dynamics of the system will, naturally, change radically. We have not gone into such an exploration of model parameters.

The Numerical methods

We solve the system for steady states by use of numerical methods, but apply a different method as the one used in [*Watson and Lovelock*, 1983]

(their method is mentioned below).

Using $a_b^* = 0$ for the white-only steady states, the system (3.1) with the simplified parameterizations (3.2)–(3.6) inserted reduces to a single equation, $F_w(a_w^*, 0) = 0$, in one unknown, $a_w^* > 0$:

$$0 = a_w^* \left[\left(p - a_w^* \right) \left(1 - \mu \left[T_0 - \left(\sqrt[4]{\frac{S}{4} \frac{1 - \left(a_w^* A_w + (1 - a_w^*) A_g \right)}{\sigma}} + q \left(a_w^* A_w + (1 - a_w^*) A_g - A_w^T \right) \right) \right]^2 \right) - \gamma \right] \tag{A.12}$$

The steady states can then be found using a numerical root-finding method, e.g. the bisection method [*Kreyszig*, 1999]. Similar reasoning applies to the black-only steady states with $a_b^* = 0$ and $a_w^* > 0$.

For the full biotic case, i.e. $a_w^* > 0$ and $a_b^* > 0$, when inserting the parameterizations (3.2)–(3.6) in the governing equations (3.1), we need to solve two equations, $F_w(a_w^*, a_b^*) = 0$ and $F_b(a_w^*, a_b^*) = 0$, in two unknowns, a_w^* and a_b^*, to find the steady states. This task can by inspection be reduced to solving a single equation in one unknown, see [*Saunders*, 1994]. A similar approach can be then used as in the simplified cases above. (Finding the zeros of a function of one variable is a simpler task to perform numerically than functions of multiple variables.) To see this, assume $a_w^* > 0$ and $a_b^* > 0$. To fulfill $\frac{da_i}{dt} = 0$ in equation (3.1) for both types of daisies a_w^* and a_b^*, we must have

$$a_{\text{bare}}(a_w^*, a_b^*) U_{\text{growth}}(T_s^i) = \gamma \tag{A.13}$$

for both a_w^* and a_b^*, and hence $U_{\text{growth}}(T_s^b) = U_{\text{growth}}(T_s^w) = U_{\text{growth}}$ is constant. By assumption, $T_s^b > T_s^w$, and therefore equation (3.3) for U_{growth} yields $T_s^b + T_s^w = 2T_0$. Futhermore, from (3.4) we find that $T_s^b - T_s^w = q(A_w^T - A_b^T)$. This combines to yield

$$\begin{array}{rcl} T_s^b & = & T_0 + \frac{q}{2}(A_w^T - A_b^T) \\ T_s^w & = & T_0 - \frac{q}{2}(A_w^T - A_b^T). \end{array} \tag{A.14}$$

The steady state local surface temperatures are thus independent of S/S_0. Re-inserting this in (3.3) gives

$$U_{\text{growth}} = 1 - \mu \left[\frac{1}{2}(A_w^T - A_b^T) \right]^2 .$$

From (A.13) we have that $a_{\text{bare}} = \frac{\gamma}{U_{\text{growth}}}$. By inserting this and the above in equation (3.2) for a_{bare} and rearranging terms, we find

$$a_w^* + a_b^* = p - a_{\text{bare}} = p - \frac{\gamma}{1 - \mu \left[\frac{1}{2}(A_w^T - A_b^T) \right]^2}. \tag{A.15}$$

The total areal cover of daisies in a steady state full biotic is thus independent of S/S_0. This relation (A.15) can then be used to reduce the system. Insert, e.g.,

$$a_w^* = -a_b^* + p - \frac{\gamma}{1 - \mu \left[\frac{1}{2}(A_w^T - A_b^T) \right]^2} \tag{A.16}$$

in (3.5) to reach an expression of A_p as function of a_b^*:

$$A_p(a_b^*) = A_w + \frac{\gamma(A_g - A_w)}{1 - \mu\left[\frac{1}{2}(A_w^T - A_b^T)\right]^2} + (A_b - A_w)a_b^*.$$

Using this expression as (3.6) is inserted in (3.4), and using (A.14), we reach a single equation in one unknown that must be solved for a_b^*:

$$T_0 + \frac{q}{2}\left(A_w^T + A_b^T\right) = qA_p(a_b^*) + \sqrt[4]{\frac{S}{4}\frac{1 - A_p(a_b^*)}{\sigma}},$$

that implies a fourth order equation in a_b^*. a_w^* is then determined by equation (A.16). As shown in chapter 3, it turns out that a single legitimate solution exists for a wide range of solar luminosities S/S_0 for version I, and likewise a single solution exists for version II, but for a more narrow range of S/S_0.

The method in [*Watson and Lovelock*, 1983] for solving the system for steady state for a given solar luminosity is by forward integration of the governing equations (3.1) in time from some initial condition by a numerical scheme. The initial condition is chosen as either the previous steady state, i.e. from the previous solar luminosity iteration, or, if this was zero, 0.01. This procedure is applied for three biotic cases: the simplified system with white daisies only, the simplified system with black daisies only, and the full system with both black and white daisies (for Daisyworld II it seems that only the last case is applied). The unstable fixed points are not found using this method. This can be justified from the fact that the system can not reside in these points of phase space, given just a minimal amount of pertubative noise. However, the abiotic fixed point is nevertheless shown, although this is actually an unstable fixed point for a range of S/S_0. Furthermore, the method only finds at most one stable fixed point for a given solar luminosity. Also, the step size in solar luminosity can also influence which steady state is found.

A.4 Transient Response of the Simple Model

Figure A.1 shows the results of a transient model run, where the governing equations (5.10)–(5.12) have been numerically integrated forward in time using a simple Runge-Kutta scheme with the model parameters in table 5.1 and the increasing solar luminosity as given by the relation (2.1). The system starts out from the warm, stable abiotic state with $T_s = 295\,\mathrm{K}$, $M_{\mathrm{bio}} = 0$ and $f\mathrm{CO}_2 = 3 \cdot 10^{-2}$ at $t = 0$, assuming $S/S_0 = 0.943$ which corresponds to $\sim$700 Ma ago. At $t = 200\,\mathrm{ka}$ we pertube the biomass so that $M_{\mathrm{bio}} = 0.01$. Figure 6.9 in section 6.3.2 is a zoom-in on this figure.

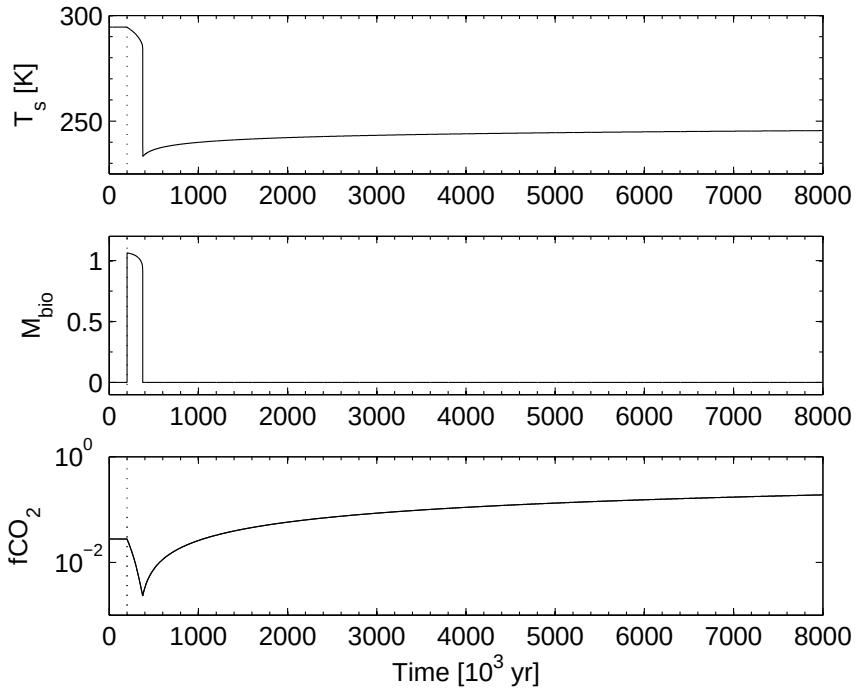

Figure A.1: Surface temperature (top panel), biomass (middle panel) and carbon dioxide mixing ratio (bottom panel) as function of time for a transient model run initiated from the stable warm abiotic state at $S/S_0 = 0.943$ which corresponds to $\sim$700 Ma ago. At $t = 200$ ka we set $M_{\rm bio} = 0.01$. This ultimately forces the transition to the cold state at $t \approx 375$ ka. $f\mathrm{CO}_2$ then slowly increases towards stable levels, with the increase in T_s following behind.

A.5 Sensitivity Study of the Simple Model

Below, the resulting bifurcation diagrams when using modified values of Ω (figure A.2) and β (figure A.3) are shown.

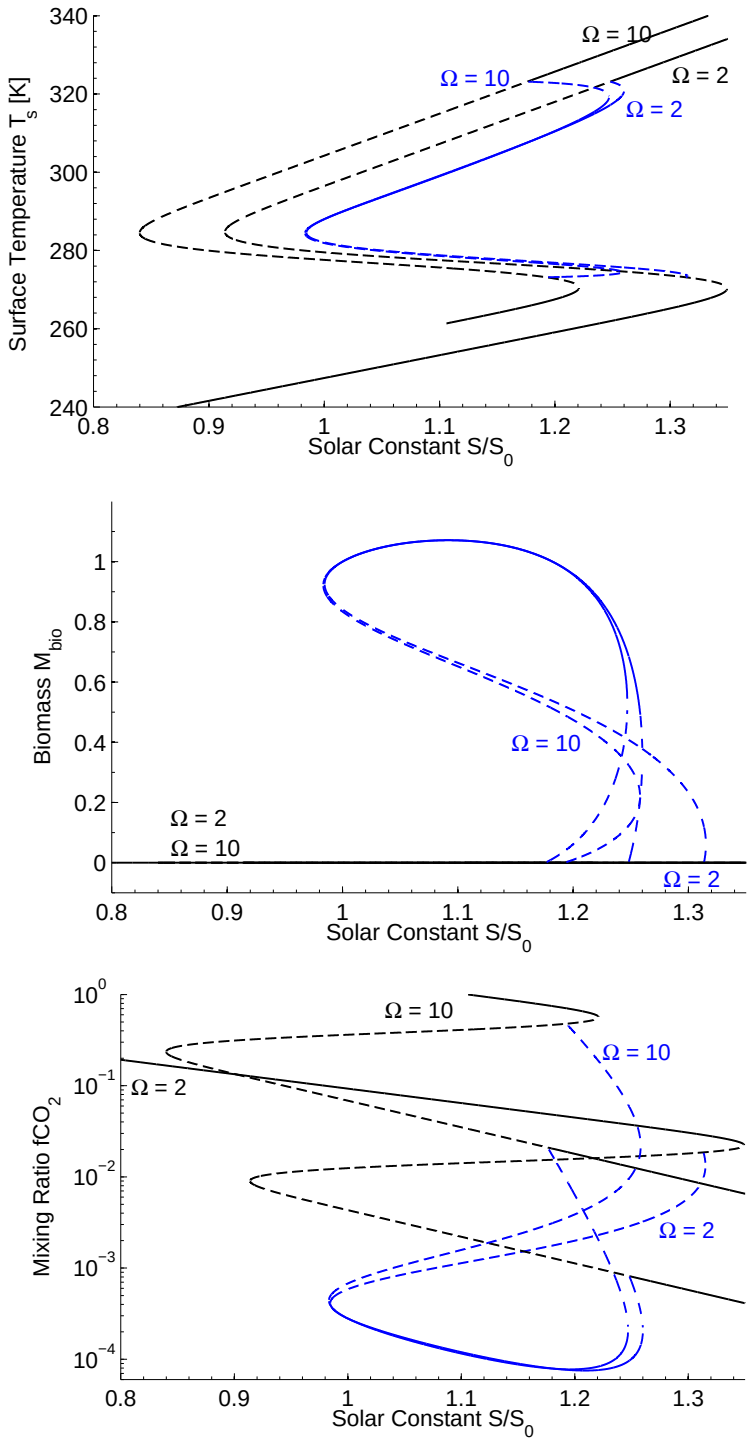

Figure A.2: Steady state surface temperature T_s (top panel), biospheric size $M_{\rm bio}$ (middle panel) and atmospheric mixing ratio of carbon dioxide $f\mathrm{CO}_2$ (bottom panel) as function of solar luminosity S/S_0 for two extreme values of the biotic enhancement factor Ω of silicate weathering rate. Solutions with $f\mathrm{CO}_2 > 1$ have been rejected.

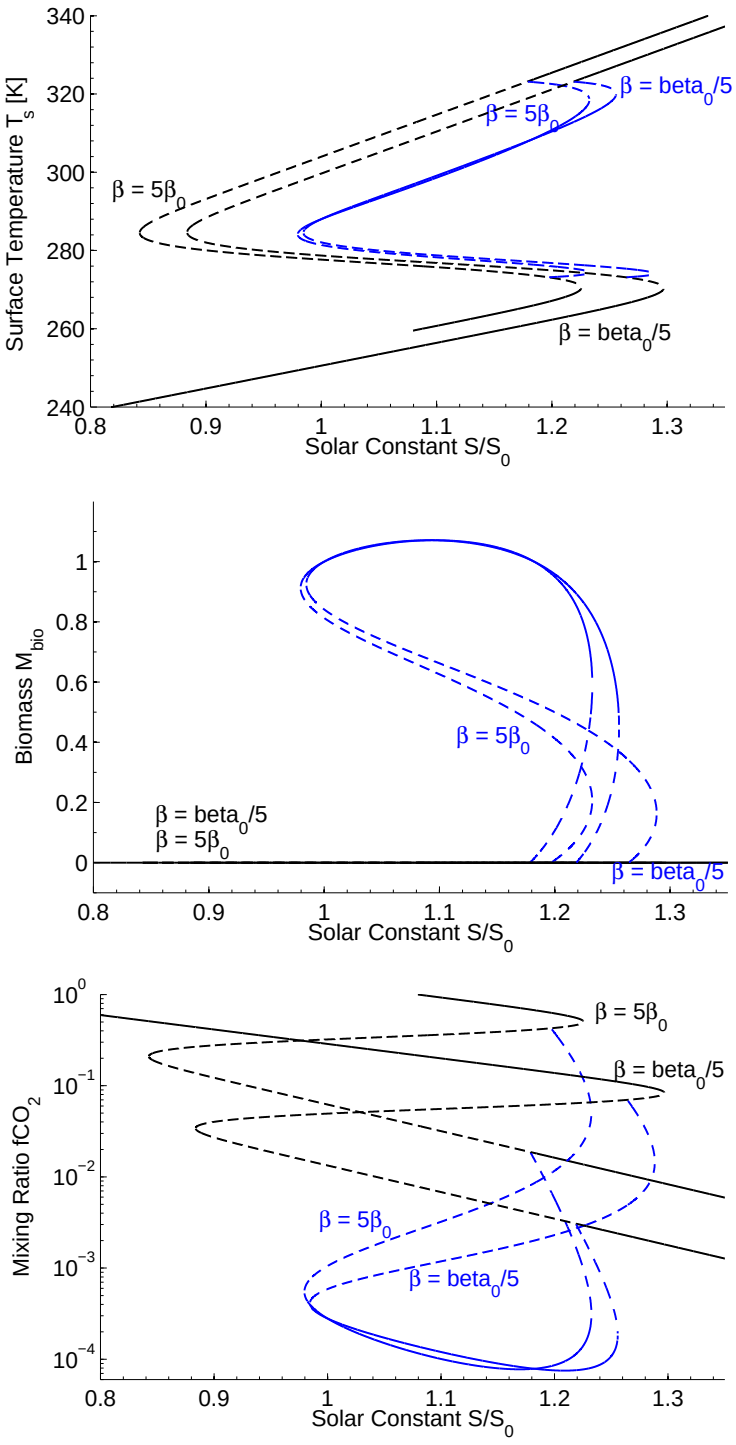

Figure A.3: Steady state surface temperature T_s (top panel), biospheric size $M_{\rm bio}$ (middle panel) and atmospheric mixing ratio of carbon dioxide $f\mathrm{CO}_2$ (bottom panel) as function of solar luminosity S/S_0 for two extreme values of the biotic carbon burial fraction β. Solutions with $f\mathrm{CO}_2 > 1$ have been rejected.

References

Bates, J. R. (2007), Some considerations of the concept of climate feedback, *Q. J. R. Meteorol. Soc.*, *133*, 545–560.

Beerling, D. J., and R. A. Berner (2005), Feedbacks and the coevolution of plants and atmospheric CO_2, *PNAS*, *102*(5), 1302–1305.

Bendtsen, J., and C. J. Bjerrum (2002), Vulnerability of climate on earth to sudden changes in insolation, *Geophysical Research Letters*, *29*(15), 1706–1710.

Berner, R. A. (1998), The carbon cycle and CO_2 over phanerozoic time: the role of land plants, *Phil. Trans. R. Soc. Lond. B*, *353*, 75–82.

Berner, R. A. (2003), The long-term carbon cycle, fossil fuels and atmospheric composition, *Nature*, *426*, 323–326.

Berner, R. A. (2005), The rise of trees and how they changed paleozoic atmospheric CO_2, climate, and geology, in *A history of atmospheric* CO_2 *and its effects on plants, animals, and ecosystems*, *Ecological Studies*, vol. 177, edited by J. R. Ehleringer, T. E. Cerling, and M. D. Dearing, chap. 1, Springer.

Caldeira, K., and J. F. Kasting (1992), The life span of the biosphere revisited, *Nature*, *360*, 721–723.

Ditlevsen, P. D. (2004), Turbulence and climate dynamics, Doctoral thesis, Copenhagen, iSBN 87-990522-0-2.

Ditlevsen, P. D. (2005), A climatic thermostat making Earth habitable, *International Journal of Astrobiology*, *4*, 3–7.

Franck, S., C. Bounama, and W. von Bloh (2006), Causes and timing of future biosphere extinctions, *Biogeosciences*, *3*, 85–92.

Goldblatt, C., T. M. Lenton, and A. J. Watson (2006), Bistability of atmospheric oxygen and the Great Oxidation, *Nature*, *443*, 683–686.

Hartmann, D. L. (1994), *Global Physical Climatology*, Academic Press, San Diego.

Harvey, L. D. (2000), *Global Warming, The Hard Science*, Prentice-Hall, Essex.

Heckman, D. S., D. M. Geiser, B. R. Eidell, R. L. Staufer, N. L. Kardos, and S. B. Hedges (2001), Molecular Evidence for the Early Colonization of Land by Fungi and Plants, *Science*, *293*, 1129–1133.

Hoffman, P. F., and D. P. Schrag (2000), Snowball Earth, *Scientific American*, pp. 68–75.

Hoffman, P. F., A. J. Kaufman, G. P. Halverson, and D. P. Schrag (1998), A Neoproterozoic Snowball Earth, *Science*, *281*, 1342–1346.

Hyde, W. T., T. J. Crowley, S. K. Baum, and W. R. Peltier (2000), Neoproterozoic 'snowball Earth' simulations with a coupled climate/ice-sheet model, *Nature*, *405*, 425–429.

Jin, Z., T. P. Charlock, W. L. S. Jr., and K. Rutledge (2004), A parameterisation of ocean surface albedo, *Geophysical Research Letters*, *31*, L22,301.

Kasting, J. F. (2004), When Methane Made Climate, *Scientific American*, pp. 78–85.

Kasting, J. F. (2005), Methane and climate during the Precambrian era, *Precambrian Research*, *137*, 119–129.

Kasting, J. F. (2006), Ups and downs of ancient oxygen, *Nature*, *443*, 643–645.

Kasting, J. F., and D. Catling (2003), Evolution of a habitable planet, *Annu. Rev. Astron. Astrophys.*, *41*, 429–463.

Kasting, J. F., and S. Ono (2006), Palaeoclimates: the first two billion years, *Phil. Trans. R. Soc. B*, *361*, 917–929.

Kasting, J. F., and J. L. Siefert (2002), Life and the Evolution of Earth's Atmosphere, *Science*, *296*, 1066–1068.

Kirchner, J. W. (2002), The Gaia hypothesis: fact, theory and wishful thinking, *Climate Change*, *52*, 391–408.

Kleidon, A. (2002), Testing the effect of life on Earth's functioning: how Gaian is the Earth system?, *Climate Change*, *52*, 383–389.

Kopp, R. E., J. L. Kirschvink, I. A. Hilburn, and C. Z. Nash (2005), The Paleoproterozoic snowball Earth: A climate disaster triggered by the evolution of oxygenic photosynthesis, *PNAS*, *102*, 11,131–11,136.

Kreyszig, E. (1999), *Advanced Engineering Mathematics*, 8th ed. ed., John Wiley and Sons, iSBN 0-471-15496-2.

Lenton, T. M. (1998), Gaia and natural selection, *Nature*, *394*, 439–447.

Lenton, T. M. (2002), Testing Gaia: the effect of life on Earth's habitability and regulation, *Climate Change*, *52*, 409–422.

Lovelock, J. E. (1991), Geophysiology - The Science of Gaia, in *Scientists on Gaia*, edited by S. H. Schneider and P. J. Boston, chap. 1, pp. 3–10, MIT Press.

Myhre, G., E. J. Highwood, K. P. Shine, and F. Stordal (1998), New estimates of radiative forcing due to well mixed greenhouse gases, *Geophysical Research Letters*, *25*(14), 2715–2718.

Nisbet, E. G., and N. H. Sleep (2001), The habitat and nature of early life, *Nature*, *409*, 1083–1091.

Pavlov, A. A., J. F. Kasting, L. L. Brown, K. A. Rages, and R. Freedman (2000), Greenhouse warming by CH_4 in the atmosphere of early Earth, *Journal of Geophysical Research*, *105*, 11,981–11,990.

Pierrehumbert, R. T. (2002), The hydrologic cycle in deep-time climate problems, *Nature*, *419*, 191–198.

Robert, F., and M. Chaussidon (2006), A palaeotemperature curve for the Precambrian oceans based on silicon isotopes in cherts, *Nature*, *443*, 969–972.

Rye, R., P. H. Kuo, and H. D. Holland (1995), Atmospheric carbon dioxide concentrations before 2.2 billion years ago, *Nature*, *378*, 603–605.

Salby, M. L. (1996), *Fundamentals of Atmospheric Physics*, Academic Press, San Diego.

Saunders, P. T. (1994), Evolution without natural selection: Further implications of the daisyworld parable, *Journal of Theoretical Biology*, *166*, 365–373.

Sharov, A. A. (1996), Quantitive Population Ecology On-Line Lectures, http://www.ento.vt.edu/ sharov/PopEcol/, cited on December 3, 2007.

Shaviv, N. J. (2003), Towards a Solution to the Early Faint Sun Paradox: A Lower Cosmic Ray Flux from a Stronger Solar Wind, *submitted to Journal of Geophysical Research*, *arXiv:astro-ph/0306477v2*, 1–8, `http://arxiv.org/pdf/astro-ph/0306477`.

Strogatz, S. H. (1994), *Nonlinear Dynamics and Chaos*, Westview Press, iSBN: 0-7382-0453-6.

Tajika, E. (2003), Faint young Sun and the carbon cycle: implication for the Proterozoic global glaciations, *Earth and Planetary Science Letters*, *214*, 443–453.

Volk, T. (2002), Toward a future for Gaia theory, An Editorial Comment, *Climate Change*, *52*, 423–430.

Walker, J. C. G., P. B. Hays, and J. F. Kasting (1981), A negative feedback mechanism for the long-term stabilization of Earth's surface temperature, *Journal of Geophysical Research*, *86*, 9776–9782.

Watson, A. J., and J. E. Lovelock (1983), Biological homeostasis of the global environment: the parable of Daisyworld, *Tellus*, *35B*, 284–289.